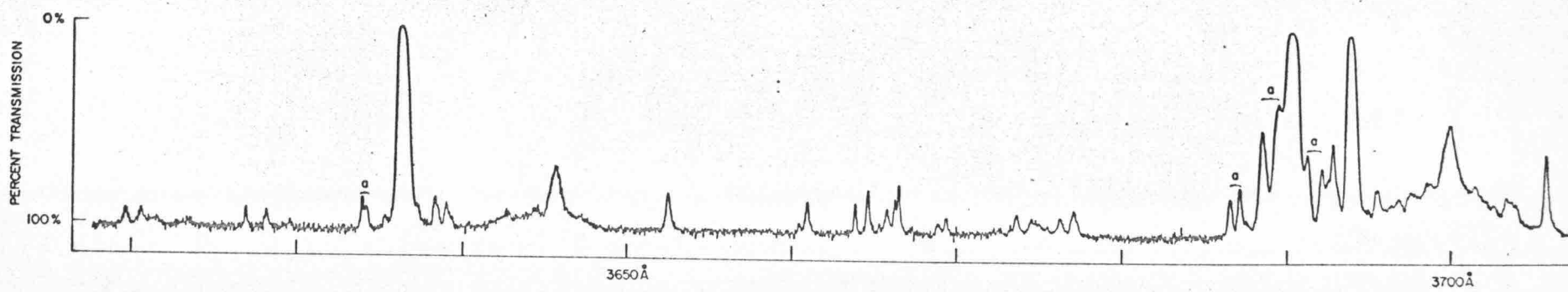
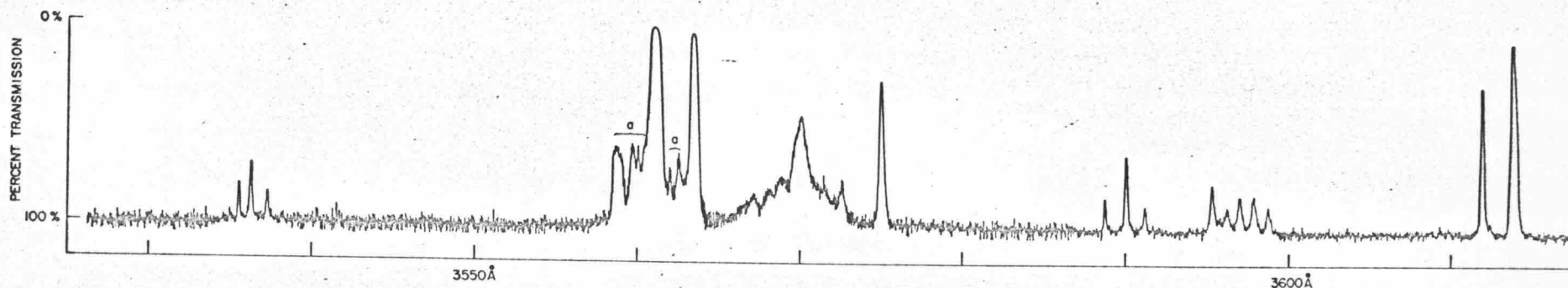
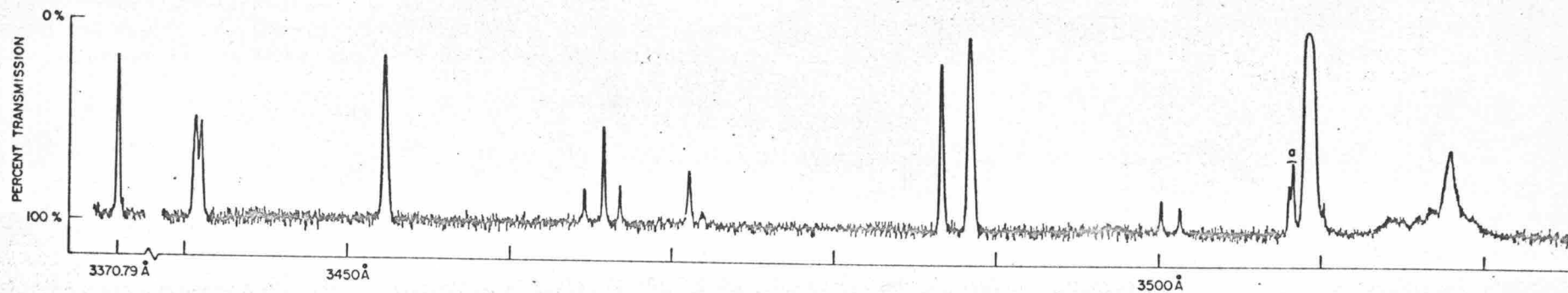


Caption for Fig. 2.

Microphotometer tracing of a lower resolution plate of the C_6H_6 phosphorescence. The bands labeled "a" are due to $^{13}C^{12}C_5H_6$ and discussed in the text.



Caption for Fig. 3.

Microphotometer tracing of the $0, 0-\nu_9$ and $0, 0-\nu_8$ C_6H_6 phosphorescence lines at the highest resolution employed.

PLATE TRANSMISSION

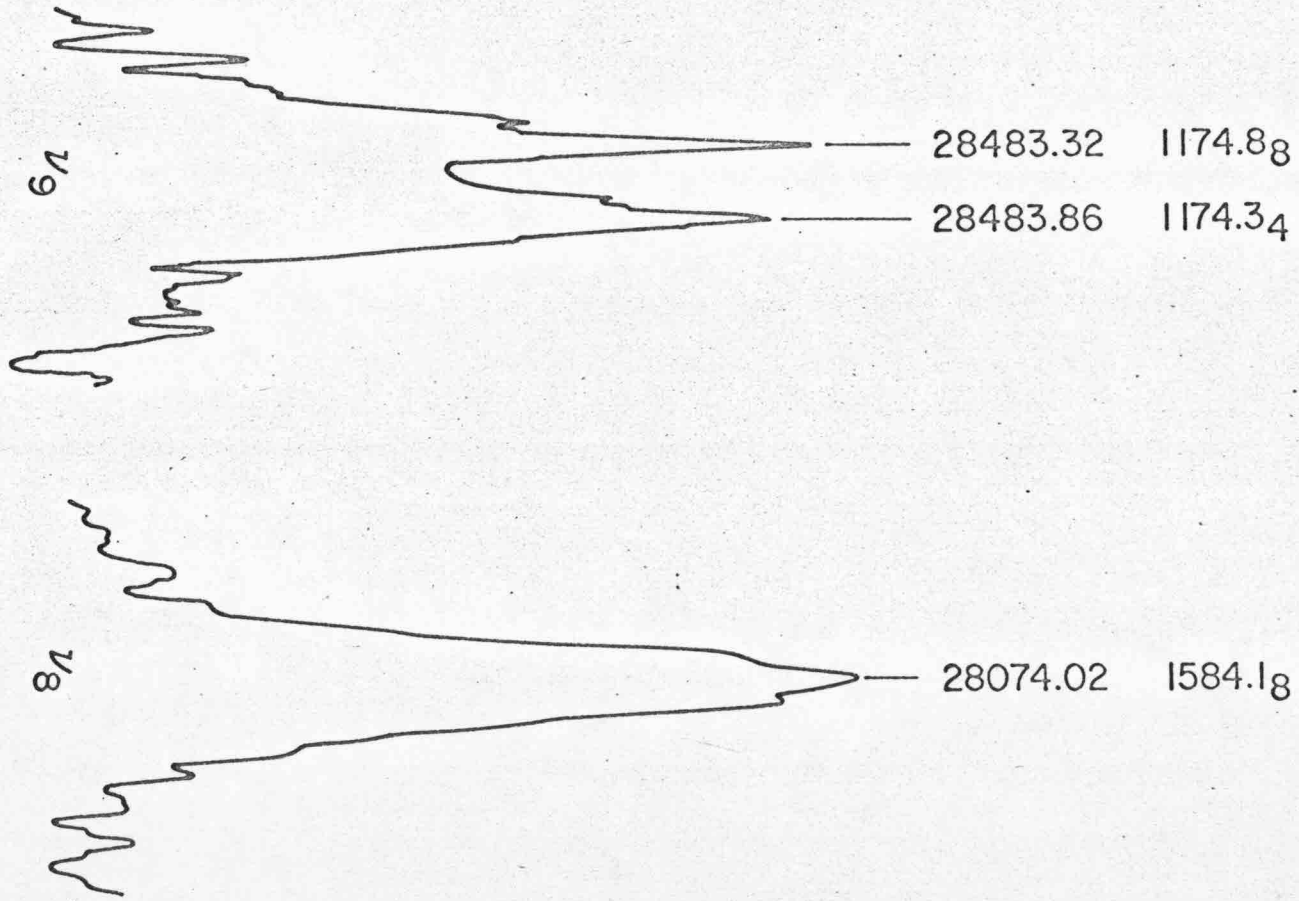
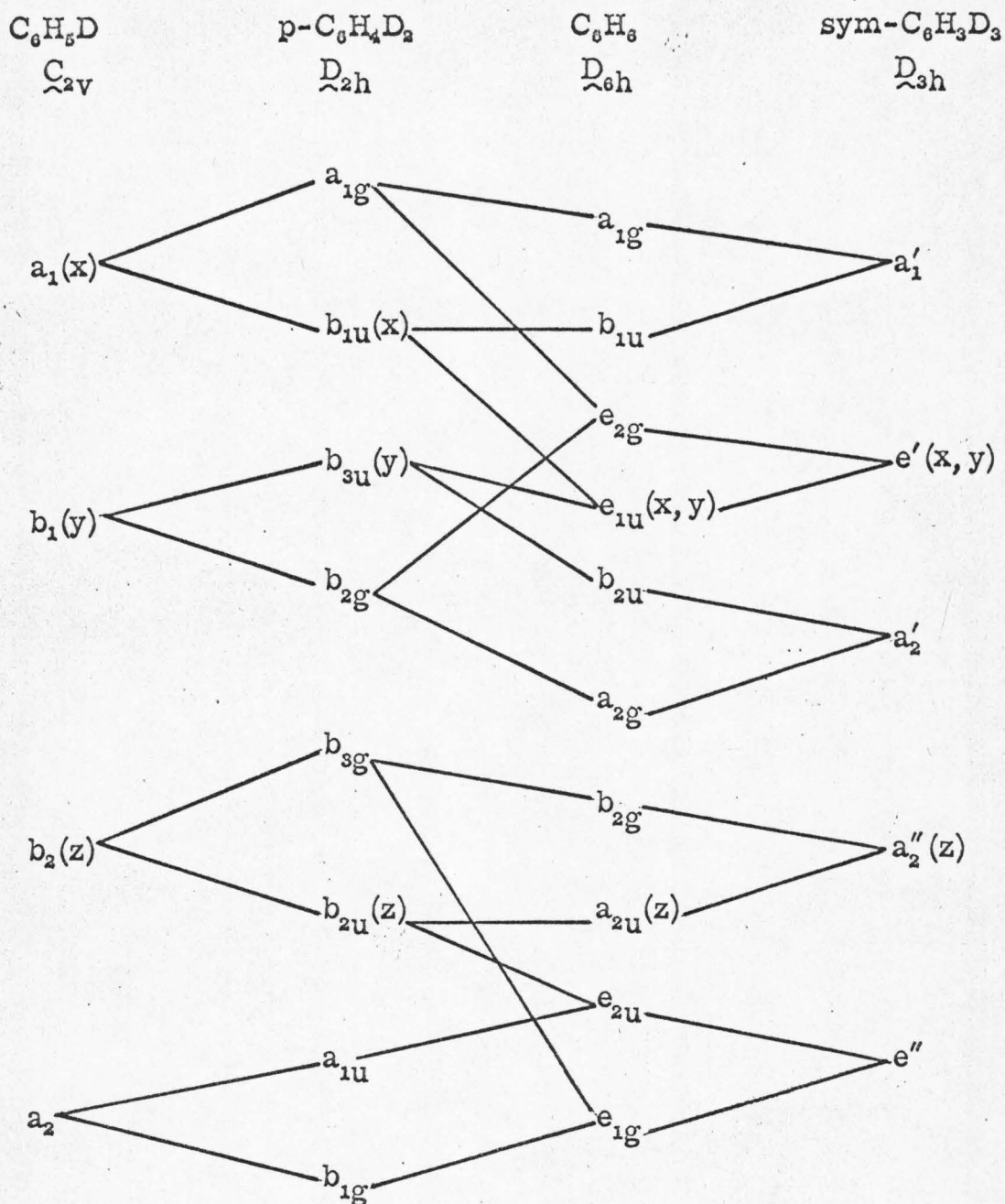


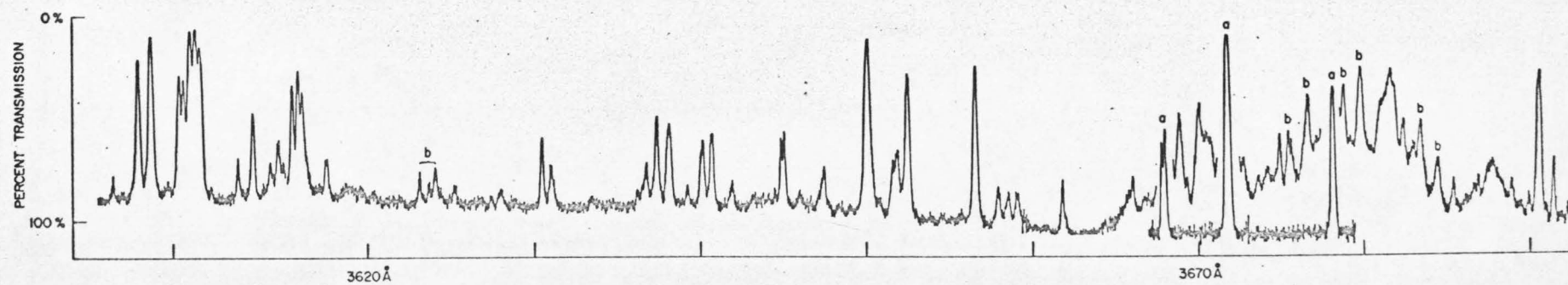
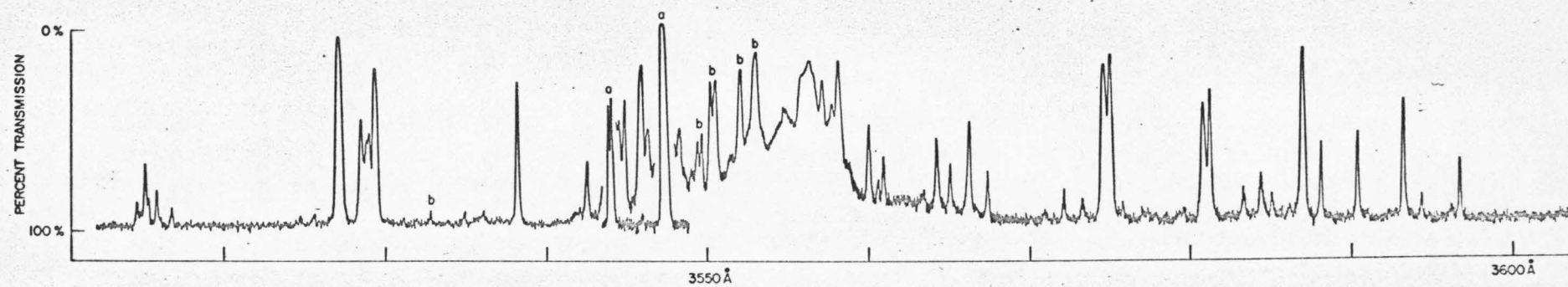
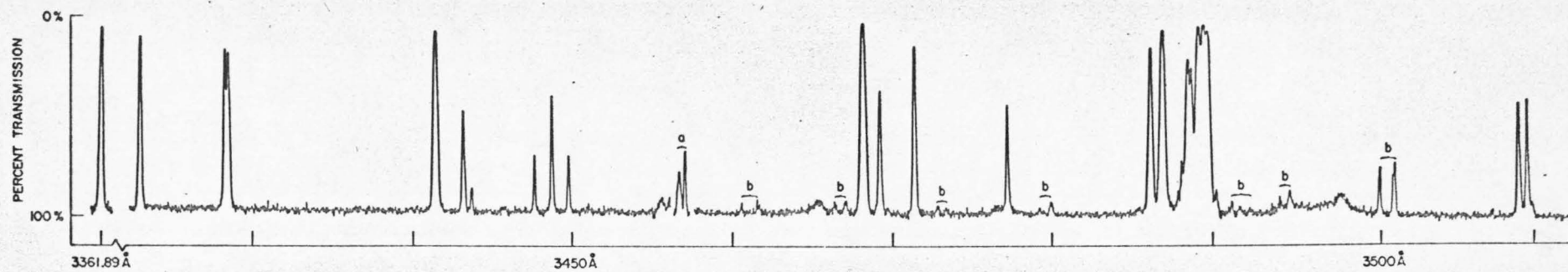
FIG. 4. Correlation diagram for the groups of benzene isotopes^a.



^a z -axis always perpendicular to the plane of molecule; y -axis through C_1 ; and x -axis between C_2 and C_3 .

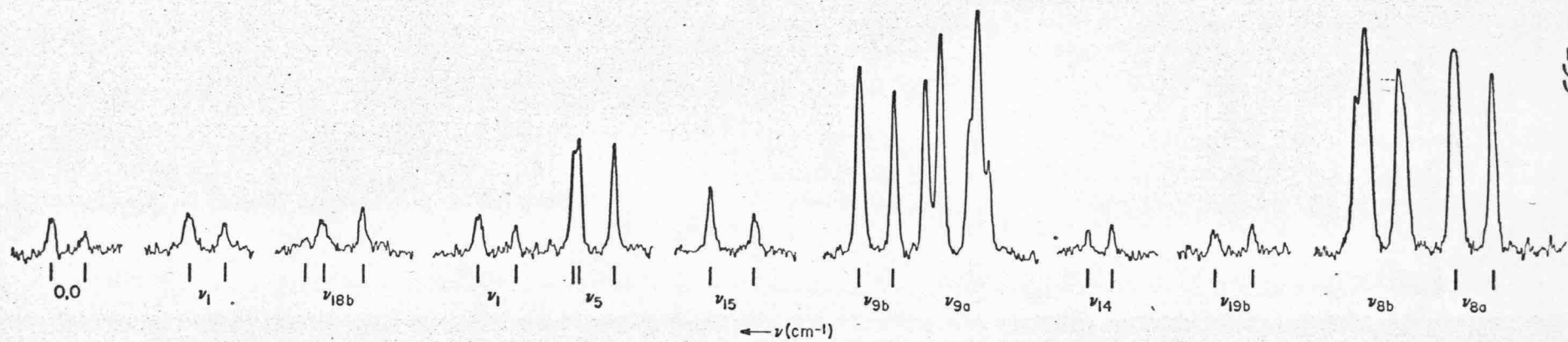
Caption for Fig. 5.

Microphotometer tracing of a lower resolution plate of the sym- $C_6H_3D_3$ phosphorescence. The bands labeled "a" are from a plate exposed 1/20 as long as the rest of the spectrum; "b" denotes bands assigned to m- $C_6H_4D_2$ and m- $C_6H_2D_4$ impurities.



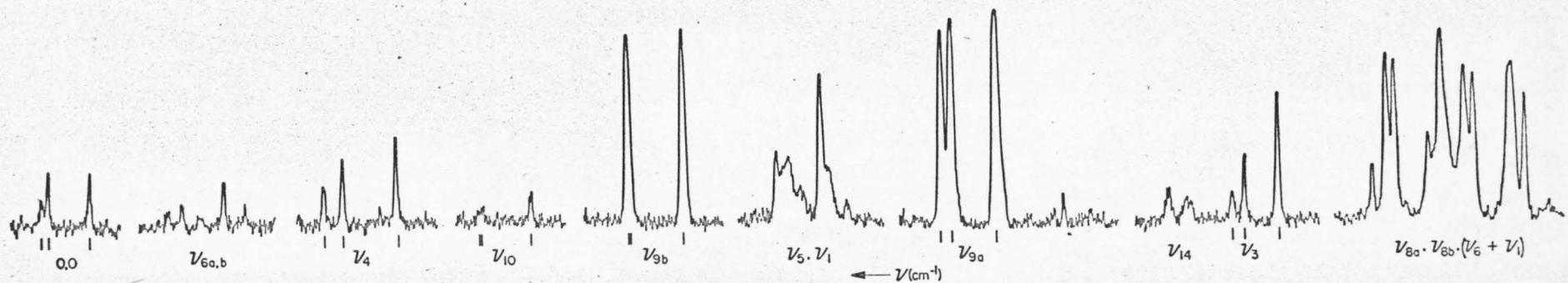
Caption for Fig. 6.

Microphotometer tracing of the stronger bands of the C_6H_5D phosphorescence. The $\nu_{8a,b}$ bands are taken from a plate exposed $1/5$ as long as the rest of the spectrum. Lines under the trace indicate assignments.



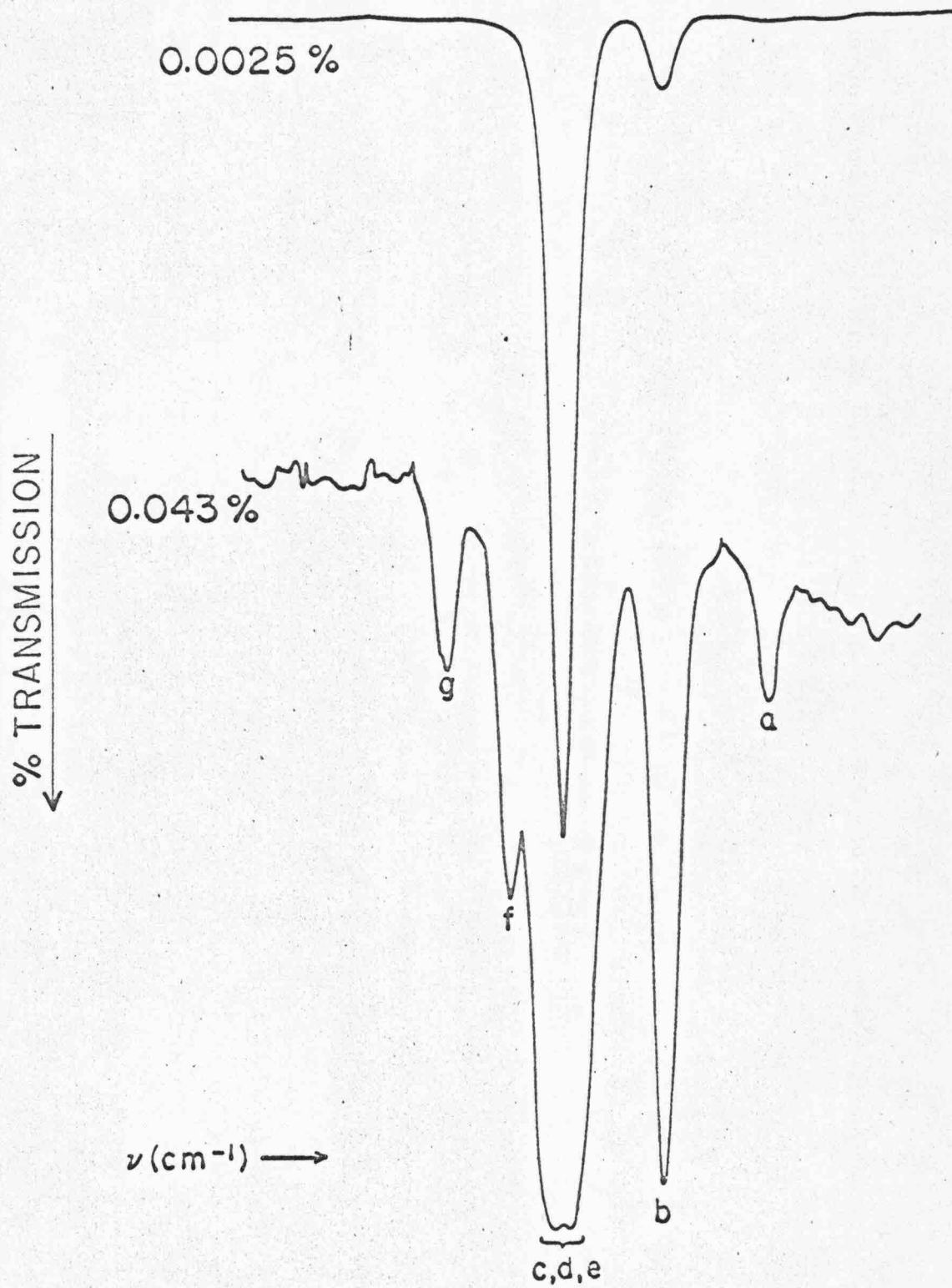
Caption for Fig. 7.

Microphotometer tracing of the stronger bands of the $p\text{-C}_6\text{H}_4\text{D}_2$ phosphorescence. The ν_8 region is taken from a plate exposed $1/5$ as long as the rest of the spectrum. Lines under the trace indicate assignments.



Caption for Fig. 8.

Microphotometer tracing of the C_6H_6 electronic origin at two concentrations in a 2 mm. thick C_6D_6 host crystal. See Table XIII for the frequencies.



Vibrational Exciton Structure in Crystals of Isotopic Benzenes*

ELLIOT R. BERNSTEIN AND G. WILSE ROBINSON

Gates and Crellin Laboratories of Chemistry[†]California Institute of Technology, Pasadena, California 91109ABSTRACT

New high resolution infrared spectra of crystalline isotopic benzenes C_6H_6 , C_6H_5D , p, m- $C_6H_4D_2$, sym- C_6H_5D , and C_6D_6 are presented. Using these data in conjunction with isotopic mixed crystal data and the polarized single crystal spectra (C_6H_6) of Zwerdling and Halford, the exciton band structures and coupling constants for non-degenerate vibrations of C_6H_6 and C_6D_6 are obtained. One vibration of sym- $C_6H_3D_3$ has also been analyzed. It is assumed that when the band shapes and splittings are nearly identical, the polarizations can be carried over from the C_6H_6 crystal to C_6D_6 and sym- $C_6H_3D_3$ crystals. It is not possible to analyze completely the degenerate bands of these isotopes since experimental data do not yield values of all the independent matrix elements appearing in the expression for the energy of the exciton components. In the isotopic modifications of lower symmetry, exciton structure is not usually observable due to an orientational effect, crystal induced Fermi resonance, and the inevitable presence of isotopic impurities.

* Supported in part by the National Science Foundation.

[†] Contribution No. 3549.

I. INTRODUCTION

The infrared spectrum of the benzene crystal has had a long and somewhat interesting history beginning in 1949 with the classic paper by Mair and Hornig.¹ Not only did these authors correctly assign all of the benzene spectrum in the infrared, but they observed and identified exciton structure on some of the bands. Their investigation was somewhat hampered by low instrumental resolution. In 1955 Zwerdling and Halford,² again using relatively low resolution, obtained polarized, single crystal spectra of benzene; this still remains the only infrared polarization data published on the benzene crystal.³ Unfortunately, the low resolution makes it very difficult to compare the data of Zwerdling and Halford with newer high resolution results. The latest infrared work on crystalline benzene (C_6H_6 and C_6D_6) was carried out by Hollenberg and Dows^{4, 5} using resolution of about 0.7 cm^{-1} . These workers also measured the absolute intensities of the infrared crystal transitions of C_6H_6 and C_6D_6 . It should be pointed out that the investigation of Hollenberg and Dows represents the first comprehensive and detailed study of the infrared spectrum of crystalline benzenes under high resolution.

Although it was clear in these early investigations that the observed structure in the benzene crystal vibrations was due to the coupling of the four molecules in the unit primitive cell, it was not at all obvious how to interpret the observed splittings in terms of specific interactions. In fact, no interpretation was presented in terms of the intermolecular coupling constants of the Davydov theory,⁶ as

transitions to one of the four exciton components from the ground state is dipole forbidden ($A_u \rightarrow A_g$). Recently Bernstein, Colson, Kopelman and Robinson (BCKR)⁷ have presented a technique for determining the position of the fourth Davydov component, employing isotopic mixed crystal data. Such data, in the limit of the ideal mixed crystal,⁷ allow the mean of the $\underline{k} = 0$ exciton multiplet to be determined and the unobserved level to be predicted. With accurate, high resolution polarization data, this in turn enables one to evaluate the magnitude and sign of the nearest-neighbor, pair-wise exciton coupling constants and, therefore, the form and magnitude of the intermolecular interactions. Clearly, such an analysis depends heavily on good dilute isotopic mixed crystal data and accurate high resolution single crystal polarization ratios. The former is presently available^{8,9} while, unfortunately, the latter is not. We must thus rely on the low resolution data of Ref. 2. A further difficulty along this line is that no polarization data is available for the non- C_6H_6 isotopes. Since such information is essential to our development we will assume that bands from different isotopic modifications with "superimposable structure" are similarly polarized.

The purpose then of this paper is threefold: 1) to understand exciton interactions in neat crystals of the isotopic benzenes; 2) to study the relationship between isotopic mixed crystal data and exciton structure of the various benzenes; and 3) to determine what, if any, are the effects of isotopic substitution upon the exciton exchange coupling constants in the neat crystal.

II. THEORY

Exciton band theory in the Frenkel limit has recently been discussed for the case of benzene in a paper by Bernstein, Colson, Kopelman and Robinson. Pertinent earlier references to the general theory are discussed in that work. For the purposes of this paper we shall require the energies of the four Davydov components ($\underline{k} = \underline{0}$),

$$E(A) = 4(+M_{I \text{ II}} + M_{I \text{ III}} + M_{I \text{ IV}})$$

$$E(B_1) = 4(+M_{I \text{ II}} - M_{I \text{ III}} - M_{I \text{ IV}}) \quad || \underline{a}$$

$$E(B_2) = 4(-M_{I \text{ II}} + M_{I \text{ III}} - M_{I \text{ IV}}) \quad || \underline{b}$$

$$E(B_3) = 4(-M_{I \text{ II}} - M_{I \text{ III}} + M_{I \text{ IV}}) \quad || \underline{c}$$

in terms of the pairwise intermolecular coupling constants $M_{qq'}$, for translationally inequivalent molecules. In Ref. 7 it was shown that the common origin (the mean energy) of these four components lies at a position $\bar{\epsilon} + \Delta + L^f(\underline{0})$, where $\bar{\epsilon}$ is the gas phase excitation energy, Δ is the total static field gas-to-crystal shift (site shift), and $L^f(\underline{0})$ is the translation group shift. The value of Δ also corresponds to the shift between the gas phase excitation energy and that in an ideal mixed crystal.⁷ The value of $L^f(\underline{0})$ is small for short range intermolecular interactions, since it depends upon the interaction between the relatively distant translationally equivalent molecules in the benzene crystal. Thus the mean energy of the Davydov components can be obtained to high precision from ideal mixed crystal results. Isotopic mixed crystal data properly corrected for quasiresonance effects approach

the ideal mixed crystal closely and therefore provide a means of obtaining Δ , the mean value of the Davydov components, and the position of the dipole forbidden A component in benzene.

Another result of Ref. 7 that should be kept in mind here is that site splitting of a molecular degenerate state is best defined in terms of ideal mixed crystal data. It is not necessarily a useful concept in the neat crystal because of the large number of independent off-diagonal interaction matrix elements associated with a pair of degenerate or nearly degenerate crystal states. (For example, in the case of benzene, there are only three independent off-diagonal elements for a molecular nondegenerate state but ten for a doubly degenerate state.) This complication arises when both site states map into the same irreducible representation of the site group, as in the case of benzene, and is particularly important when the magnitude of the site splitting in the ideal mixed crystal is comparable to the width of the exciton band in the neat crystal. The latter condition applies to many vibrational exciton bands in crystalline benzene.

It is important to realize too that vibrational states of the crystal are more susceptible to Fermi resonance than vibrational states of the free molecule.⁸ There are more levels in the crystal, and therefore more chance for accidental degeneracies to occur,¹¹ the symmetry restriction on interactions are more relaxed, and intermolecular coupling as well as intramolecular anharmonicity can mix the states.

Orientalional effects in isotopic mixed crystals of benzene have been observed recently^{8,9} for C_6H_5D , *p*, *m*- $C_6H_4D_2$, *m*- $C_6H_2D_4$, and

This is not a missing page. It is a result of page misnumbering.

and C_6HD_5 in host crystals of C_6H_6 and C_6D_6 . The "apparent splitting" of nondegenerate transitions is due to the random positioning, with respect to the molecular sixfold axis, of the non- \widetilde{D}_{3h} molecular isotopes of benzene in the \widetilde{C}_i site of the crystal. This observation indicates that the non-symmetry related site directions or positions can and do affect the site vibrations differently. In other words, when the molecular vibration can have specific orientations with respect to its environmental field and the molecule can orient itself in more than one way in this field, the various (differently oriented) vibrational transitions can have different energies and thus display an orientational effect. These energy differences, δ_{OE} , have been empirically determined to be roughly of the same order as the site group splittings and the exciton splittings ($\sim 2-10 \text{ cm}^{-1}$).^{8,9} It can be further shown¹⁰ that all these energy differences ("splittings") are determined by the same interactions. Thus, one would suspect that in the pure crystal spectra of the above listed isotopes little if any well-defined exciton splitting would be observable on transitions showing a sizable orientational effect in mixed crystals.

III. EXPERIMENTAL METHODS AND RESULTS

The general technique for the preparation of the sample has been described in BCKR. For weak transitions such as ν_{14} or any of the gerade vibrations of a benzene with no center of symmetry, a 0.015 in. indium spacer was used between the two CsI windows comprising the cell. This cell produces a sample on the order of $150\ \mu$ thick, estimated from both the compression of the indium spacer and intensity of the transitions. For strong transitions, such as the e_{1u} and a_{2u} vibrations of C_6H_6 and C_6D_6 , the samples were made with windows whose centers were machined and polished such that when the cell was assembled the sample thickness was roughly $10\text{-}20\ \mu$. Both techniques produce very transparent polycrystalline samples containing no empty volume. These samples were then attached to the cold finger of a helium temperature dewar and brought to 77°K in about 10-15 min. Although many runs were carried out at 4.2°K , most of the data were obtained at 77°K . Using $0.5\ \text{cm}^{-1}$ resolution, there is no observable difference in exciton structure at these two temperatures. All spectra were obtained on a Beckman IR-12.

The isotopic benzenes used in these experiments were either unpurified or cesium-purified.¹² The C_6H_6 was obtained from Phillips Petroleum Company (Research Grade), and the isotopic modifications from Merck, Sharpe and Dohme of Canada, Ltd. Differences have been detected in the spectra from these three types of samples and will be discussed in the next Section. From these observations it is possible to make some remarks concerning the limitations of Cs purification

(Section III-B). The results are reported in Tables I through III and some representative tracings are given in Figs. 1 through 14.

A. C₆H₆ and C₆D₆

Some of the spectra for the C₆H₆ and C₆D₆ vibrations are given in Figs 1 through 9 and the data are reported in Tables I and II.¹³ They should be compared with Ref. 4, and it is quite clear that the agreement in both absolute energy and band shapes is for the most part excellent.¹⁴ We do not, however, attempt to report ν_{20} and ν_{13} (3000 cm⁻¹ in C₆H₆ and 2200 cm⁻¹ in C₆D₆) since we feel they are inherently quite complex in the crystal because of increased Fermi resonance among the fundamentals themselves and the numerous combinations and overtones in these regions. Such complications are known to be present in the gas phase spectrum¹⁵ and have recently been discussed for isotopic mixed crystals of benzene.^{8,9} The extent of the Fermi resonance will be further amplified in the neat crystal as mentioned earlier.

In Table IV are contained the exciton coupling constants ($M_{qq'}$) for the nondegenerate \underline{u} molecular vibrations (a_{2u} , b_{1u} , b_{2u}) of C₆H₆ and C₆D₆ obtained from the neat and isotopic mixed crystal data employing the C₆H₆ polarization ratios of Ref. 2.

$\nu_{11}(a_{2u})[697 \text{ cm}^{-1} \text{ and } 511 \text{ cm}^{-1}]$ -- The ν_{11} band for C₆H₆ and C₆D₆ (Fig. 1 and Fig. 6) look quite similar to one another. As can be seen in Table IV, the exciton coupling constants are about the same, though those belonging to C₆D₆ appear somewhat smaller. It should be noted that the bands

are broad and thus the $M_{qq'}$'s are reported to only $\pm 0.5 \text{ cm}^{-1}$. Both samples were Cs purified¹² so that chemical impurities cannot be called upon to explain any of the structure. That part of the absorption in the exciton band could be due to isotopic impurities is eliminated since absorptions of all the isotopic benzenes in C_6H_6 and C_6D_6 mixed crystals are known, and none fall within the limits of the ν_{11} exciton band absorptions. The broad lines are probably caused by the fact that the band is intense and is thus quite sensitive to crystal quality. The discrepancy between the M's for C_6H_6 and C_6D_6 might be attributable to the line uncertainty, but there could be real causes for this difference. The C-C and C-H contact distances are smaller in C_6D_6 than in C_6H_6 due to the zero point motion of the H(D) atoms. Thus the C-C and C-H(D) interactions could be larger in the more closely packed C_6D_6 crystal. Just how these changes would affect the M's is very difficult to judge, since the geometry and number of contacts are involved in a very complicated fashion. Such changes in the exciton coupling constants should not be confused with isotopic effects on the interactions. In the latter case we mean that a change in the atom-atom potentials caused by a change in the electronic charge distribution has occurred. The changes in $M_{qq'}$ that we are talking about here could be best termed as a zero point or bond length effect.

$\nu_{14}(b_{2u}) [1312 \text{ cm}^{-1} \text{ and } 1285 \text{ cm}^{-1}]$ -- For ν_{14} (Figs. 2 and 7) the pairwise interactions appear somewhat larger in C_6D_6 than C_6H_6 but as can be seen from the band structure as well as the M's the exciton splitting is very similar. We consider the M's to be in agreement for these

two isotopes. From these data and the Raman work of Gee and Robinson¹⁶ one expects that such agreement is the rule rather than the exception.

$\nu_{15}(b_{2u})$ [1147 cm^{-1} and 821 cm^{-1}] -- For this band the M's for C_6D_6 and C_6H_6 , obtained from the isotopic mixed crystal data and the neat crystal data, do not agree. The major reason for this difference can be seen from Table II. The ν_{15} and ν_{18} bands of C_6D_6 (Fig. 9) interact considerably in the pure crystal due to the exciton splitting of each band, but not as much in the isotopic mixed crystal. This difference in Fermi resonance in the pure and mixed crystal considerably shifts the band from its ideal mixed crystal value; the predicted A_u level then appears to be much further away from the B_u levels than it actually is. Thus the large calculated exciton band structure for ν_{15} is an artifact caused by stronger intermolecular Fermi resonance in the pure crystal than in the mixed crystal. If all the $\underline{k} = \underline{0}$ exciton components were observed in the neat crystal and they all interacted equally under the Fermi resonance coupling, no such problem would exist. However, in this instance the "ideal mixed crystal" concept, which implies that the only difference between mixed and neat crystals is the exciton coupling interaction, breaks down.

Conclusions -- We can extract two general conclusions from the above data: The isotopic effects on the exciton coupling constants (exciton bands) are quite small; and increased Fermi resonance in the neat crystal with respect to both the gas and mixed crystal is a very important and significant phenomenon for the exciton structure. Most small

differences in exciton coupling constants associated with isotopic substitution can probably be associated with zero-point C-H or C-D bond changes.

B. Sym-C₆H₃D₃

Although it has been shown group theoretically and experimentally that no orientational effect can occur for sym-C₆H₃D₃ in the \underline{C}_i site of a C₆H₆ or C₆D₆ host crystal,^{8,9} it is clear that for the neat crystal of sym-C₆H₃D₃, where the site symmetry group is now reduced to \underline{C}_i , two distinct (in principle, energetically different) orientations can occur for this isotope. This is a consequence of the loss of inversion symmetry in the molecule itself. However, the crystal site field should not be greatly perturbed by such a change, as the bulk geometrical arrangement of the molecules remains unchanged and the isotopic effects on the potentials are small for ground state vibrations.^{8,17} In other words, this orientational effect should be considerably smaller than that which occurs for a molecule like C₆H₅D or p-C₆H₄D₂ in C₆H₆ or C₆D₆ host crystals. Therefore some bands in neat crystalline sym-C₆H₃D₃ are well-resolved (for example ν_{11} , ν_1 , ν_{12} , and ν_{16} in Figs. 10 and 11). The presumably random orientation of the molecules in the crystal will also affect the translational symmetry; and thus the entire \underline{k} band structure, as well as the $\Delta\underline{k} = 0$ selection rules,¹⁸ should now be altered. In light of the above ideas however, these effects may again be assumed to be small. Still there are many fundamentals that are quite broad, showing no discernable exciton

structure (Figs. 11 and 12). The two principal causes of this are Fermi resonance (ν_{15} , ν_5 , ν_{17} , and ν_1 --see Fig. 11) and the presence of a large amount of *m*-C₆H₄D₂ impurity (ν_{18} --see Fig. 11). Interference from other isotopes can be seen from the difference between spectra of the Cs purified and unpurified samples (Fig. 12). Cs purification¹² appears to cause exchange of H and D atoms in an isotope or mixture of isotopes containing both H and D atoms. Figures 10 and 11 show ν_{11} and ν_{16} in which regions (545 and 360 are cm⁻¹, respectively) the complication from Fermi resonance and other isotopes are believed to be minimized.¹⁹ Since however, ν_{16} is a free molecule degenerate vibration, the only band for which we can obtain M's is the $\nu_{11}(a_2'')$. These are: $M_{I \text{ II}} = 0$, $M_{I \text{ III}} = 1.5$, and $M_{I \text{ IV}} = 1 \text{ cm}^{-1} (\pm 0.5 \text{ cm}^{-1})$. The large error is due to the greater line position error in sym-C₆H₃D₃. While it is difficult to comment extensively on these exciton coupling constants they are in rough agreement with those of the ν_{11} bands of C₆H₆ and C₆D₆.

C. Other Isotopes

For C₆H₅D, *m-p*-C₆H₄D₂, and *m*-C₆H₂D₄ in which "first order" site orientational effects are possible ($\Lambda \sim \delta_{SS} \sim \delta_{OE}$), Fermi resonance is extensive and isotopic impurities are numerous, the pure crystal spectra are quantitatively uninformative (see Figs. 13 and 14). Where impurities and orientational effects do not obscure the exciton structure, Fermi resonance takes over to complicate matters even further. The ν_{16a} region of *p*-C₆H₄D₂ for example is probably

complicated due to the presence of C_6H_6 (Fig. 14).

An interesting point to make concerning the $p-C_6H_4D_2$ spectra (Fig. 14) is that the g vibrations ν_{9b} (910 cm^{-1}) and ν_{10a} (850 cm^{-1}) appear to be induced due to the loss of the \tilde{C}_i site symmetry in the crystal. This decrease in the symmetry occurs because of the orientational disorder in the crystal, and graphically illustrates the importance of site symmetry for the selection rules.

IV. CONCLUSIONS AND SUMMARY

Our experimental results demonstrate the following:

- a. For the case of benzene there does not appear to be any need to invoke large isotopic effects on the nearest-neighbor pairwise interactions (that is, changes in the interaction potential with isotope substitution), in order to account for the data on the ground state interactions. Any change in the M 's for a given vibration from isotope to isotope can be ascribed to either Fermi resonance or the increase in C-C and C-H(D) interactions due to the zero point decrease in the C-D bond length with respect to the C-H bond length.
- b. The orientational effects observed in mixed crystals (C_6H_5D , $m-p-C_6H_4D_2$, and $m-C_6H_2D_4$ in C_6H_6 or C_6D_6) for the \tilde{C}_i site symmetry can be observed in pure crystals, and usually serve to broaden the exciton structure to such an extent that neither the orientational effect nor the exciton structure can be extracted from the spectra. Of course, a further orientational effect

occurs due to the loss of the \underline{C}_i site symmetry in crystals of the above isotopes, which can, in principle at least, cause twice as many orientational lines to appear for a given vibration. In addition, an orientational effect for sym- $C_6H_3D_3$ is postulated in the pure crystal due to the reduction of the site symmetry to \underline{C}_1 . However, this effect is small as it is not due to the "bulk crystal" structure, which is assumed not to change from that of C_6H_6 (\underline{C}_i site, D_{2h}^{15} space group), but to the substitution of D for H atoms. Other effects, such as a breakdown of the $\Delta \underline{k} = 0$ selection rule and the disruption of the general \underline{k} band structure due to the loss of translational symmetry in the crystal, may also contribute to the broadening of the exciton structure of the non- \underline{D}_{6h} isotopic crystals.

- c. The importance of Fermi resonance for the crystal vibrational spectra is emphasized. It becomes especially significant when the ideal mixed crystal concept is employed to obtain the complete $\underline{k} = \underline{0}$ exciton band structure, as we have done in order to locate the unobserved exciton component of the nondegenerate band of benzene. If such resonances are not identically equal in both mixed and pure crystals, employing this technique to find the band structure can lead to what appear to be large exciton band distortions as a function of isotopic substitution. Such an occurrence is graphically illustrated by the ν_{15} vibration of C_6D_6 in resonance with the ν_{18} mode. One expects the ν_{15} exciton structure of C_6H_6 and of C_6D_6 to be nearly the same (vide infra) but they clearly are not (see Tables I, II and IV).

Since Fermi resonance in the neat crystal is greatly enhanced with respect to the mixed crystal, where Fermi resonance is possible, the ideal mixed crystal energy level must be used with caution to obtain the band structure. In essence the concept of the ideal mixed crystal is no longer valid, in that the difference in interactions for the mixed and neat crystals are no longer simply the resonance exchange terms $M_{qq'}$.

REFERENCES AND FOOTNOTES

1. R. D. Mair and D. F. Hornig, *J. Chem. Phys.* 17, 1236 (1949).
2. S. Zwerdling and R. S. Halford, *J. Chem. Phys.* 23, 2221 (1955).
3. Although there are some questions concerning this work, a careful analysis of their experimental apparatus and procedure reveals that any difficulty can be cleared up when one considers the divergence of their light beam (R. Kopleman, private communication) and the fact that they employed the incorrect crystal structure. They believed that, although the space group was D_{2h}^{15} , the benzene molecules were oriented parallel to the crystal axes. With the "new" crystal structure their oriented gas arguments are not greatly altered and their conclusions concerning the spectra observed along the a and c axes remain likewise unaltered.
4. J. L. Hollenberg and D. A. Dows, *J. Chem. Phys.* 37, 1300 (1962).
5. Some doubt is cast on these values as the authors did not realize for example that the 3000 cm^{-1} was complicated by crystal enhanced Fermi resonance and combinations. They also included a C_6D_5H transition in the C_6D_6 (ν_{11}) band [see also J. L. Hollenberg and D. A. Dows, *J. Chem. Phys.* 39, 495 (1963) and Ref. 8].
6. A. S. Davydov, *Usp. Fiz. Nauk* 82, 393 (1964) [English transl. : *Soviet Phys. --Usp.* 7, 145 (1964)].
7. E. R. Bernstein, S. D. Colson, R. Kopelman and G. W. Robinson, "Electronic and Vibrational Exciton Structure in Molecular Crystals--Benzene", *J. Chem. Phys.* (to be published).

8. E. R. Bernstein, "Site Effects in Molecular Crystals--Site Shift, Site Splitting, Orientational Effect and Intermolecular Fermi Resonance for Benzene Crystals", J. Chem. Phys. (to be published).
9. E. R. Bernstein, S. D. Colson, D. S. Tinti and G. W. Robinson, "Static Crystal Effects on the Vibronic Structure of the Phosphorescence, Fluorescence, and Absorption Spectra of Benzene Isotopic Mixed Crystals", J. Chem. Phys. (to be published).
10. See, however, E. R. Bernstein "Calculation of the Ground State Vibrational Structure and Phonons of the Benzene Isotopic Crystals", J. Chem. Phys. (to be published).
11. V. L. Strizhersky, Opt. i Spektroskopiya 8, 165 (1960) [English transl.: Opt. Spectry. (USSR) 8, 86 (1960)].
12. S. D. Colson and E. R. Bernstein, J. Chem. Phys. 43, 2661 (1965).
13. Some other tracings can be found in Ref. 7.
14. Even though we only report our frequencies to 0.1 cm^{-1} and claim an absolute accuracy of $\pm 0.5 \text{ cm}^{-1}$ we believe our number to be as good as those of Ref. 5, in which the frequencies are reported to $\pm 0.01 \text{ cm}^{-1}$, as they also use a commercial spectrometer and calibrate with various gas phase spectra. In many cases, due to our somewhat higher resolution, our numbers may actually be better.
15. G. Herzberg, Infrared and Raman Spectra (D. van Nostrand and Co., 1964), p. 362 ff.
16. A. R. Gee and G. W. Robinson, J. Chem. Phys. 00, 0000 (1967).
17. This is very obvious in the work of Ref. 8 which shows that 0.1% $\text{C}_6\text{H}_5\text{D}$ in $m\text{-C}_6\text{H}_4\text{D}_2$ (Fig. 19 of this reference) gives very

sharp lines for the orientational effect. (See also Ref. 9.)

18. S.D. Colson, R. Kopelman and G.W. Robinson, J. Chem. Phys. 00, 0000 (1967).
19. The ν_{11} band of m-C₆H₂D₄ should fall around 538 cm⁻¹ and could change the band shape of the sym-C₆H₃D₃ band. However, since Cs purification which makes m-C₆H₄D₂ from sym-C₆H₃D₃ has no large effect on this band, the above conclusion is probably justified.

TABLE I. C₆H₆ exciton structure (cm⁻¹).

Vibration Number and D _{6h} Symmetry ^a		Gas Phase Value ^b	IMC Value ^c	Exciton Components ^d	Polarization ^e	
ν ₁₁	a _{2u}	672	696.9	681-683	a	B _{1u}
				689.2	c	B _{3u}
				707.8	b	B _{2u}
				[709.0] ^f		A _u
ν ₁₂	b _{1u}	1011	1011.3	1006.9	c	B _{3u}
				1008.6	b	B _{2u}
				1009.7	a	B _{1u}
				[1020.0]		A _u
ν ₁₄	b _{2u}	1309	1312.6	1312.2	g	A _u
				1313.4		
				1315.3		
				[1309.5]		
ν ₁₅	b _{2u}	1146	1146.9	1142.5	c	B _{3u}
				1148.6	a	B _{1u}
				1150.3	b	B _{2u}
				[1146.2]		A _u
ν ₁₆	e _{2u}	398	404.8	i		
			413.0			
			419.0			
ν ₁₇	e _{2u}	967	978.3	g		
			972.0			
			974.7			
			978.6			
			982.3			
			987.5			
988.1						
ν ₁₈	e _{1u}	1037	1034.8	g		
			1038.6			
			1030.0			
			1032.5			
			1033.5			
			1034.6			
1038.9						
1039.8						
ν ₁₉	e _{1u}	1482	1470.0 ^h	1469.8	g	
				1470.2		
				1473.5		
				1474.9		
				1475.6		
				1477.7		
				1478.9		
				1480.2		

¹³C

TABLE I. (continued)

^a ν_{20} and ν_{13} are in Fermi resonance in crystal and cannot be separated into distinct vibrations.

^bJ. H. Callomon, T. M. Dunn and I. M. Mills, *Phil. Trans. Roy. Soc. (London)*, A259, 499 (1966).

^cIdeal mixed crystal energy--see text and Ref. 8.

^dComponent in brackets not observed--calculated from IMC level and other exciton components, see Ref. 7.

^eS. Zwerdling and R. S. Halford, *J. Chem. Phys.* 23, 2221 (1955).

^fPosition not well known due to inaccuracy in the determination of the a-polarized component.

^gPolarization data not conclusive due to low resolution.

^hBroad and structureless.

ⁱNot observed by Zwerdling and Halford (Ref. 2).

TABLE II. C_6D_6 exciton structure (cm^{-1}).

Vibration Number and D_{6h} Symmetry ^a		Gas Phase Value ^b	IMC Value ^c	Exciton Components ^d	Polarization ^e	
ν_{11}	a_{2u}	498	511.3	502.0	a	B_{1u}
				506.0	c	B_{3u}
				519.0	b	B_{2u}
				[518.0] ^g		A_u
ν_{12}	b_{1u}	970	971.0	966.8	c	B_{3u}
				969.6	b	B_{2u}
				970.3	a	B_{1u}
				[978.1]		A_u
ν_{14}	b_{2u}	1285	1285.1	1286.2	f	
				1287.5		
				1288.7		
				[1278.0]		
ν_{15}	b_{2u}^h	824	820.6	823.4	c	B_{3u}
				824.1	a	B_{1u}
				826.9	b	B_{2u}
				[808.0] ^j		A_u
ν_{16}	e_{2u}	348	354.8 364.6	351.3	i	
				353.7		
				354.0		
				367.3		
				370.1		
				373.2		
ν_{17}	e_{2u}	787	791.3 797.8	789.4	f	
				790.3		
				795.0		
				795.4		
				797.8		
				801.2		
ν_{18}	e_{1u}^h	814	810.5 814.6	808.2	f	
				809.3		
				811.2		
				812.5		
				814.9		
				815.5		
ν_{19}	e_{1u}	1333	1329.2	1325.4	f	¹³ C
				1328.4		
				1329.5		
				1330.3		
				1335.1		
				1336.0		

TABLE II. (continued)

^a ν_{20} and ν_{13} are in Fermi resonance in the crystal and cannot be separated into distinct vibrations.

^bJ. A. Callomon, T. M. Dunn and I. M. Mills, *Phil. Trans. Roy. Soc. (London)*, A259, 499 (1966).

^cIdeal mixed crystal energy--see text and Ref. 8.

^dComponents in brackets are obtained from IMC level and observed exciton components.

^eThese polarizations are obtained from the C_6H_6 data by assuming the same band structure for the two isotopes; square brackets indicate Fermi resonance.

^fDue to low resolution the C_6H_6 polarizations are not known (Ref. 2).

^gNot well known due to inaccuracy in the determination of the polarized components.

^h ν_{15} and ν_{18} are in resonance in the pure crystal and to a less extent in the IMC.

ⁱNot studied by Zwerdling and Halford in C_6H_6 (Ref. 2).

^jCalculated on the basis of the ideal mixed crystal level in the same fashion as the other bands. Not believed to be the true neat crystal exciton structure due to the increase of Fermi resonance between ν_{18} and ν_{15} in the neat crystal with respect to the mixed crystal. See text for discussion of this point.

TABLE III. sym-(1, 3, 5)C₆H₃D₃ Exciton structure.

Vibration Number and D _{3h} Symmetry		Gas Phase Value ^a	IMC Value ^b	Exciton Components ^c	Polarization ^d	
ν_{11}	a''_2	531	545.5	536.0	a	B _{1u}
				541.0	c	B _{3u}
				550.0	b	B _{2u}
				[555.0] ^e		A _u
ν_{12}	a'_1	1002	1002.7	1002.7		
ν_{15}	a'_2	912	908.1	922.0		
				925.0		
				935.0		
ν_5	a''_2	917	928.0	940.0 946.0		
ν_{17}	e''	924	935.7 939.4	955.0		
ν_1	a_1	955	954.6			
ν_{16}	e''	368	377.5 385.0	376.6		
				378.1		
				390.3		
				395.9	f	
				399.6		
ν_{18}	e'	833	831.6 834.4	830.0		
				830.6	f	
				832.4		
				835.1		
				837.1		

^aS. Brodersen and L. Langseth, Mat. Fys. Skr. Dan. Ved. Selsk.

1, 7 (1959).

^bIdeal mixed crystal energy--see Refs. 7 and 8.

^cComponents in brackets are obtained from IMC level and observed exciton components.

^dFrom the C₆H₆ data of Zwerdling and Halford, J. Chem. Phys. 23, 2221 (1955).

TABLE III. (continued)

^eNot well known due to inaccuracy in the determination of the polarized components.

^f C_6H_6 polarization not known.

TABLE IV. Nearest-neighbor pairwise exciton interaction constants for C_6H_6 and C_6D_6 nondegenerate u ground state vibration (in cm^{-1}).

Vibration	IMC (C_6H_6)	IMC (C_6D_6)	Coupling Constants	
			C_6H_6	C_6D_6
ν_{11} a_{2u}	696.9	511.3	$M_{I II} = 0.5 \pm 0.5$	-0.3 ± 0.5
			$M_{I III} = 0.4$	+0.2
			$M_{I IV} = 2.8$	+1.8
ν_{12} b_{1u}	1011.3	971.0	$M_{I II} = 0.9 \pm 0.2$	0.7 ± 0.2
			$M_{I III} = 0.8$	0.7
			$M_{I IV} = 0.6$	0.3
ν_{14} b_{1u}	1312.6	1285.1	$M_1^a = -0.4 \pm 0.2$	-0.8 ± 0.2
			$M_2 = -0.3$	-0.6
			$M_3 = +0.1$	-0.5
ν_{15} b_{2u}	1146.9	820.6	$M_{I II} = 0.4 \pm 0.2$	-1.1 ± 0.2^b
			$M_{I III} = 0.1$	-0.8
			$M_{I IV} = -0.7$	-1.2

^aPolarizations not known and thus it is not possible to assign each coupling constant to a given pair of molecules.

^bNot correct values of the exciton coupling constants due to Fermi resonance between ν_{15} and ν_{18} (see text).

Fig. 1. Neat crystal C_6H_6 ν_{11} (a_{2u}).

Neat Crystal C_6H_6 $\nu_{11}(a_{2u})$

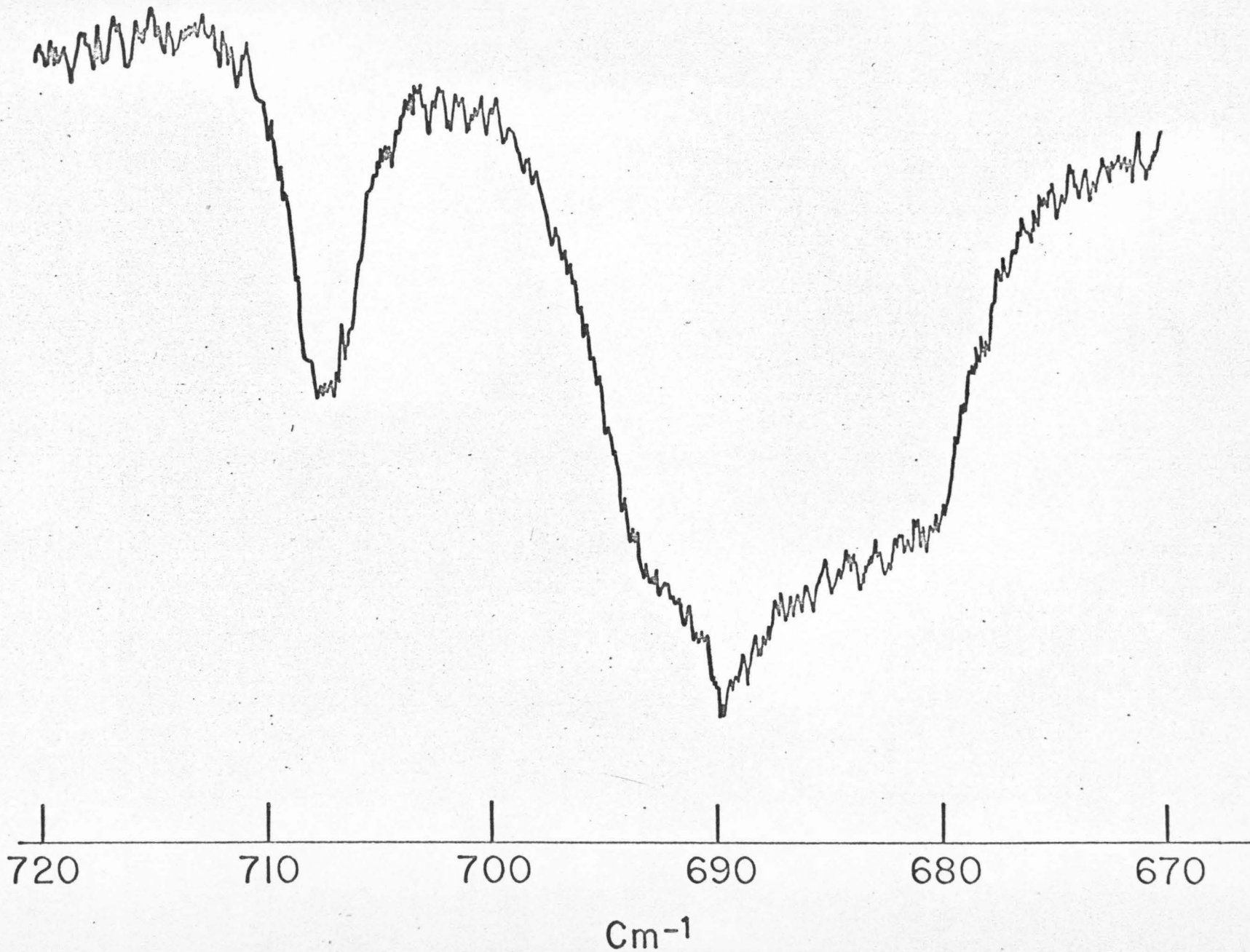


Fig. 2. Neat crystal C_6H_6 ν_{14} (b_{2u}). The feature at c. 1307 cm^{-1} is due to $^{13}CC_5H_6$ (Ref. 8).

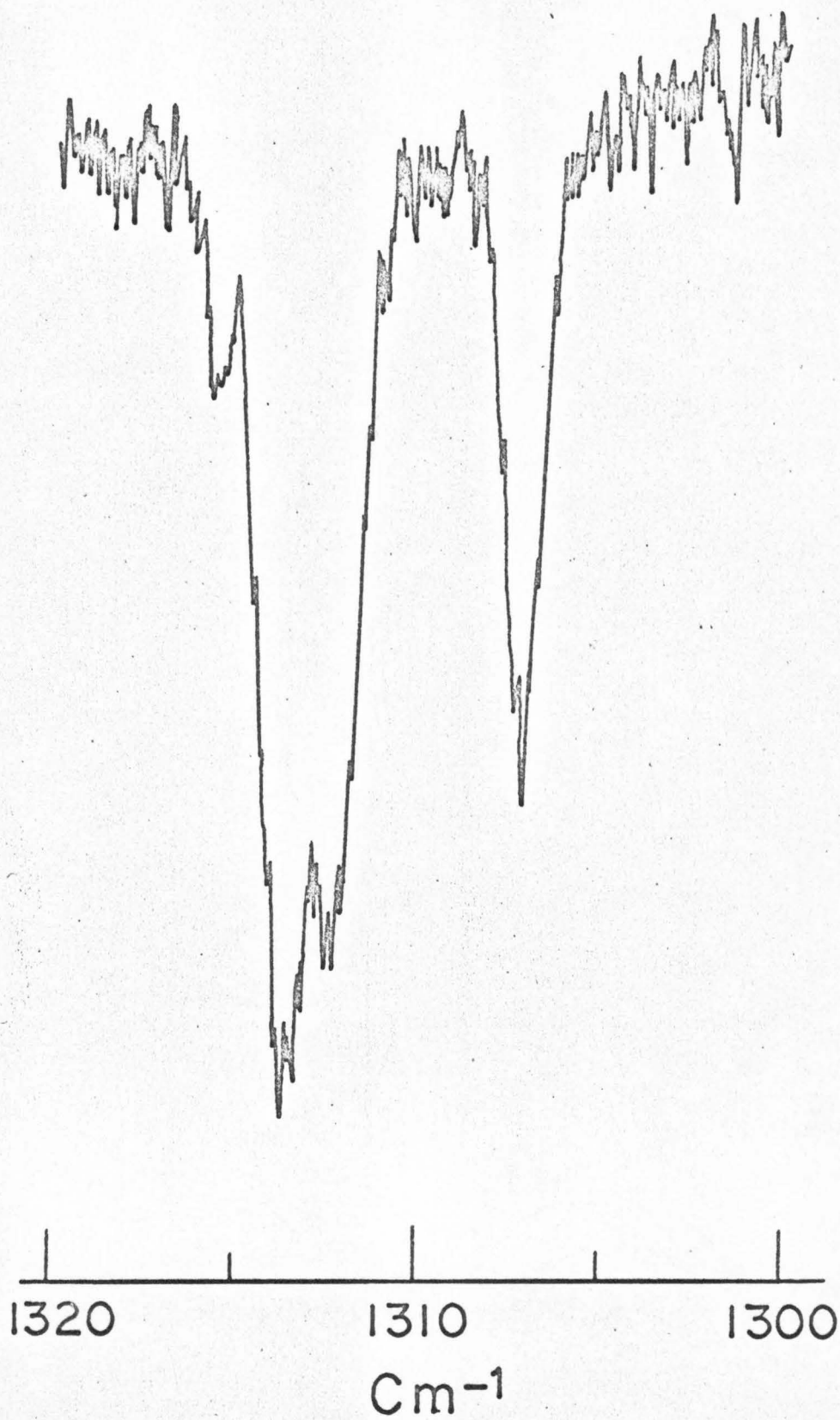
$\nu_{14} \text{C}_6\text{H}_6$ 

Fig. 3. Neat crystal $C_6H_5 \nu_{16}$ (e_{2u}).

Neat Crystal C_6H_6 $\nu_{16}(e_2u)$

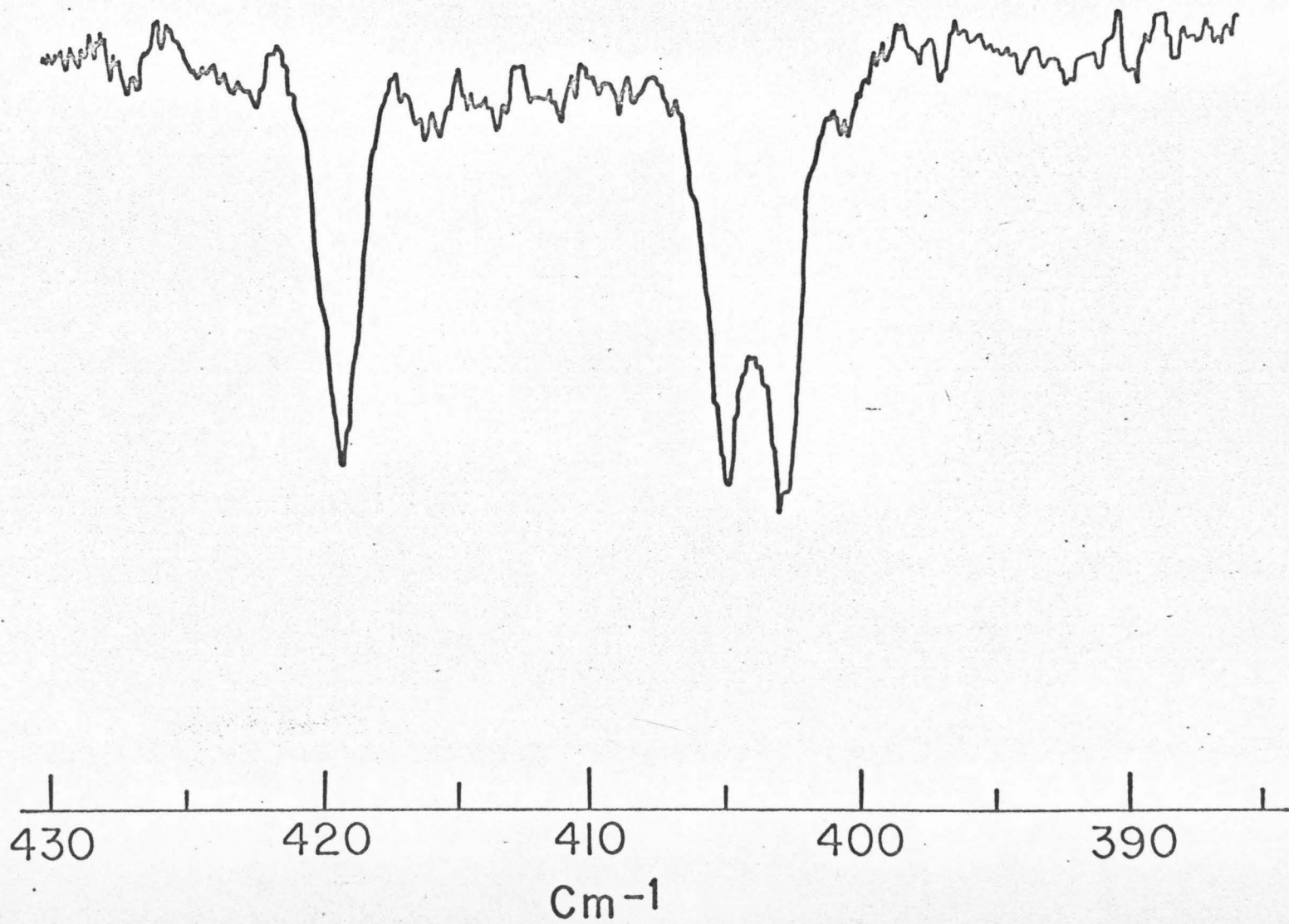


Fig. 4. Neat crystal C_6H_6 ν_{17} (e_{2u}).

271

ν_{17} C₆H₆

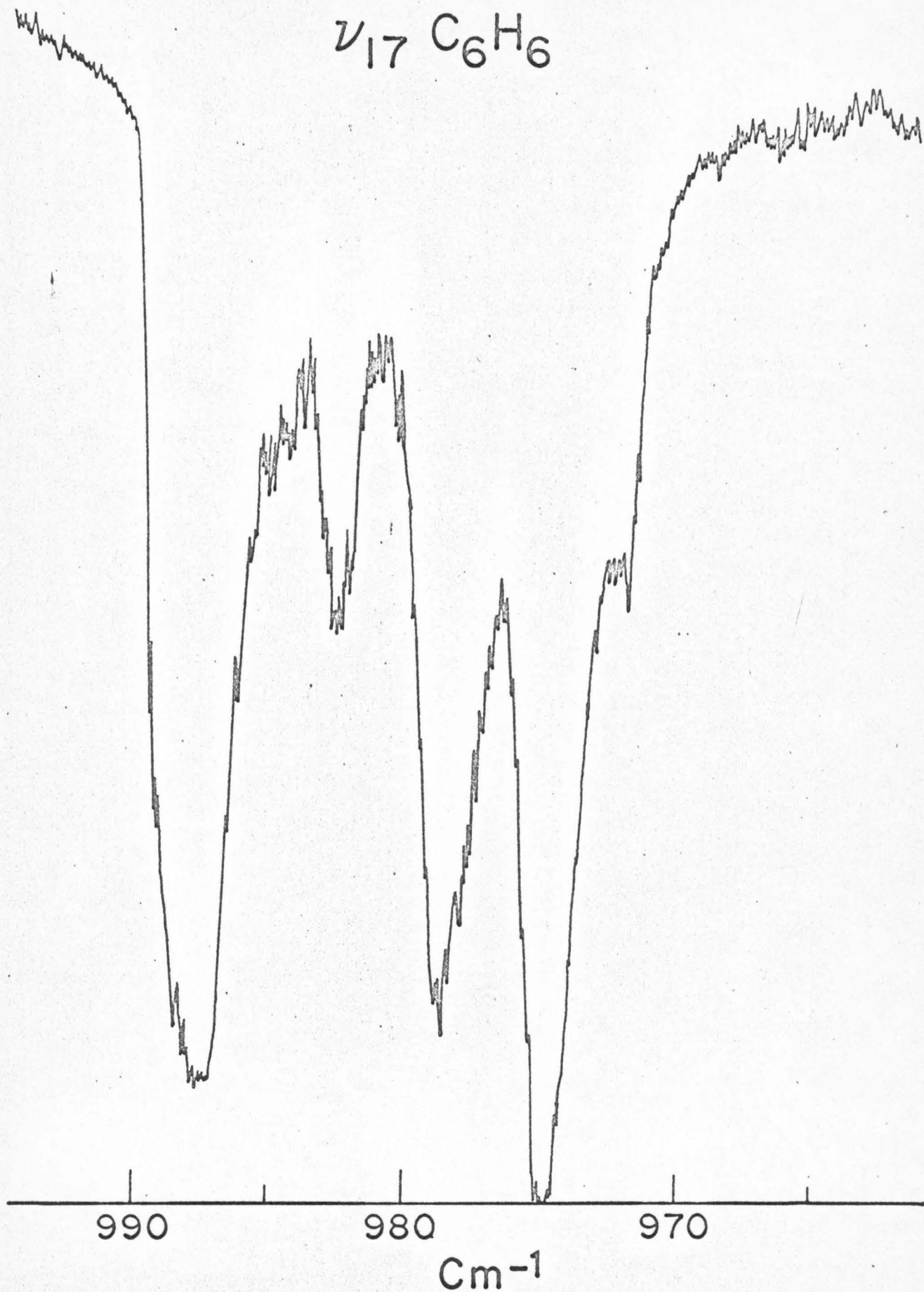
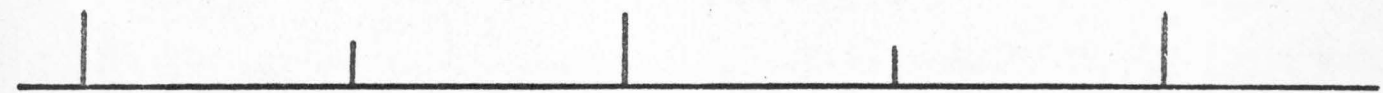
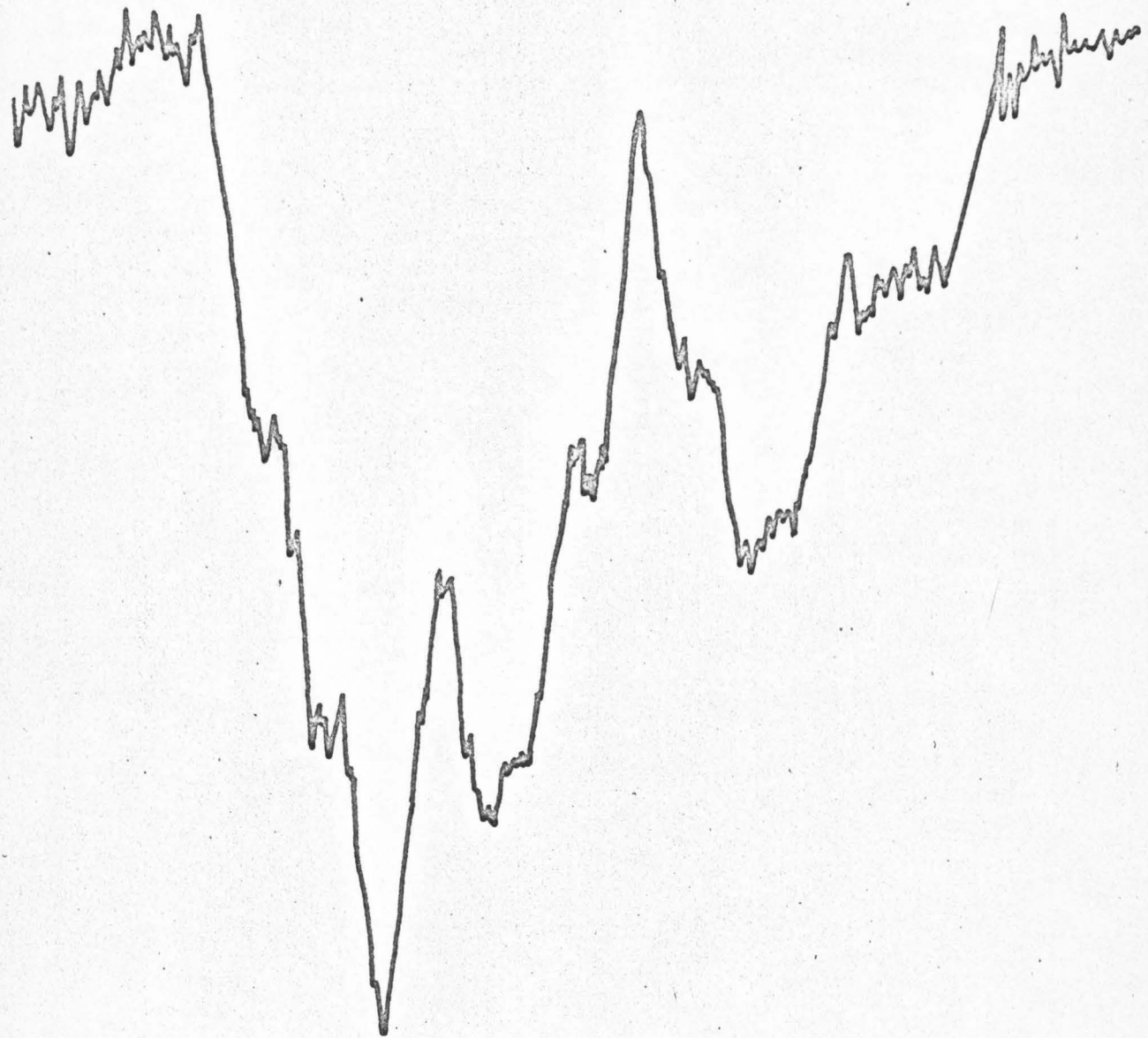


Fig. 5. Neat crystal C_6H_6 ν_{19} (e_{1u}). The feature at c. 1470 cm^{-1} is due to $^{13}CC_5H_6$ and should contain two lines due to the removal of the ν_{19} degeneracy (Ref. 8).

²⁷³
 ν_{19} C₆H₆



1485

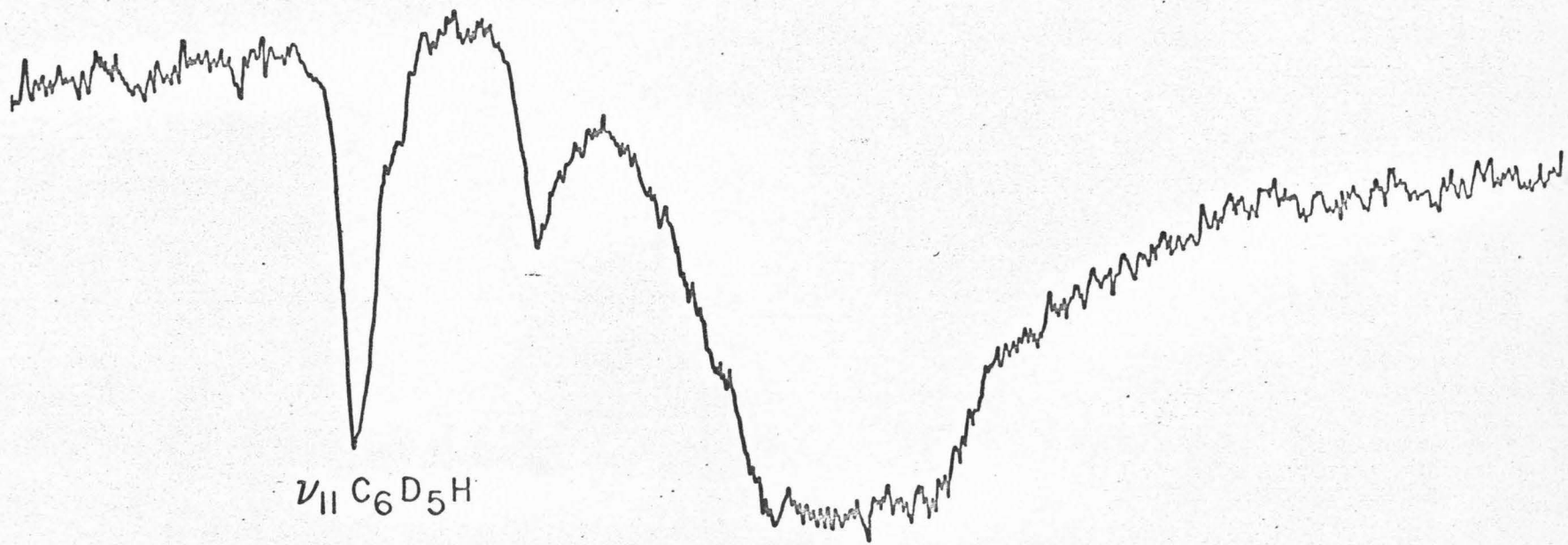
1475

1465

Cm⁻¹

Fig. 6. Neat crystal $C_6D_6 \nu_{11}$ (a_{2u}). The absorption at c. 528 cm^{-1} is due to the ν_{11} of C_6D_5H . The intensity of this peak may be due to intermolecular Fermi resonance with the $C_6D_6 \nu_{11}$. (See Ref. 8.)

Neat Crystal C_6D_6 $\nu_{11}(a_2u)$



$\nu_{11} C_6D_5H$

$\nu_{11} C_6D_6$

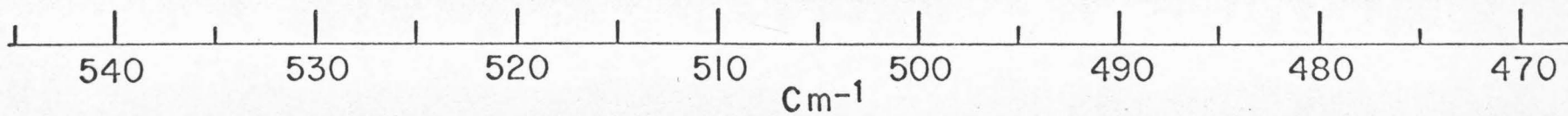


Fig. 7. Neat crystal C_6D_6 ν_{12} (b_{1u}), ν_{14} (b_{2u}) and ν_{19} (e_{1u}) absorption. The feature at c. 528 cm^{-1} is due to $^{13}CC_5D_6$ (Ref. 8). ν_{14} is the weakest observed u vibration in the C_6D_6 spectrum.

Neat Crystal C_6D_6

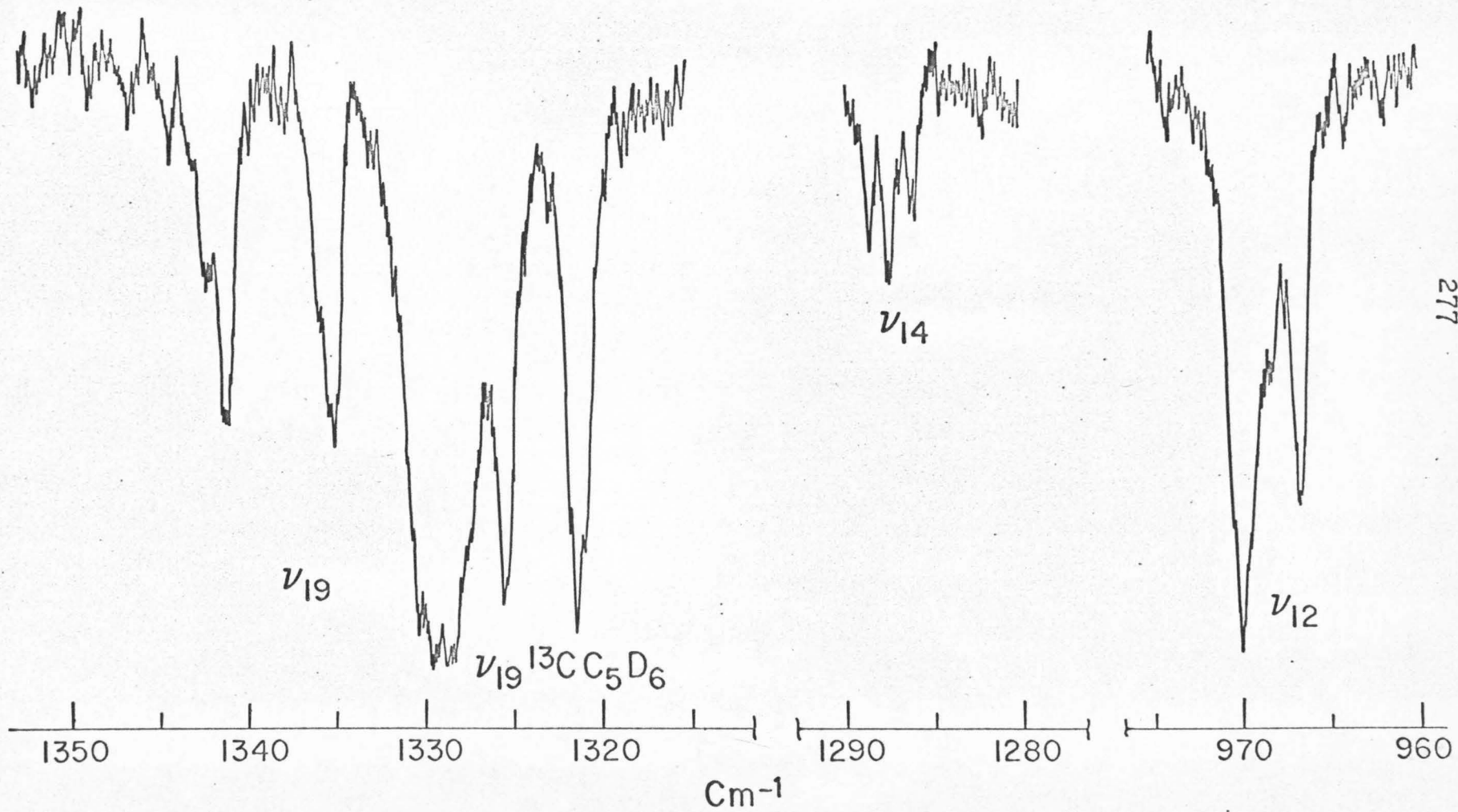
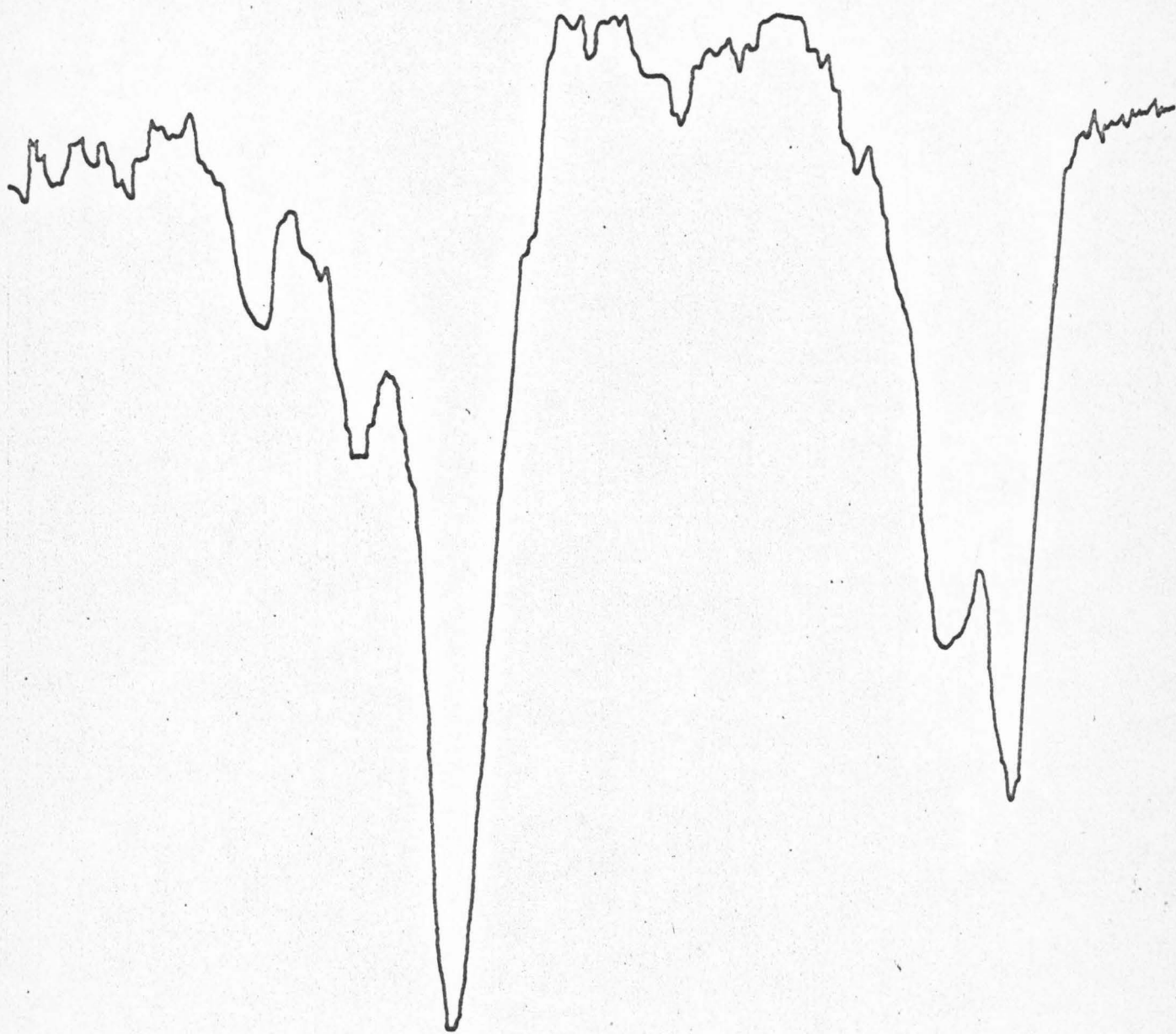


Fig. 8. Neat crystal spectrum of $C_6D_6 \nu_{16} (e_{2u})$.

ν_{16} C_6D_6 

380 370 360 350
 cm^{-1}

Fig. 9. Neat crystal C_6D_6 ν_{17} (e_{2u}), ν_{18} (e_{2u}) and ν_{15} (b_{2u}). There is Fermi resonance between all three of these transitions in the C_i crystal site. The absorption at c. 818 cm^{-1} (to the high energy site of ν_{18}) is due to C_6D_5H .

Neat Crystal C_6D_6

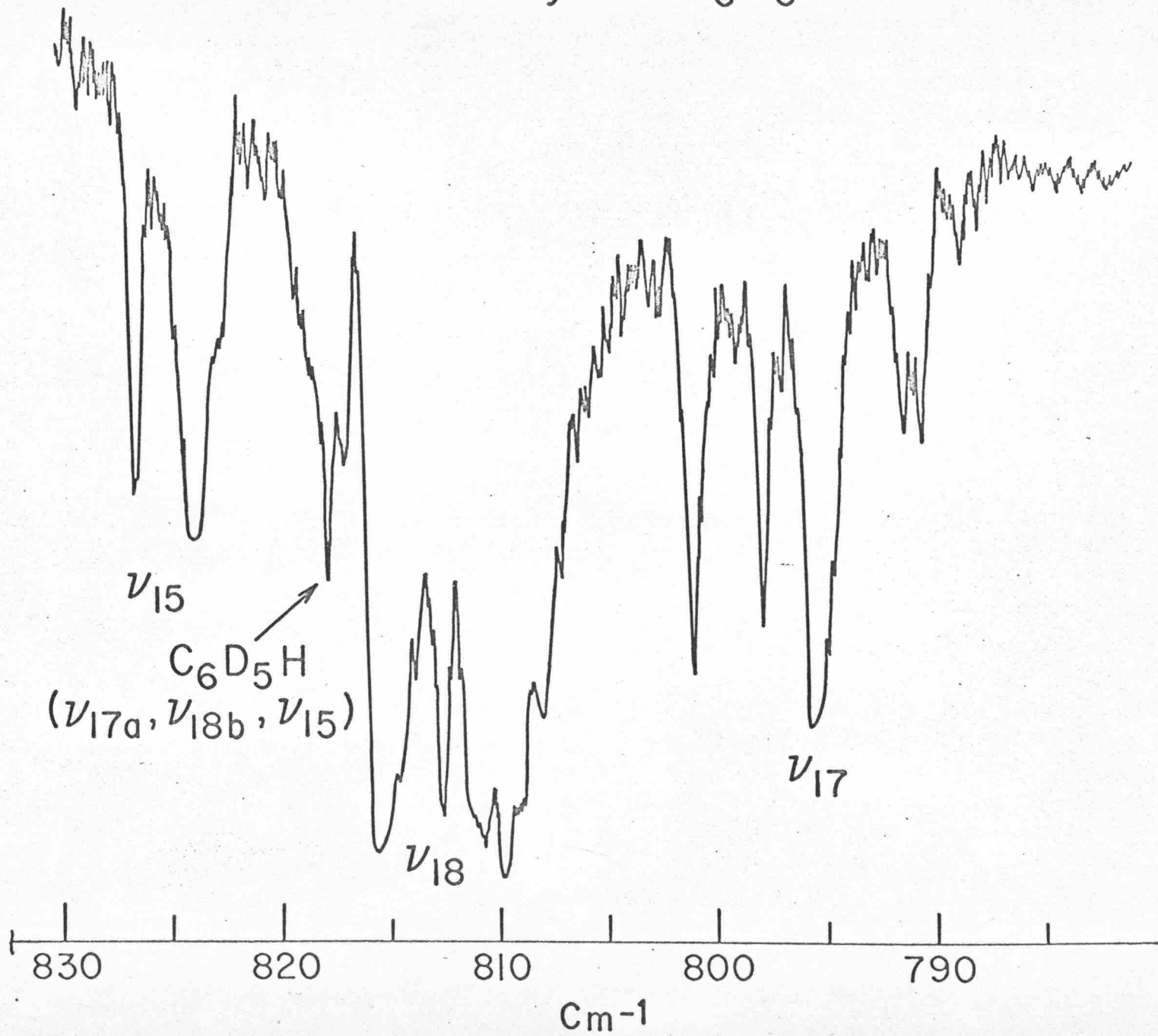


Fig. 10. Neat crystal ν_{11} (a_{2u}) sym- $C_6H_3D_3$. In the region from 570-600 cm^{-1} are the ν_{11} of m- $C_6H_4D_2$ and ν_6 (e_{2g}) of sym- $C_6H_3D_3$.

Neat Crystal sym $C_6H_3D_3$

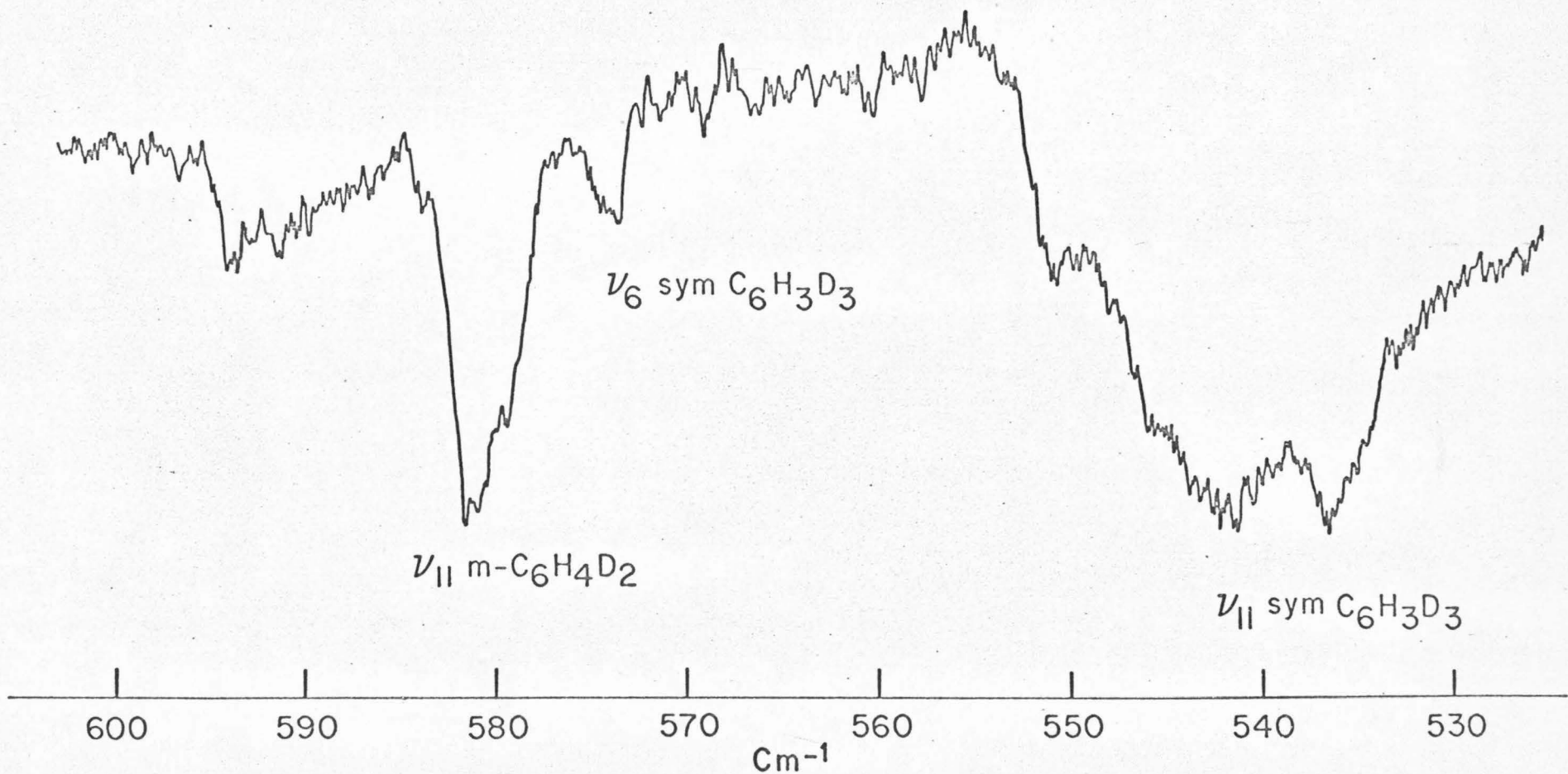


Fig. 11. A tracing of several of the sym- $C_6H_3D_3$ neat crystal bands. ν_{16} is observed to show clear splitting because the various exciton components are well separated and this band is isolated from any others. ν_1 and ν_{12} show no exciton structure but are broadened from the various crystal effects (see text). ν_3 and ν_{14} (which mix strongly in the molecule) are broadened and distorted in the neat crystal (see text). The ν_8 , $(\nu_6 + \nu_1)$ region cannot be uniquely assigned.

Neat Crystal Sym $C_6H_3D_3$

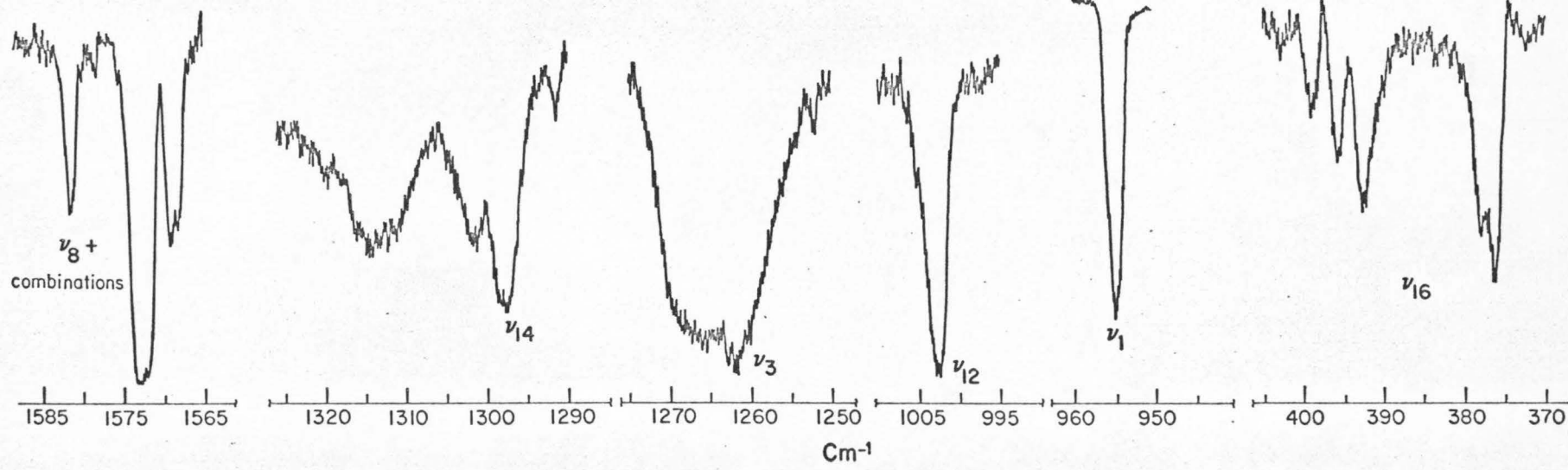


Fig. 12. A trace of the neat crystal spectrum of sym- $C_6H_3D_3$ showing the ν_{18} band and the ν_{12} band. The region from $920-955\text{ cm}^{-1}$ contains ν_5 , ν_{17} , ν_{15} and ν_1 all in resonance in the crystal. The effect of Cs purification on the isotopic composition of a non- C_6H_6 or C_6D_6 sample can be seen from the ν_{18} trace. The lower ν_{18} spectra were taken with a sample that was not Cs purified. ν_{18a} of m- $C_6H_4D_2$ and m- $C_6H_2D_4$ falls at c. 835 cm^{-1} .

Neat Crystal Sym $C_6H_3D_3$

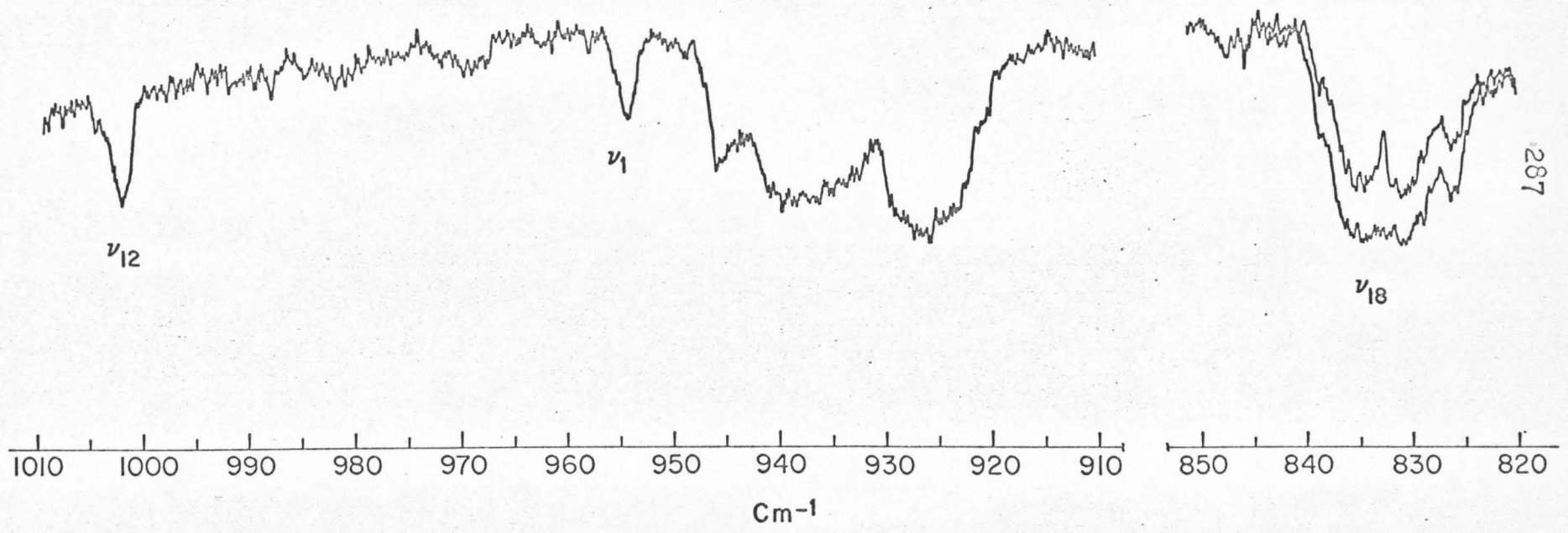


Fig. 13. Neat crystal C_6H_5D tracing showing the effect of resonance between the vibration ($\nu_1, \nu_5, \nu_{12} - 990$ to 1010 cm^{-1}) and the orientational effect (see text and Refs. 8 and 9).

Neat Crystal C_6H_5D

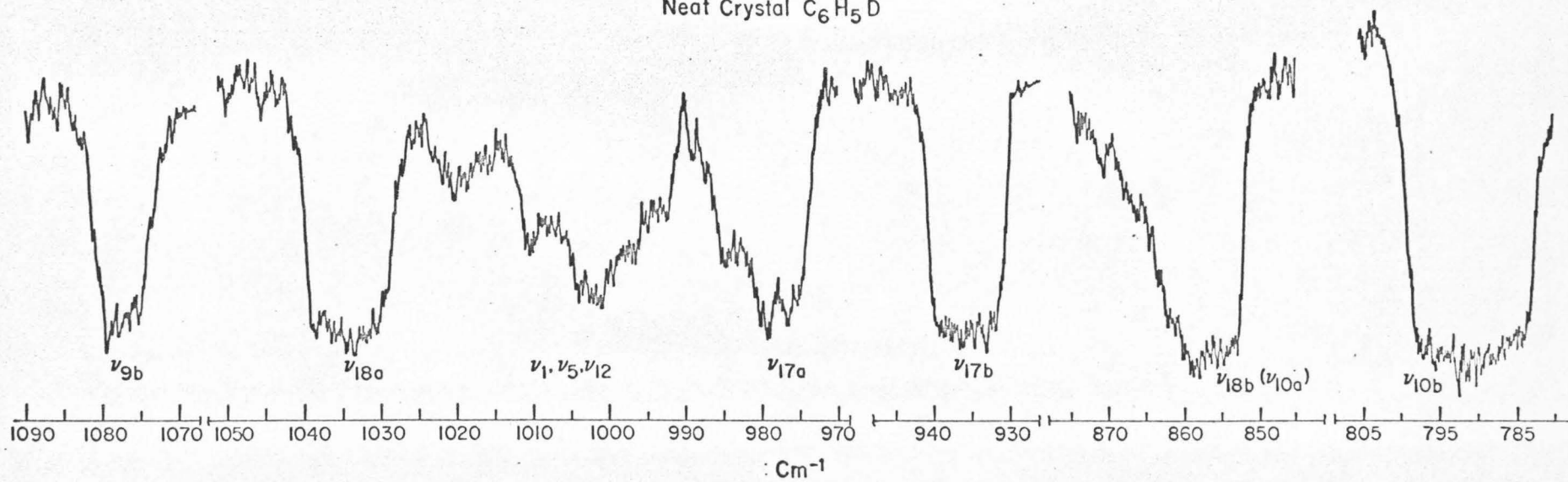
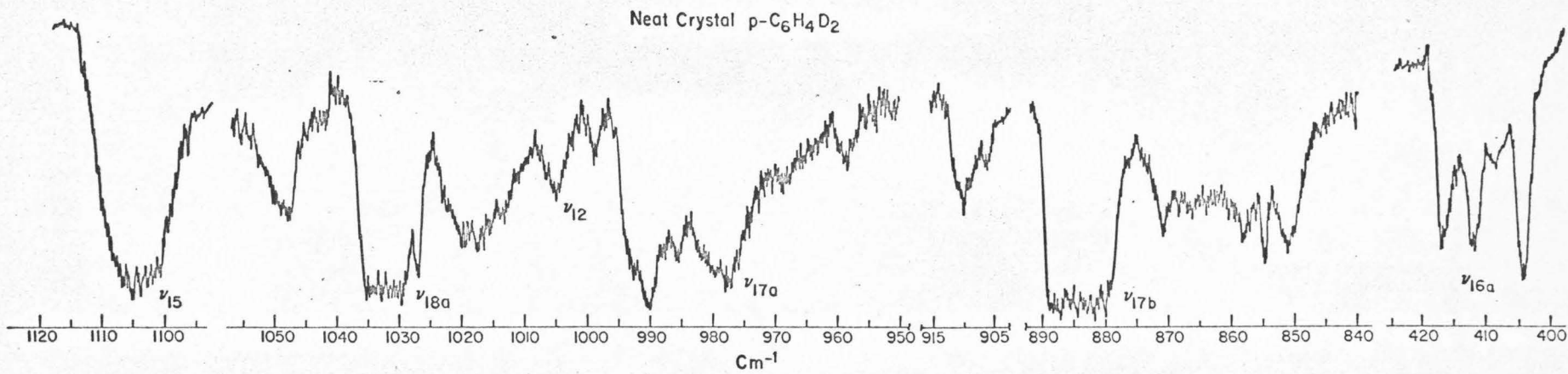


Fig. 14. Neat crystal spectrum of p-C₆H₄D₂. The orientational effect can be seen to obscure most of the exciton structure. ν_{16} (c. 410 cm⁻¹) where the orientational and exciton splittings are both quite large shows resolved structure but the presence of the ν_{16} C₆H₆ complicates this interpretation. Due to the orientational disorder of the p-C₆H₄D₂ molecules the \underline{g} vibrations ν_{10a} (c. 850 cm⁻¹) and ν_{9b} (c. 910 cm⁻¹) have been observed. This is due to the loss of the \underline{C}_i site symmetry in the crystal.



Calculation of Ground State Vibrational Structure and Phonons of
the Isotopic Benzene Crystals*

Elliot R. Bernstein

Gates and Crellin Laboratories of Chemistry, California Institute of
Technology, Pasadena, California 91109

Abstract

Using the "giant molecule" technique and existing potentials derived from thermodynamic and structural aromatic crystal data, the normal modes, exciton structure, site shifts, site splitting, and orientational effect for the isotopic benzene crystals are calculated. The agreement between the calculations and the experimental observations is excellent for an H-H, C-H and C-C potential set recently obtained by Williams. This set was also found to give the best results for the thermodynamic and structural properties of many aromatic crystals. The calculation as presented here serves to unify not only thermodynamic structure and spectral crystal properties in general, but also the various, and apparently diverse, spectral properties themselves. This calculation emphasized that all atom-atom interactions, not just H-H interactions must be considered for good agreement

* Supported in part by the National Science Foundation.

between calculated and observed results; indeed, not including all types of atom-atom interactions can be grossly misleading concerning a physical understanding of the forces and interactions involved in crystals and, in a few instances, has led to the misassignment of data. A detailed discussion of the potentials, their form and their relation to standard exciton theory is presented. It is further indicated that future improvements in such calculations must be directed, not toward more extended parametric data fitting, but toward the model employed (pair-wise, atom-atom, two center interactions of the form $V(\underline{r}) = Be^{-Cr} - A/r^6$).

I. INTRODUCTION

Complete understanding of the binding or cohesive forces in molecular aromatic crystals has been a long sought-after goal for both theoreticians and experimentalists alike. The general problem has typically been approached in the following manner: with the aid of a greatly simplifying model usually atom-atom interactions of which only H-H interactions are considered, one tries to calculate experimentally observable thermodynamic and spectral properties of the crystal. Since even these calculations for all but the simplest of systems are prohibitively difficult, a perturbation method containing many adjustable parameters is often employed. One usually expands integrals in terms of parametrically adjustable potential functions $V(\underline{r})$ varied in a way that invariably justifies the chosen model.^{1,2} Unfortunately, such calculations accurately render only those properties for which they were designed; in many cases it has not even been possible to transfer the potentials from crystal to crystal for the calculation of the identical properties.^{1,3} Parametric potential calculations are significant only if they are able to reproduce data for many crystals and for many crystal properties,^{4,5} or if potentials used to successfully calculate one type of crystal property are transferred to obtain another.⁶ Thus, it would be quite informative to use a single set of potentials in the calculation of crystal spectral data such as phonons, site splittings, orientational effects, or exciton structure, that have been successfully fit to a large number of thermodynamic or structural properties of many different crystals.

Such a procedure would not only be satisfying from the point of view of getting more out of the calculation than was put into it; it would be informative in the sense that it would yield an accurate test of the model and its approximations. Furthermore such a procedure would lead to a better understanding of the relationship between thermodynamic and spectral crystal properties. Thus in terms of a basic physical appreciation of crystal interaction, how they can be approximated and what their essential features are, we find the above variety of data fitting quite unrewarding, as it only re-enforces old prejudices, oversimplifies the physics, and many times leads to incorrect conclusions.

Recent calculations have been completed on the thermodynamic structural properties of many aromatic crystals.^{4, 5} Such a variety of varied data has been successfully fit that it is quite reasonable to assume that the atom-atom potentials employed in these calculations are near optimism. These potentials are tested here on the

spectral crystal properties. The goals of this work, in the light of the foregoing discussion, are then: a) to show that good intermolecular potentials are not only transferable from crystal to crystal but are useful in the calculation and understanding of all crystal properties; b) to determine what parts, repulsion or attraction, of the intermolecular C-C, C-H and H-H atom-atom potentials are important for the spectroscopic data; c) to elucidate what improvements are to be made if the calculations of such properties are to be improved in the future; and d) to relate and unify the various spectroscopically observed phenomena such as isotopic mixed crystal spectra, neat crystal spectra and phonons.

In Section II we shall discuss the theoretical considerations⁸ leading to the calculation of the crystal normal modes and show the relationship between standard exciton theory^{9,10} and the "giant molecule approach"⁸ to such problems. We shall further demonstrate how phonons, exciton structure,^{11,12} ideal mixed crystal energies^{13a,b} site group splittings,^{13a,b} and the orientational effect^{13a,b} are inter-related. Section IIIa will contain a complete description of the intermolecular potentials considered, their approximations and their theoretical basis. This will be followed (Section IIIb) with a short description of crystal geometry including all "nearest neighbor" atom-atom contacts out to 4.0 Å. We shall then compare the calculated results for various potential sets

(H-H; C-H; H-H and C-H; and H-H, C-H, and C-C) and magnitudes of potential parameters (A, B, C) with the available experimental data (Sec. IV).

II. THEORETICAL CONSIDERATIONS

The calculations of the normal modes of the benzene isotopic mixed and neat crystals were made employing the \underline{G} \underline{F} method of Wilson¹⁴ as modified by Shiminouchi.⁸ This is the so-called "giant molecule" technique in that the primitive unit cell of the crystal is treated as one molecule whose motion is then assumed to be in phase with the rest of the crystal. The technique produces then the $\underline{k} = 0$ or "optically active" modes⁸. The essence of these combined notions is as follows: a) Since it is best to determine the force constants in the normal coordinate system, we obtain the molecular (site) force field¹⁵ in molecular symmetry coordinates and the intermolecular force field in the intermolecular symmetry coordinate system. Our force fields, both molecular and intermolecular, are therefore respectively diagonal in these coordinate systems. b) In order to combine or algebraically add these two sets (matrices) of force constants together we must transform them to the same coordinate system in this instance the Cartesian coordinate system of the site. c) When this transformation is applied to the intermolecular force constants they separate into two groups or blocks: one "diagonal block" involving only the coordinates of one site and the other an "off-diagonal block" involving the coordinates of two sites. d) All "one site" force treated together yield the eigenvalues of the ideal mixed crystal¹⁰ while the exciton structure and phonons are obtained by "adding" (in the symmetry of the interchange group¹⁰) the three two-site force constant matrices to all the

diagonal ones; e) These "super matrices", for the ideal mixed crystal and the neat crystal, are then numerically diagonalized and the eigenvalues and eigenvectors found. Since the above scheme has been amply represented in the literature,¹⁸ we shall now proceed to show how it can be related to the general Davydov formalism.^{9,10}

The energy, to first order in crystal site wave functions χ_{nq}^f of the crystal "optically active" transition $f\alpha \leftarrow 0$, where α is an irreducible representation of the interchange group and f represents the f^{th} excited state of the site, is given by

$$\Delta E^{f\alpha}(\underline{k}=0) = \epsilon + D + L^{f\alpha}(\underline{k}=0) \quad (1)$$

where

$$\epsilon = \langle \chi_{nq}^f | H_{nq}^0 | \chi_{nq}^f \rangle - \langle \chi_{nq}^0 | H_{nq}^0 | \chi_{nq}^0 \rangle, \quad (2)$$

$$D = \sum \{ \langle \chi_{nq}^f \chi_{n'q'}^0 | H'_{nq, n'q'} | \chi_{nq}^f \chi_{n'q'}^0 \rangle - \langle \chi_{nq}^0 \chi_{n'q'}^0 | H'_{nq, n'q'} | \chi_{nq}^0 \chi_{n'q'}^0 \rangle \} \quad (3)$$

$$L^{f\alpha} = L^f(\underline{k}=0) + \sum_{q=II}^{IV} a_q^\alpha L_{Iq}^f(\underline{k}=0), \quad (4)$$

$$L_{Iq}^f(\underline{k}=0) = 4M_{Iq}(\underline{k}=0) = 4 \langle \chi_{nI}^f \chi_{n'q'}^0 | H'_{nq, n'q'} | \chi_{nI}^0 \chi_{n'q'}^f \rangle \quad (5)$$

and

$$L^f(0) \propto \langle \chi_{nI}^f \chi_{n'I}^0 \mid H'_{nq n'q} \mid \chi_{nI}^0 \chi_{n'q}^f \rangle . \quad (6)$$

We have assumed only nearest neighbor interactions are possible, that is, $H'_{nq n'q}$ connects only neighboring sites. A more complete discussion of these equations and the notation can be found in Ref. 10. ϵ is clearly an intrasite term while $(D + L^{of})$ is the intersite contribution to the energy; D and ϵ however are the first-order contributions to the ideal mixed crystal energy while the M_{Iq} 's are the only pure crystal splitting terms (vide infra and Ref. 16). Thus, the D and M terms of equation (1) must come from the intermolecular interactions ($H'_{nq n'q}$) while ϵ must be calculated for the sites or molecules separately, where F is the molecular force field, and depends on the form of H_{nq}^0 only. We can calculate ϵ using the $|\underline{G} \underline{F} - \underline{\lambda}| = 0$ technique of Wilson¹⁴ assuming the gas phase energy is the same as the crystal site energy. This is the first approximation we make, and in that the gas-to-crystal shift is not too large ($\lesssim 1\%$ of ΔE^f),¹³ it is probably not a very bad one. On the other hand, contributions to the ideal mixed and neat crystal energy from the intermolecular terms D and L^{of} are obtained by expanding the integral of $H'_{nq n'q}$ over the crystal wave functions¹⁰ $\Psi^{f\alpha}(\underline{k} = 0)$ in terms of a potential function. From this potential function are obtained the force constants that, upon transformation to the Cartesian coordinate system of the sites, render the "diagonal" and "off-diagonal" intermolecular contribution to the crystal energy, ΔE^{of} . All site interactions are given by considering the "diagonal" or one-site contributions from

the intermolecular force constants to the molecular or site force constants. We will thus add (in the proper coordinates system and symmetry--that of the crystal site) to the "site" force constants the "diagonal" (one site) contributions to the energy from the intermolecular force constants in order to obtain the ideal mixed crystal energy ($E_{\text{IMC}} = \epsilon + D$).¹⁰ This force field ($\underline{F} + \underline{F}'$) gives us the site splitting of degenerate molecular states, as the F' contribution has C_i symmetry and the orientational effect, if the ideal mixed crystal force field is rotated with respect to the deuterium substitutions. To the matrix ($F + F'$) will then be "added" (in the interchange group symmetry) the various "off-diagonal" or two site terms ($M_{\text{I II}}, M_{\text{I III}}, M_{\text{I IV}}$ become matrices of force constants $F_{\text{I II}}, F_{\text{I III}}, F_{\text{I IV}}$) and the pure crystal $k = 0$ exciton states and optical phonons are found.

With respect to the Davydov formalism as outlined in ref. 10 we have considered neither the site distortion energy P (the difference between the gas phase and crystal site energy) nor the higher order terms in site wave functions. These approximations are believed to be quite reasonable (vide infra) because we are dealing with the ground state vibrations for which increased crystal site mixing of molecular states and van der Waals contributions to the energy should be generally unimportant. A large site distortion and van der Waals energy would evidence themselves in a distorted molecular geometry in the crystal and such distortions are known to be small (see Sec. IIIb). These assumptions can indeed be checked by the calculation itself as we do

not vary the potentials to obtain final agreement. Any other approximations made in this calculation deal with the potential functions and force constants and will be discussed explicitly in the following section.

III. THE POTENTIALS AND FORCE CONSTANTS

As discussed in the last section, calculation of the ground electronic state vibrational frequencies of the crystal will be accomplished through the use of intra- and inter-site force constants. Assuming the intra-site force constants are the molecular ones, we then proceed with the determination of the inter-site forces and further divide these into "diagonal" (approximating D) and "off diagonal" (approximating $L^{\alpha f}$) contributions to the unit cell vibrational energy. Such intermolecular force constants are found from the intermolecular potential by making the harmonic approximation; that is, by assuming that the force constant is the second derivative of the potential $V(\underline{r})$. We are therefore confronted with the problem of finding a $V(\underline{r})$ that represents quantum mechanical integrals such as $[D + L^{\alpha f}(0)]$ of the form,

$$\{ \langle \chi_{nq}^f \chi_{n'q'}^0 | H'_{nq, n'q'} | \chi_{nq}^f \chi_{n'q'}^0 \rangle + \langle \chi_{nq}^f \chi_{n'q'}^0 | H'_{nq, n'q'} | \chi_{nq}^0 \chi_{n'q'}^f \rangle \} \quad (6)$$

where $H'_{nq, n'q'}$ is the nearest neighbor, site pairwise, intersite interaction term in the crystal Hamiltonian. de Boer⁷ has shown that nonspherical repulsion terms can be best represented in the form of a potential which decreases exponentially with distance; the wave functions are themselves sums and products of exponentials and this form is retained through the integration. The attractive part of the interaction on the other hand can be shown to arise from the dipolar terms in second order and thus a spherical form of A/r^6 can be quite accurately used.^{7, 17} The entire intermolecular potential is represented then as

$$V(\underline{r}) = B e^{-Cr} - A/r^6 \quad (7)$$

Since we have three constants in the potential it is actually possible to represent more than dipolar attraction in second order and single exponential dependence of the repulsive interaction by experimentally fitting these parameters instead of calculating them.

We next assume that these molecular pairwise site interaction potentials be broken down into sums of pairwise atom-atom interactions (H-H, C-H, C-C) as follows

$$\begin{aligned} V(I, II) = \sum_{i,j} \{ & (B_{HH} e^{-C_{HH} r_{ij}} - A_{HH} r_{ij}^{-6}) \\ & + (B_{CH} e^{-C_{CH} r_{ij}} - A_{CH} r_{ij}^{-6}) \\ & + (B_{CC} e^{-C_{CC} r_{ij}} - A_{CC} r_{ij}^{-6}) \} \end{aligned} \quad (8)$$

The sum in equation (8) goes over all atoms of each molecule ($12 \times 12 = 144$ terms for two benzene molecules). The other site pairwise potentials $V(I, III)$ and $V(I, IV)$ can be obtained in the same fashion. The r_{ij} are the atom-atom intersite distances and are thus the symmetry coordinates in which the pairwise intermolecular force constant matrices are diagonal. The second derivative of this potential function with respect to these distances gives the force constant for that atom-atom interaction such that

$$\begin{aligned}
 F_{ij} = \sum_{ij} \{ & (B_{HH} C_{HH}^2 e^{-C_{HH} r_{ij}} - 42 A_{HH}^2 / r_{ij}^8) \\
 + & (B_{CH} C_{CH}^2 e^{-C_{CH} r_{ij}} - 42 A_{CH}^2 / r_{ij}^8) \\
 + & (B_{CC} C_{CC}^2 e^{-C_{CC} r_{ij}} - 42 A_{CC}^2 / r_{ij}^8) \} \quad (9)
 \end{aligned}$$

Eq. (9) gives only the harmonic contribution to the interactions. F_{ij} is the diagonal of a (144×144) matrix for two benzene molecules.

Before specifically discussing how the various A , B , and C parameters can be obtained, let us review the approximations, both explicit and implicit, we have thus far made. To begin with, the P term and any higher order contributions were omitted from the Davydov crystal energy equation [eq. (1)ff and Ref. 10]. Assuming $H'_{nq, n'q'}$, the pairwise intersite (intermolecular) interaction term in the crystal Hamiltonian only connects neighboring sites, we expand those integrals [D and $L^{\alpha f}(0)$] containing $H'_{nq, n'q'}$ as a pairwise sum of two center atom-atom potentials. From these terms we extract only the harmonic contributions to the force constants and thus the crystal energy. The neglect of three and four center terms in the repulsion energy is probably the most serious of these assumptions as such terms usually account for about 5% of the lattice energy.¹⁸ Their absence from our potential could cause the calculation of the spectroscopic splitting and shifts to be far worse, however. We further assume the attractive terms in the interaction, those that hold the crystal together, are simply given by the second order dipole-

dipole interactions or van der Waals forces. Lastly we completely ignore π -electron effects, static dipole and quadrupole effects and any bond-centered interaction. Of course, underlying all these approximations is the ubiquitous Born-Oppenheimer separation.

In the light of the just enumerated approximations necessary to obtain a viable form for the crystal energy in terms of the Davydov equation [eq. (1)], one can justifiably wonder if any crystal spectroscopic data can be calculated if the specific data are not carefully "fit", as much of the specific detail of the interaction has been lost through the introduction of these approximations. On the other hand, however, it is strongly felt that such a "fitting" procedure would indeed render the calculation useless and void of physical meaning. We can test the above approximations by using the well-known thermodynamic and structural crystal data to calibrate the potentials, that is, to determine values of A, B, and C, and then employing these potentials the calculation of the observed spectroscopic data. These latter, due to their strong short range order dependence, should be much more sensitive to the three and four center terms, the neglected anharmonic effects and any non-pairwise additivity of the various components. One would hope however that the general form of the experimental data could be obtained through the use of such potential functions. Any improved calculation must address itself directly to the approximations and not try to fit the data; certainly a next step would be to include three and four center terms. We thus resort to the bulk crystal properties to find a good form for these potentials and the best parameters to use.

Our best information concerning the potentials, their form and the parameter associated with them, is thermodynamic; such considerations have been extensively discussed by Kitaigorodskii⁴ and Williams⁵. One can characterize the equilibrium structure of a molecular crystal for all intra- and inter-molecular geometries by a minimum in the free energy. However, at constant entropy and volume, the minimum in the potential energy can also characterize the equilibrium geometry. The lattice energy is equated to the observed enthalpy of sublimation with the neglect of zero point contributions. The stress and strain tensors and the elastic constants can be respectively represented as derivatives of the entropy and free energy of the crystal.¹⁹ Knowing these quantities experimentally, it is possible to obtain the potentials and such calculations have recently been made available.⁵ There are some general conclusions which can be extracted from these calculations and are of interest to us here:

a) Within a factor of two σ - σ , π - π , σ - π interactions contribute equally to the lattice energy.²⁰

b) The relative molecular orientation in these crystals is probably dominated by the pairwise atom-atom repulsions of which H-H interactions have been assumed the most important.^{1,2} on the other hand, C-H and C-C interactions are the largest overall contributors to the total energy.⁵ C-H and C-C interactions however have been found to contribute substantially to the relative molecular orientations in the crystal.⁵

c) Geometrical combining laws, especially for the repulsions,

parameters B and C, are only good to about 2-4% of the total energy of even simple systems: they should be worse for the geometrically complex atom-atom arrangement of aromatic molecular crystals, as they tend to further gloss over the specifics of the interactions.

d) If the individual electron and excitation exchange integrals are not highly orientation and shape dependent, we can expect the additive pairwise atom-atom potentials to give reasonable results for the spectroscopic crystal properties.

In Table I are found the A_{HH} , B_{HH} , and C_{HH} parameters for a number of well-regarded potentials available in the literature, and the force constants derived from some of the more promising ones are plotted in Figs. 1-5. In this table are the H-H and C-H potentials obtained simultaneously and the potential parameter for four sets of H-H, C-H, and C-C potentials obtained by Williams.⁵ These latter are clearly the best due to the extent of data they fit, and are the ones used in the calculation. They were obtained by simultaneously fitting the heat of sublimation, molecular rotations and translations, lattice constants and elastic moduli of benzene, naphthalene, anthracene, phenanthrene, pyrene, chrysene, terphenylene, pyrylene and ovalene. For a comparison, other potentials are used in the calculation but not only are the calculated spectroscopic quantities in much poorer agreement with the observed values, the thermodynamic and structural data obtained from these potentials are also poor. It is very satisfying indeed to find that the potentials obtained by Williams (Table I) are general for both the thermodynamic crystal properties (transferable from crystal to crystal) as well as the spectral crystal properties.

IV. THE CRYSTAL STRUCTURE, ATOM-ATOM DISTANCES AND THE MOLECULAR GEOMETRY

The crystal structure of benzene has been determined to be $D_{2h}^{15}(P_{bca})$ with four molecules per primitive unit cell all occupying equivalent sites of inversion symmetry.²¹ The molecules are labeled I, II, III, and IV in accordance with the notation of Cox et al.²¹ For the benzene molecule I, the carbon atoms are labeled counter clockwise, 11, 12, 13, 21, 22, 23, and the hydrogen atoms are labeled (in like fashion), 31, 32, 33, 41, 42, 43, as given in Figure 6. The site or molecular axis system is the right-handed system with the axis, y, through C_{11} and H_{31} , the x axis lies between C_{22} , H_{42} , and C_{23} , H_{43} , and the z axis perpendicular to the x and y. All the other molecules (sites) are generated from I using the operations of the D_2 interchange group.¹⁰ This technique uniquely creates molecules (sites) II, III, IV, in such a fashion as to preserve the atomic numbering system, the right-handed coordinate system, and define the phasing of the crystal site states. Explicitly, $C_2^a I = II$, $C_2^b I = III$, and $C_2^c I = IV$, where $C_2^{a,b,c}$ represents the twofold rotation operations about the a, b, or c crystal axes, respectively (in the space group these are actually screw-rotation operations; C_2 point operations, and a translation).

Bacon et al.²² give the neutron diffraction data at 138°K which can be extrapolated to 77°K. The relation between the crystal a, b, c axes and the site z, y, z axes, the direction cosines of (a, b, c) and (x, y, z) are given in Table II. The bond lengths, extrapolated to 77°K,

are given in Fig.6. With these data it is possible to calculate all atom-atom contacts in the crystal which are given in Table III for I-II contacts, Table IV for I-III contacts and Table V for I-IV contacts to 4.0 Å. The closest translationally equivalent atom-atom contacts are greater than 5.0 Å. The above bond lengths, and atom-atom contacts, were computed from the reduced atomic positions and cell parameters of Bacon *et al.*²² extrapolated to 77°K, using the Cryrm crystallographic program.²³ These represent all the unique contact distances in the crystal to 4.0 Å. The direction cosines of these vectors in the a, b, c axes system can be obtained from the positions of the atoms involved in the contact. Since each molecule has 12 nearest neighbors (four of each of the other three translationally inequivalent molecules), the related direction cosines, and thus the contact vectors, can be obtained straightforwardly from the crystal geometry and the known contact. Therefore, each unique contact generates three others, related to it by the crystal symmetry.

From an examination of the potentials and the force constants as a function of distance (Section III and tables and figures), we cut off the contacts for C-H and H-H interaction at 3.4 Å and for C-C interaction at 4.0 Å, as at these distances the intermolecular atom-atom force constants are less than 10^{-3} m dynes/Å and will no longer significantly contribute to the frequency. It should be noted that this eliminates any translationally equivalent interaction ($I-I'_{a,b,c}$) which means $L^f(0) = 0$ and the ideal mixed crystal frequency is the center of the neat crystal exciton band for nondegenerate states. It can be seen from the tables of atom-atom contacts, that seriously mis-

leading conclusions could be reached concerning, for example, which molecules interacted most strongly if just one type of contact was employed in the calculation.

V. RESULTS OF THE CALCULATION AND DISCUSSION

The force constant matrix for the neat crystal can be written as

$$F_{\text{cryst}}^{\alpha} = F_{\text{mol}} + F' + \sum_{q=II}^{IV} a_q^{\alpha} F' (I, q) \quad (10)$$

where α is one of the representations of the D_2 interchange group.¹⁰

The ideal mixed crystal force constants are then

$$F_{\text{IMC}} = F_{\text{mol}} + F' \quad (11)$$

Equation (11) is simply the "diagonal" or one-site component of the crystal force constant matrix for a unit cell.

Tables VI-XI contain the calculated frequencies for the ideal mixed crystal(s) and exciton structure of some isotopic benzenes of some representative potentials using eqns. (10) and (11). In Tables XII-XV are the calculation site (gas-to-crystal) shifts Δ , the site splittings δ_{SS} , the orientational effects δ_{OE} , exciton structure and phonons for the isotopes. The experimental data,^{11, 12, 13, 24} where available, are also given in these tables for the site effects while the exciton structures and phonons of C_6H_6 and C_6D_6 are presented in Tables XVI and XVII. New high resolution Raman phonon data,²⁵ obtained at 77°K, are also presented (Table XVIII).

From the tables of C_6H_6 data, calculated with the various potentials, it is clear that all the experimental spectroscopic data are best reproduced using the H-H, C-H and C-C potential set of Williams.⁵

This result is quite satisfying, as set I is also the one that best fits the thermodynamic and structural data for many aromatic crystals. Thus good potentials not only are transferable from crystal to crystal for the thermodynamic and structural properties, but also from these to the spectroscopic crystal properties as well; the same potential set being best for all the spectroscopic data. Thus it is firmly believed that potential calculations of the intermolecular forces in other aromatic crystals should also use this same set determined by Williams. If such future calculations were to disagree with experimental results, one would know that interactions other than two center pairwise atom-atom terms made significant contributions to the binding forces between the molecules or that the form $(V = B e^{-Cr} - A/r^6)$ is not proper. The latter alternative is of course not anticipated.⁷

Although employing the set I of Williams we find the best agreement with all the combined data, some calculated properties for certain of the vibration simply do not at all agree with measured values. In such cases we believe that "higher order" interactions become important (three and four body or anharmonic terms, for example), and that the terms we consider, by some coincidence cancel. It is not, of course,

possible to uniquely eliminate other contributions to the disagreement such as the site distortion energy P.

a) Phonons:

Phonons, as purely intermolecular phenomena, represent the most lucid test of the pairwise atom-atom interactions as a model for the intermolecular potential of crystals.

It can be seen from the calculated C_6H_6 and C_6D_6 data for the various potentials (Tables VI-XI) that the phonons are most sensitive to the form and size of the intermolecular force constants. Although all the calculated data, not just the phonons, show the same trend, that of set I being the best potential, the changes in the phonon frequencies with different potentials are the most dramatic. The calculations for both C_6H_6 and C_6D_6 lattice modes are excellent; the only significant differences between observed and calculated frequencies are B_{2g} and B_{3g} phonons for both C_6H_6 and C_6D_6 , neither of which have been observed in the Raman.^{24, 25} They are predicted to be inactive²⁶ and qualitative arguments place them degenerate with observed ones.²⁶ Since the other phonons are so well calculated we must reject these arguments and place the unobserved B_{2g} phonons at $\sim 110 \text{ cm}^{-1}$ (C_6H_6) and 105 cm^{-1} (C_6D_6) and the unobserved B_{3g} phonons at 125 cm^{-1} (C_6H_6) and 115 cm^{-1} (C_6D_6). Recently C_6H_6 u lattice modes have been observed²⁷ and again rough estimates have been used to assign their polarization properties. Our calculations however require that the phonons be reassigned as given in Table XVI. Such misassignments indicate the necessity of using good potentials and of considering all the atom-atom interactions in crystal calculations.

We find the grouping of the unassigned B_{2u} and B_{3u} phonons at

65 cm^{-1} , corresponding to the broad feature at 74 cm^{-1} in the far infrared spectrum,²⁷ the worst calculated of all the phonons. These modes may be sensitive to intermolecular anharmonicities or many center interactions. The generally excellent agreement between the experiments and calculations is a rewarding confirmation of both the potential model and the parameters.

b) Exciton Structure (C_6H_6 and C_6D_6):

While the same potential set which gave the best agreement between the calculated and experimental results for the phonons is also the best potential here, the exciton structure of C_6H_6 and C_6D_6 seems less accurately described by our model. With few exceptions, however, the general trends are reproduced. It is clear that the experimental data is far from complete as not all components of the bands are observed, polarization data²⁸ is scanty and taken at low resolution and especially for C_6D_6 ν_{17} , ν_{18} , and ν_{15} and ν_5 and ν_9 , there is strong interaction between the vibrational modes. However, there are cases of real disagreement (ν_{15} and ν_{12} in particular). All that can really be said here is that although the potential model does with few exceptions predict the overall size and nature of the exciton splitting, the detailed structure of the bands is not always obtained. Again this indicates that anharmonic or three and four body terms must be important (especially when the other terms are small or cancel); our calculation thoroughly explores the harmonic two center contributions of the form $V(\underline{r})$ (eq. 7) to the exciton splitting. The possible contribution of the site distortion energy and higher order two center terms can be eliminated from the calculation of site shifts, site

splittings, and orientational effects (vide infra). Many bands, notably ν_1 , ν_6 , ν_9 , ν_{10} , ν_{11} , ν_{14} , ν_{16} , ν_{17} , and ν_{18} are however, quite well characterized by our model. The above indicated Fermi resonance complicates the comparison of experiments and calculation in some cases since the separation of calculated vibrations (even in the free molecule) is sometimes different than actually observed.

c) Site (gas-to-crystal) shift:

Site shifts have been calculated for all the isotopes and are tabulated here for C_6H_6 , C_6D_6 and sym- $C_6H_3D_3$ (Tables XII and XIII). The agreement between theory and experiment is a direct check on the approximation in which the site distortion energy was assumed to be small ($P \equiv 0$ in this calculation); the entire shift is then due to the approximated D term or the "diagonal" contribution of the intermolecular force field to the molecular (site) one. We present data on these isotopes alone as the experimental data are most reliable for them. Site shifts have been discussed extensively recently¹³ and the problems involved with them have been enumerated (increased Fermi resonance in the condensed phase, gas-phase experimental error for unresolved bands, to mention just a few). From the data presented in Tables XII and XIII, it is obvious that the agreement between the theoretical model and the observed values is excellent. Three bands are however at complete variance with the experimental findings in all the isotopes; ν_9 , ν_{15} , and ν_{18} . For ν_{15} the calculated exciton structure seems also to be incorrect but ν_{18} .

and ν_9 appear to be otherwise in agreement. While this seems to imply that $P \neq 0$ for ν_9 and ν_{18} the case is not completely straightforward and it is difficult to uniquely explain the breakdown of the model in terms of the approximations made. It is interesting to note that these three modes are $H^{||}$ in which both the carbon and the hydrogen atoms move parallel to one another in the molecular plane but in opposite directions. The calculated shifts are all much too large for these vibrations while the set I H-H potential employed in the presented calculated data is relatively a weak one.

d) Site (group) splitting:

The splitting of a degenerate vibration into two or more crystal site states has been demonstrated experimentally and theoretically discussed for benzene.^{10, 13} Only C_6H_6 , C_6D_6 and sym- $C_6H_3D_3$ have degenerate molecular fundamentals and thus show the effect. In our model it is the force constants of the ideal mixed crystal ($F'_{mole} + F' = F'_{IMC}$) that give the site splitting. Tables XII and XIII contain both the calculated and observed values for these isotopes. Agreement is again very good (it should be remembered that in C_6D_6 ν_{18} and ν_{17} are in Fermi resonance and that the experimental splittings of ν_7 and ν_{20} are also perturbed by Fermi resonance in all the isotopes). It is necessary to comment on ν_6 , ν_8 and ν_9 of C_6H_6 and sym- $C_6H_3D_3$. The experimental observations have already been noted to be somewhat peculiar^{13b} and this apparent discrepancy seems also to apply to the calculations. From the calculated data there appear to be large isotopic effects on these vibrations. For example, the calcula-

tions show that for ν_6 $\delta_{SS}(\text{C}_6\text{H}_6) = 0.7$, $\delta_{SS}(\text{C}_6\text{H}_3\text{D}_3) = 2.0$ and $\delta_{SS}(\text{C}_6\text{D}_6) = 1.1 \text{ cm}^{-1}$ while the observed values are 3.1, 1.7, and 1.2 cm^{-1} , respectively: the experimental value for C_6H_6 appears to be out of line with both the calculated and the observed δ_{SS} for the other isotopes. For the C_6H_6 band ($\nu_6 + \nu_1$), in Fermi resonance with ν_8 , the $\delta_{SS} = 1.2 \text{ cm}^{-1}$. It is difficult to understand why for a given vibration of one isotope the atom-atom potential would appear to work while it does not for another isotope. Likewise the ν_8 band of C_6H_6 and sym- $\text{C}_6\text{H}_3\text{D}_3$ [also in Fermi resonance with ($\nu_6 + \nu_1$)] is difficult to understand. It is of course conceivable that a host state can perturb the mixed crystal levels to some extent but this could not be the case for ν_6 of C_6H_6 . The same problem arises in ν_9 where the calculated and experimental values agree for sym- $\text{C}_6\text{H}_3\text{D}_3$ but not at all for C_6H_6 . Again it is not clear at all why this happens; it apparently is noteworthy in both the calculations and the experiments. ^{13b}

e) Orientalional effect:

The orientational effect, calculated by changing the relative numbering of the mass matrix with respect to the site force constant matrix, has been obtained for all isotopes of lower than \underline{D}_{3h} symmetry. It has been verified by direct calculation that sym- $\text{C}_6\text{H}_3\text{D}_3$ does not show an orientational effect in the \underline{C}_1 crystal site. The experimental data and calculated results for $\text{C}_6\text{H}_5\text{D}$ and p- $\text{C}_6\text{H}_4\text{D}_2$ using potential set I are given in Tables XIV and XV. The agreement in most cases is remarkably good. It should be pointed out that while the calculated splittings are always known in an absolute sense ("sites" 1, 2, 3 referring to a deuterium substitution position), the experimental ones

are arbitrarily determined (i. e. , the specific orientation of the molecule in the site is unknown). Thus the calculated sign of the orientational effect is of little significance when we compare these numbers with the experimental results; the quantity that is of concern is the "splitting" pattern or the relative positions of the lines with respect to one of them. For C_6H_5D only ν_{9b} seems to be not in agreement with the experimental results, at least qualitatively, while for $p-C_6H_4D_2$, only ν_{12} appears grossly incorrect.

V. CONCLUSIONS

The most important conclusions which this calculation indicates are: the model of pairwise, atom-atom, interaction potentials is a quantitatively reasonable one for the calculation of intermolecular interactions (exciton structure, phonons, site shifts and splittings, and the orientational effect) and such potentials are not only transferable from crystal to crystal for the thermodynamic and structure data but to spectroscopic properties as well. To improve on this model or to better the calculation of such crystal properties and site effects, attention must be directed to the approximations upon which this model is founded. Therefore, general potentials which take into account three and four center interactions and force constants including anharmonic contributions in the calculations of both types of observables should be considered in order to better fit the experimental results. Further, this calculation graphically demonstrates the need to consider all atom-atom interactions and not just H-H terms. Indeed, grossly misleading results and conclusions can be obtained by assuming only one set of interactions is important and then fitting the potential for this interaction to the experimental data used to prove the assumption.

In conclusion we remark that no isotopic effects are obvious in the calculations, that is, the same potentials in general work equally well for H-H, H-D, D-D, C-H, and C-D interactions, and it does not appear to be necessary to resort to higher order contributions¹⁰ (in terms of pairwise exciton theory) to account for the interactions as exemplified in the isotopic mixed and neat crystal spectra of benzene.

ACKNOWLEDGMENTS

The author wishes to express his gratitude to Professor G. W. Robinson for discussions and suggestions concerning this work. Many fruitful hours were also spent with Dr. C. -H. Ting and Mr. D. M. Burland in discussing the programs needed for these calculations.

REFERENCES AND FOOTNOTES

- ¹ See for example I. Harada and T. Shiminouchi, *J. Chem. Phys.*, 44, 2016 (1966), *J. Chem. Phys.* 46, 2708 (1967).
- ² D. P. Craig, R. Mason, P. Pauling and D. P. Santry, *Proc. Roy. Soc. (London)* A286, 98 (1965).
- ³ D. A. Dows, *J. Chem. Phys.* 32, 1342 (1960); *J. Chem. Phys.* 36, 2836 (1962).
- ⁴ A. I. Kitaigorodskii, *Acta Cryst.* 18, 585 (1965) and A. I. Kitaigorodskii and K. V. Mirskaya, *Kristallografiya* 9, 174 (1964). [English translation: *Soviet Physics-Cryst.* 9, 137 (1964)].
- ⁵ D. E. Williams, *Science* 147, 605 (1965) and *J. Chem. Phys.* 45, 3770 (1966).
- ⁶ S. Kimel, A. Ron, and D. F. Hornig, *J. Chem. Phys.* 40, 3351 (1964).
- ⁷ J. de Boer, *Physica* 9, 363 (1942).
- ⁸ T. Shiminouchi, M. Tsoboi, and T. Miyazawa, *J. Chem. Phys.* 35, 1897 (1961).
- ⁹ A. S. Davydov, *Usp. Fiz. Nauk* 82, 393 (1964). [English Translation: *Soviet Physics - Uspekhi* 7, 145 (1964)].
- ¹⁰ E. R. Bernstein, S. D. Colson, R. Kopelman and G. W. Robinson, "Electronic and Vibrational Exciton Structure of Crystalline Benzene", *J. Chem. Phys.* (to be published).

¹¹ E. R. Bernstein and G. W. Robinson, "Vibrational Exciton Structure in Crystals of Isotopic Benzenes", J. Chem. Phys. (to be published).

¹² A. R. Gee and G. W. Robinson, J. Chem. Phys. 00, 0000 (1967).

¹³_a) E. R. Bernstein, "Site Effects in Molecular Crystals--Site Shifts, Site Splitting, Orientational Effect and Intermolecular Fermi Resonance", J. Chem. Phys. (to be published);

b) E. R. Bernstein, S. D. Colson, D. S. Tinti and G. W. Robinson, "Static Crystal Effects on the Vibronic Structure of the Phosphorescence, Fluorescence and Absorption Spectra of Benzene Isotopic Mixed Crystals", J. Chem. Phys. (to be published).

¹⁴ E. B. Wilson Jr., J. C. Decius, and P. C. Cross, Molecular Vibrations, McGraw Hill, N. Y., N. Y. (1955).

¹⁵ D. H. Whiffen, Phil. Trans. Roy. Soc. (London) A248, 131 (1955) and A. C. Albrecht, J. Mole. Spec. 5, 236 (1960).

¹⁶ In Ref. 11 and 13 it has been shown that experimentally for the ground state vibrations of benzene $L^f(0) = 0$.

¹⁷ H. Margenau, Rev. Mod. Phys. 11, 1 (1939).

¹⁸ H. Margenau and J. Stamper, Adv. In Quantum Chem. 3, 129 (1967) and S. Doniach, Phil. Mag. 8, 129 (1963).

¹⁹ A. I. Kitaigorodskii, Kristallografiya 9, 171 (1964) [English Translation: Soviet Physics - Cryst. 9, 135 (1964)] and Ref. 4.

²⁰ K. Banerjee and L. Salem, *Mole. Phys.* 11, 405 (1966)
and K. Banerjee, *Mole. Phys.* 12, (1967).

²¹ E. G. Cox, *Rev. Mod. Phys.* 30, 159 (1958); E. G. Cox,
D. W. J. Cruickshank and J. A. S. Smith, *Proc. Roy. Soc. (London)*
A247, 1 (1958).

²² G. E. Bacon, N. A. Curry and S. A. Wilson, *Proc. Roy.*
Soc. (London) A289, 98 (1964).

²³ Cryrm Crystallographic Computing System, D. Duchamp
California Institute of Technology, 1964.

²⁴ M. Ito and T. Shigeoka, *Spectrochimica Acta.* 22, 1029 (1966).

²⁵ A. R. Gee and E. R. Bernstein, unpublished results.

²⁶ A. Fruhling, *J. Chem. Phys.* 18, 1119 (1950); *Ann. Phys.*
(Paris), 6, 40 (1951).

²⁷ I. Harada and T. Shiminouchi, *J. Chem. Phys.* 46, 2708
(1967).

²⁸ S. Zwerdling and R. S. Halford, *J. Chem. Phys.* 23, 2221
(1955).

TABLE I. Potentials for H-H, C-H, and C-C interactions in the form $[V = Be^{-CR} - A/R^6]$.
 Constants in atomic units.

Type of Potential and Set Number		Parameters (a. u.)			Reference and Figure Number
		A	B	C	
H-H	1	3.397	13.207	2.434	J. Chem. Soc. 340 (1948), Eq. (2.4)
	2	1.312	55.46	2.996	J. Chem. Phys. 14, 465 (1946); 16, 399, 938 (1948)
	3	5.886	10.892	2.257	Tetrahedron 19, 527 (1963)
	4	8.529	10.685	2.158	Tetrahedron 19, 527 (1963)
	5	3.573	29.14	2.636	J. Am. Chem. Soc. 83, 2938 (1967)
	6	3.573	15.93	2.434	J. Am. Chem. Soc. 83, 4537 (1961)
	7	3.573	21.66	2.497	J. Am. Chem. Soc. 83, 4537 (1961)
	8	3.397	18.926	2.434	J. Chem. Soc. 340 (1948)
	9	3.573	10.51	2.160	J. Chem. Phys. 32, 831 (1960); Fig. 1
	10	3.247	2.960	1.625	Tetrahedron 19, 527 (1963); Fig. 1
	11	4.496	100.9	2.645	Proc. Roy. Soc. A154, 624 (1936); A178, 223 (1941); Fig. 1
	12	6.495	5.921	1.625	J. Am. Chem. Soc. 77, 5808 (1955); Fig. 1
	13	0.00	4.02	1.92	graph; Fig. 2
	14	0.00	2.75	1.86	J. Chem. Phys. 32, 1342 (1960); Fig. 2
	15	-0.209	4.39	1.95	calc.; Fig. 2

325

TABLE I. (continued)

Type of Potential and Set Number		Parameters (a. u.)			Reference and Figure Number
		A	B	C	
I	16	5.12	6.35	1.98	J. Chem. Phys. <u>45</u> , 3770 (1966); Fig. 4
II	17	4.19	6.35	1.98	J. Chem. Phys. <u>45</u> , 3770 (1966); Fig. 4
III	18	3.59	6.35	1.98	J. Chem. Phys. <u>45</u> , 3770 (1966); Fig. 4
IV	19	2.61	6.35	1.98	J. Chem. Phys. <u>45</u> , 3770 (1966); Fig. 4
	20	3.10	47.9	2.645	Tetrahedron <u>14</u> , 230 (1961); Fig. 3
C-H	21	10.30	47.9	2.210	Tetrahedron <u>14</u> , 230 (1961); Fig. 3
I	22	6.21	10.77	1.94	J. Chem. Phys. <u>45</u> , 3770 (1966); Fig. 4
II	23	11.55	20.09	1.94	J. Chem. Phys. <u>45</u> , 3770 (1966); Fig. 4
III	24	12.02	21.10	1.94	J. Chem. Phys. <u>45</u> , 3770 (1966); Fig. 4
IV	25	10.00	15.00	1.94	J. Chem. Phys. <u>45</u> , 3770 (1966); Fig. 4
C-C I	26	43.47	142.15	1.904	J. Chem. Phys. <u>45</u> , 3770 (1966); Fig. 5
II	27	31.76	66.17	1.904	J. Chem. Phys. <u>45</u> , 3770 (1966); Fig. 5
III	28	31.27	69.98	1.904	J. Chem. Phys. <u>45</u> , 3770 (1966); Fig. 5
IV	29	38.49	118.68	1.904	J. Chem. Phys. <u>45</u> , 3770 (1966); Fig. 5

TABLE II. Direction cosines of the molecular (site) axes (x, y, z) with respect to the crystallographic axes (a, b, c) for molecule I (at 77°K-- see Ref. 22).

		x	y	z
T^I	= a	0.6379	-0.3248	0.6814
	= b	0.1999	0.9456	0.2532
	= c	-0.7265	-0.0339	0.6867

$$T^{II} = C_2^a T^I, T^{III} = C_2^b T^I \text{ and } T^{IV} = C_2^c T^I$$

TABLE III. Unique atom-atom contact distances to 4.0 Å between molecule I [(0, 0, 0) \Rightarrow unit cell origin] and molecule II ($\frac{1}{2} + X, \frac{1}{2} - Y, -Z$) $\Rightarrow C_2^a$.

New Atom ^a (Molecule II)	Old Atom ^a (Molecule I)	Type of Contact	Distance Å
11	23	C-C	3.762
11	43	C-H	3.303
12	23	C-C	3.965
12	43	C-H	3.243
31	11	H-C	3.519
31	22	H-C	3.474
31	23	H-C	2.922
31	31	H-H	3.689
31	42	H-H	3.630
31	43	H-H	2.652
32	11	H-C	3.812
32	23	H-C	3.374
32	31	H-H	3.410
32	43	H-H	2.526

^aSee Fig. 6 for numbering system.

TABLE IV. Unique atom-atom contact distances to 4.0 \AA between molecule I $[(0,0,0) \Rightarrow \text{unit cell origin}]$ and molecule III $[(-X, \frac{1}{2} + Y, \frac{1}{2} - Z) \Rightarrow C_2^b]$.

New Atom ^a (Molecule III)	Old Atom ^a (Molecule I)	Type of Contact	Distance Å
13	11	C-C	3.686
13	31	C-H	3.237
13	32	C-H	3.987
21	11	C-C	3.968
21	12	C-C	3.902
21	31	C-H	3.589
21	32	C-H	3.487
33	11	H-C	2.955
33	12	H-C	3.491
33	23	H-C	3.504
33	31	H-H	2.694
33	32	H-H	3.697
33	43	H-H	3.715
41	11	H-C	3.519
41	12	H-C	3.120
41	31	H-H	3.385
41	32	H-H	2.616

^aSee Fig. 6 for numbering system.

TABLE V. Unique atom-atom contact distances to 4.0 Å between molecule I [(0, 0, 0) ⇒ unit cell origin] and molecule IV [$(\frac{1}{2} - X, -Y, \frac{1}{2} + Z)$ ⇒ C₂^c].

New Atom ^a (Molecule IV)	Old Atom ^a (Molecule I)	Type of Contact	Distance Å
22	13	C—C	3.858
22	21	C—C	3.752
22	22	C—C	3.860
23	21	C—C	3.641
23	22	C—C	3.976
23	41	C—H	3.657
42	11	H—C	3.063
42	12	H—C	3.077
42	13	H—C	3.089
42	21	H—C	3.079
42	22	H—C	3.075
42	23	H—C	3.062
42	31	H—H	3.659
42	32	H—H	3.702
42	33	H—H	3.700
42	41	H—H	3.718
42	42	H—H	3.687
42	43	H—H	3.669
43	13	H—C	3.429
43	21	H—C	2.839
43	22	H—C	3.325
43	33	H—H	3.690
43	41	H—H	2.668
43	42	H—H	3.517

^aFor numbering see Fig. 6 .

TABLE VI. C_6H_6 factor group and phonons for potential set I. (See Table XVI.)

#	D_{6h} Sym	Exciton Components						
		Gas	IMC	A	B_1	B_2	B_3	Mean
ν_1	a_{1g}	992.3	995.1	994.4	995.5	996.1	994.4	995.1
ν_2	a_{1g}	3072.7	3078.7	3079.1	3078.3	3078.6	3078.7	3078.7
ν_3	a_{2g}	1351.2	1362.0	1356.9	1358.2	1366.2	1367.1	1362.0
ν_4	b_{2g}	697.1	705.8	709.1	701.9	708.0	703.0	705.8
ν_5	b_{2g}	1004.6	1019.5	1025.1	1013.9	1024.7	1014.6	1019.5
ν_6	e_{2g}		611.0	616.1	617.8	617.1	616.9	616.6
				615.3	615.0	613.5	615.1	613.4
ν_7	e_{2g}		3043.7	3050.8	3050.6	3050.9	3051.2	3050.6
				3048.3	3048.1	3048.4	3047.9	3048.5
ν_8	e_{2g}		1601.1	1603.1	1603.6	1603.5	1603.2	1603.3
				1602.8	1602.5	1602.4	1602.6	1602.6
ν_9	e_{2g}		1174.2	1189.4	1197.7	1198.8	1189.0	1187.7
				1186.2	1185.2	1183.0	1180.1	1181.2
ν_{10}	e_{1g}		853.6	875.2	872.0	881.8	871.8	819.5
				867.4	864.4	867.0	863.7	869.9

TABLE VI. (continued).

#	D_{6h} Sym	Gas	IMC	Exciton Components				Mean
				A	B_1	B_2	B_3	
ν_{11}	a_{2u}	672.9	698.3	709.1	687.9	706.7	688.9	698.3
ν_{12}	b_{1u}	1012.1	1015.0	1015.2	1016.1	1015.2	1013.8	1015.0
ν_{13}	b_{1u}	3067.5	3073.0	3073.3	3072.9	3073.2	3072.8	3073.0
ν_{14}	b_{2u}	1307.1	1310.2	1309.0	1309.2	1311.3	1311.5	1310.2
ν_{15}	b_{2u}	1147.7	1160.7	1154.5	1156.6	1165.3	1167.1	1160.8
ν_{16}	e_{2u}	400.0	421.7	417.2	429.8	416.7	426.7	
			414.7	411.9	413.7	412.6	415.8	
ν_{17}	e_{2u}	994.2	1010.6	1007.1	1013.6	1007.5	1014.4	
			1004.9	1002.6	1005.5	1002.5	1005.2	
ν_{18}	e_{1u}	1035.5	1046.9	1052.9	1051.1	1048.3	1046.2	
			1044.0	1042.2	1041.5	1042.7	1041.1	
ν_{19}	e_{1u}	1480.9	1487.7	1491.1	1491.8	1487.8	1487.1	
			1486.3	1485.6	1485.1	1483.9	1484.3	
ν_{20}	e_{1u}	3078.6	3085.9	3086.0	3085.7	3086.0	3086.1	
			3083.2	3082.9	3083.5	3083.0	3083.4	

TABLE VI. (continued).

#	D_{6h} Sym	Gas	IMC	Exciton Components				Mean	
				A	B_1	B_2	B_3		
				g {	98.2	138.2	134.6	137.7	
					87.0	81.8	108.5	125.7	
					62.7	65.9	102.7	101.4	
		PHONONS		u {	97.1	105.9	63.1	64.8	
						73.8	94.5	62.4	60.6
						45.1	0	0	0

TABLE VII. C_6H_6 factor group and phonons for potential set IV. (See Table XVI.)

#	D_{6h} Sym	Exciton Components						
		Gas	IMC	A	B_1	B_2	B_3	Mean
ν_1	a_{1g}	992.3	995.6	994.8	996.0	996.7	994.8	995.6
ν_2	a_{1g}	3072.7	3080.4	3081.0	3080.0	3080.3	3080.4	3080.4
ν_3	a_{2g}	1351.2	1365.8	1358.7	1360.8	1371.7	1373.2	1365.8
ν_4	b_{2g}	697.1	708.1	713.2	703.2	711.0	704.4	708.0
ν_5	b_{2g}	1004.6	1025.2	1033.4	1022.3	1032.5	1020.7	1025.2
ν_6	e_{2g}		611.0	617.0	618.9	618.2	618.0	617.8
				616.2	615.6	614.2	616.1	613.8
ν_7	e_{2g}		3043.7	3052.7	3052.5	3052.8	3053.2	3052.4
				3049.8	3049.6	3050.0	3049.3	3050.1
ν_8	e_{2g}		1601.1	1603.6	1604.4	1604.0	1603.7	1603.9
				1603.2	1602.7	1602.6	1603.0	1602.9

TABLE VII. (continued).

#	D_{6h} Sym	Gas	IMC	A	Exciton Components			Mean
					B_1	B_2	B_3	
ν_9	e_{2g}	1174.2	1194.7	1206.0	1207.5	1194.1	1192.7	
			1190.6	1189.1	1186.6	1171.3	1183.6	
ν_{10}	e_{1g}	853.6	883.2	878.2	893.0	877.8	890.0	
			872.7	868.1	872.0	867.5	875.8	
ν_{11}	a_{2u}	672.9	707.8	722.8	692.6	720.1	694.1	707.4
ν_{12}	b_{1u}	1012.1	1017.0	1016.0	1017.1	1016.1	1017.8	1016.8
ν_{13}	b_{1u}	3067.5	3074.6	3075.1	3074.4	3074.8	3074.3	3074.6
ν_{14}	b_{2u}	1307.1	1311.2	1309.5	1309.8	1312.8	1313.0	1311.2
ν_{15}	b_{2u}	1147.7	1165.2	1157.2	1159.8	1171.3	1173.3	1165.2
ν_{16}	e_{2u}	400.0	427.9	422.2	438.2	421.5	434.4	
			419.1	415.3	417.8	416.0	420.5	

TABLE VII. (continued)

#	D_{gh} Sym	Gas	IMC	Exciton Components				Mean
				A	B_1	B_2	B_3	
ν_{17}	e_{2u}	994.2	1015.0	1011.4	1015.4	1011.0	1015.0	
			1009.0	1006.0	1009.2	1005.7	1009.0	
ν_{18}	e_{1u}	1035.5	1050.5	1058.6	1056.3	1053.5	1049.9	
			1046.9	1044.8	1043.7	1044.9	1043.4	
ν_{19}	e_{1u}	1480.9	1490.0	1494.6	1495.7	1490.5	1489.3	
			1488.3	1487.3	1486.4	1484.6	1485.4	
ν_{20}	e_{1u}	3078.6	3087.9	3087.9	3087.6	3088.0	3088.1	
			3084.8	3084.3	3085.2	3084.5	3085.0	

TABLE VII. (continued).

#	D _{6h} Sym	Gas	IMC	Exciton Components				Mean
				A	B ₁	B ₂	B ₃	
				g {	106.2	155.6	151.9	155.1
					96.1	85.5	116.1	141.9
					67.9	74.4	115.3	109.1
				u {	110.3	118.8	69.5	69.7
					81.3	101.7	68.2	69.2
					50.1	0	0	0

PHONONS

TABLE VIII. C_6H_6 factor group components and phonons for H-H interactions only of Ref. 1. (See Table XVI for comparison.)

#	D_{6h} Sym	Exciton Components						Mean
		Gas	IMC	A	B_1	B_2	B_3	
ν_1	a_{1g}	992.27	992.99	993.1	992.9	993.1	992.7	992.99
ν_2	a_{1g}	3072.71	3072.19	3075.3	3074.7	3075.2	3075.1	3074.9
ν_3	a_{2g}	1351.24	1361.89	1354.05	1356.33	1368.39	1369.99	1361.9
ν_4	b_{2g}	697.07	703.7	706.86	700.4	706.15	700.89	703.7
ν_5	b_{2g}	1004.58	1020.81	1029.33	1011.98	1027.4	1016.34	1020.8
ν_6	e_{2g}	610.99	613.4	614.89	613.77	614.1	613.87	
			612.79	611.89	611.93	612.57	611.78	
ν_7	e_{2g}	3043.71	3046.41	3046.43	3046.69	3046.36	3046.37	
			3045.46	3045.16	3045.42	3045.35	3045.73	
ν_8	e_{2g}	1601.14	1602.34	1603.28	1602.96	1602.73	1602.6	
			1602.14	1601.73	1601.68	1601.72	1601.4	
ν_9	e_{2g}	1174.2	1190.00	1202.00	1202.90	1188.72	1188.17	
			1185.30	1183.32	1181.66	1177.08	1177.80	
ν_{10}	e_{1g}	853.6	877.77	870.48	888.16	872.03	885.71	
			867.94	863.83	867.85	864.33	869.02	

TABLE VIII. (continued).

#	D_{6h} Sym	Gas	IMC	Exciton Components				Mean
				A	B_1	B_2	B_3	
ν_{11}	a_{2u}	672.91	701.07	715.46	686.05	713.28	687.72	701.0
ν_{12}	b_{1u}	1012.12	1013.32	1013.3	1012.37	1013.05	1013.75	1013.3
ν_{13}	b_{1u}	3067.47	3069.65	3070.05	3069.54	3069.70	3069.3	3069.7
ν_{14}	b_{2u}	1307.13	1309.72	1308.04	1308.4	1311.24	1311.53	1309.7
ν_{15}	b_{2u}	1147.74	1160.65	1152.63	1154.56	1167.46	1168.70	1160.7
ν_{16}	e_{2u}	399.99	419.48	413.95	426.42	415.6	424.52	
			411.79	409.37	411.84	409.1	412.52	
ν_{17}	e_{2u}	994.19	1011.64	1006.39	1018.82	1005.77	1012.77	
			1005.06	1003.0	1004.24	1002.32	1004.85	
ν_{18}	e_{1u}	1035.51	1045.58	1053.49	1052.76	1050.15	1047.26	
			1043.75	1041.37	1040.29	1039.39	1038.27	
ν_{19}	e_{1u}	1480.87	1487.67	1492.9	1493.6	1487.78	1486.90	
			1485.44	1484.62	1483.22	1481.84	1482.49	
ν_{20}	e_{1u}	3078.58	3081.27	3081.12	3081.38	3081.44	3081.38	
			3080.36	3080.11	3080.35	3080.21	3080.62	

TABLE VIII. (continued).

#	D_{6h} Sym	Gas	IMC	Exciton Components				Mean
				A	B_1	B_2	B_3	
				91.7	123.9	127.2	126.0	
			g	67.4	79.0	72.5	116.0	
				35.0	50.2	66.2	55.3	
		PHONONS		68.1	60.5	50.8	55.3	
			u	59.4	43.3	38.5	33.8	
				27.9	0	0	0	

TABLE IX. C_6H_6 factor group components and phonons for C-H interactions only of Ref. 1. (See Table XVI for comparison.)

#	D_{6h} Sym	Exciton Components						Mean
		Gas	IMC	A	B_1	B_2	B_3	
ν_1	a_{1g}	992.27	994.96	994.2	995.4	995.86	994.4	995.0
ν_2	a_{1g}	3072.71	3080.07	3080.3	3079.9	3079.78	3080.2	3080.0
ν_3	a_{2g}	1351.24	1358.49	1359.2	1358.8	1358.1	1357.9	1358.5
ν_4	b_{2g}	697.07	702.20	704.5	700.8	702.9	700.6	702.2
ν_5	b_{2g}	1004.58	1010.02	1008.5	1011.0	1009.5	1011.15	1010.1
ν_6	e_{2g}	610.99	615.84	616.23	617.14	617.02	614.5	
			613.81	613.95	612.94	613.32	613.3	
ν_7	e_{2g}	3043.71	3052.61	3052.61	3052.66	3052.69	3052.60	
			3049.08	3048.98	3049.13	3049.16	3049.02	
ν_8	e_{2g}	1601.14	1602.85	1602.85	1602.13	1603.16	1603.38	
			1602.10	1601.97	1602.06	1601.87	1602.42	
ν_9	e_{2g}	1174.2	1184.31	1184.90	1184.47	1183.99	1184.09	
			1182.79	1182.39	1183.44	1182.25	1183.03	
ν_{10}	e_{1g}	853.6	861.66	864.02	860.02	861.81	862.29	
			858.52	859.33	857.62	857.38	858.05	

TABLE IX. (continued).

#	D_{6h} Sym	Gas	IMC	Exciton Components				Mean
				A	B_1	B_2	B_3	
ν_{11}	a_{2u}	672.91	681.81	680.77	683.40	680.90	682.23	681.8
ν_{12}	b_{1u}	1012.12	1014.7	1014.3	1015.4	1015.3	1013.7	1014.8
ν_{13}	b_{1u}	3067.47	3074.09	3074.24	3073.82	3073.91	3074.41	3074.1
ν_{14}	b_{2u}	1307.13	1309.11	1309.15	1308.82	1309.39	1309.1	1309.1
ν_{15}	b_{2u}	1147.74	1156.55	1156.55	1156.93	1156.26	1156.58	1156.6
ν_{16}	e_{2u}	399.99	411.34	409.19	416.82	408.98	412.92	
			407.81	407.52	406.16	407.03	407.71	
ν_{17}	e_{2u}	994.19	1000.42	1001.43	999.85	1001.53	1000.06	
			998.21	998.11	997.20	998.04	997.95	
ν_{18}	e_{1u}	1035.51	1044.31	1045.09	1042.96	1045.28	1044.27	
			1040.91	1041.35	1041.07	1040.60	1040.56	
ν_{19}	e_{1u}	1480.87	1485.79	1485.66	1486.01	1485.85	1486.17	
			1484.45	1483.85	1484.63	1484.39	1484.46	
ν_{20}	e_{1u}	3078.58	3087.41	3087.43	3087.39	3087.39	3087.46	
			3084.69	3084.55	3084.98	3084.84	3084.36	

TABLE IX. (continued).

#	D_{6h} Sym	Gas	IMC	A	Exciton Components			Mean
					B_1	B_2	B_3	
				g {	95.0	107.9	105.5	109.9
					70.1	86.6	94.9	104.5
					46.3	85.0	92.6	86.3
				u {	78.9	62.2	69.6	56.3
					60.3	58.1	48.2	39.0
					34.7	0	0	0

PHONONS

TABLE X. C_6H_6 factor group components and phonons for C-H and H-H interactions of Ref. 1. (See Table XVI for comparison.)

#	D_{6h} Sym	Exciton Components						
		Gas	IMC	A	B_1	B_2	B_3	Mean
ν_1	a_{1g}	992.27	995.71	995.0	996.0	996.8	995.1	995.7
ν_2	a_{1g}	3072.71	3082.23	3082.8	3081.9	3082.1	3082.2	3082.2
ν_3	a_{2g}	1351.24	1369.14	1362.0	1363.9	1375.3	1376.6	1369.2
ν_4	b_{2g}	697.07	708.70	714.0	704.1	711.6	704.4	708.6
ν_5	b_{2g}	1004.58	1026.41	1033.5	1019.1	1032.5	1020.4	1026.4
ν_6	e_{2g}	610.99	617.69	619.2	619.1	618.9	617.0	
			616.04	615.1	614.6	616.0	614.4	
ν_7	e_{2g}	3043.71	3054.53	3054.4	3054.5	3054.9	3054.6	
			3051.67	3051.5	3052.0	3051.3	3051.7	
ν_8	e_{2g}	1601.14	1603.99	1605.0	1604.0	1604.2	1604.3	
			1603.22	1602.6	1602.6	1603.0	1603.2	
ν_9	e_{2g}	1174.2	1198.38	1209.9	1211.7	1198.1	1197.4	
			1195.19	1193.6	1191.8	1185.2	1187.0	
ν_{10}	e_{1g}	853.6	885.11	880.8	893.8	880.0	890.5	
			873.40	869.8	872.7	868.6	877.0	

TABLE X. (continued)

#	D_{6h} Sym	Gas	IMC	Exciton Components				Mean
				A	B_1	B_2	B_3	
ν_{11}	a_{2u}	672.91	709.69	723.2	696.3	721.0	697.1	709.8
ν_{12}	b_{1u}	1012.12	1014.86	1016.2	1016.0	1012.6	1014.2	1014.8
ν_{13}	b_{1u}	3067.47	3076.50	3077.1	3076.1	3076.4	3076.5	3076.5
ν_{14}	b_{2u}	1307.13	1311.95	1310.2	1310.2	1313.9	1313.9	1312.0
ν_{15}	b_{2u}	1147.74	1168.94	1161.2	1163.5	1175.1	1176.6	1169.0
ν_{16}	e_{2u}	399.99	430.11	422.5	441.4	423.3	436.3	
			419.36	416.8	418.0	416.8	420.1	
ν_{17}	e_{2u}	994.19	1018.87	1012.6	1021.8	1018.0	1021.7	
			1009.63	1007.4	1009.8	1006.6	1010.2	
ν_{18}	e_{1u}	1035.51	1053.68	1061.9	1046.3	1055.1	1052.7	
			1049.05	1047.7	1021.8	1047.6	1045.7	
ν_{19}	e_{1u}	1480.87	1491.45	1496.1	1497.5	1492.5	1491.7	
			1490.35	1489.5	1488.4	1485.8	1486.8	
ν_{20}	e_{1u}	3078.58	3089.39	3089.3	3089.3	3089.6	3089.5	
			3086.94	3086.6	3087.5	3086.8	3086.9	

TABLE X. (continued).

#	D_{6h} Sym	Gas	IMC	Exciton Components				Mean
				A	B_1	B_2	B_3	
				g {	117.7	161.7	163.1	159.3
					96.3	117.5	117.3	150.0
					67.3	85.4	119.9	117.1
	PHONONS			u {	110.3	100.7	73.7	70.3
					82.9	81.0	71.8	65.5
					52.0	0	0	0

TABLE XI. C_6D_6 factor group components and phonons for potential set I. (See Table XVIII.)

#	D_{6h} Sym	Gas	IMC	Exciton Components				Mean
				A	B_1	B_2	B_3	
1	\bar{a}_{1g}	943.3	946.4	945.7	946.9	947.3	945.7	946.4
2	a_{1g}	2286.4	2290.0	2290.4	2289.7	2289.8	2290.2	2290.0
3	a_{2g}	1051.0	1056.9	1054.4	1055.0	1059.1	1059.5	1056.9
4	b_{2g}	589.8	602.2	609.0	596.4	606.5	597.5	602.2
5	b_{2g}	839.9	845.1	845.8	844.2	846.2	844.1	845.1
6	e_{2g}	576.0	580.8	580.4	578.7	581.0	578.5	
			581.9	583.4	583.1	582.2	582.2	
7	e_{2g}	2274.7	2277.4	2277.4	2277.4	2277.4	2277.4	2277.6
			2278.9	2278.5	2279.0	2278.9	2278.5	2278.5
8	e_{2g}	1546.2	1547.4	1547.3	1547.2	1547.3	1547.5	
			1547.5	1547.5	1547.6	1547.6	1547.8	
9	e_{2g}	863.7	871.9	871.5	869.9	867.3	868.7	
			863.8	879.3	880.2	873.4	872.9	
10	e_{1g}	664.0	672.3	671.2	671.5	670.3	674.2	
			676.6	675.3	680.0	674.6	678.6	

TABLE XI. (continued).

#	D_{6h} Sym	Gas	IMC	Exciton Components				Mean
				A	B_1	B_2	B_3	
11	a_{2u}	494.1	510.8	517.7	504.4	515.9	505.1	510.9
12	b_{1u}	961.5	964.6	964.7	964.7	964.5	964.3	964.6
13	b_{1u}	2284.2	2287.4	2287.6	2287.3	2287.5	2287.3	2287.4
14	b_{2u}	1285.6	1286.3	1286.2	1286.3	1286.3	1286.4	1286.3
15	b_{2u}	825.5	836.5	831.3	833.2	841.7	842.7	837.2
16	e_{2u}	344.2	358.3	355.2	357.4	355.9	359.4	}
			365.2	360.9	373.2	360.6	370.3	
17	e_{2u}	809.2	817.0	815.2	814.1	815.0	813.5	}
			819.9	821.9	822.9	817.2	817.9	
18	e_{1u}	817.4	822.8	824.0	823.5	822.5	822.7	}
			825.5	825.9	828.1	826.6	827.3	
19	e_{1u}	1324.5	1326.6	1326.3	1326.6	1326.1	1326.1	}
			1326.8	1327.3	1327.5	1327.0	1326.5	
20	e_{1u}	2287.9	2290.7	2290.5	2290.0	2290.6	2290.7	}
			2292.3	2292.4	2292.2	2292.3	2292.5	

TABLE XI. (continued).

#	D _{6h} Sym	Gas	IMC	Exciton Components				Mean
				A	B ₁	B ₂	B ₃	
				g {	95.1	126.8	123.2	125.8
					79.3	78.9	105.0	115.0
					60.5	60.0	93.7	97.9
		PHONONS		u {	88.8	96.7	60.2	62.5
					71.2	91.2	57.4	55.3
					44.1	0	0	0

TABLE XII. Observed and calculated site shifts (Δ) and splittings (δ_{SS}) for C_6H_6 and C_6D_6 (potential set I).

Vibration Number	$C_6H_6^a$				$C_6D_6^a$			
	Δ		δ_{SS}		Δ		δ_{SS}	
	Calc.	Obs.	Calc.	Obs.	Calc.	Obs.	Calc.	Obs.
1	+ 2	- 3			+ 3			
2	+ 6	0			+ 4			
3	+11				+ 5			
4	+ 8	- 2			+12			
5	+15	+13			+ 5			
6	+ 4	0	0.7	3.1	+ 5		1.1	1.2
7	+ 6	+ 4	2.5	5.5	+ 4		1.4	
8	+ 2		0.3	<0.3	+ 1		0.1	
9	+13	- 2	3.2	0.54	+ 9		1.9	
10	+18	+19	7.8	7.5	+10		4.3	
11	+25	+23			+17	+15		
12	+ 3	0			+ 4	+ 1		
13	+ 6				+ 3	- 7 ^b		
14	+ 3	+ 4			+ 1	+ 3		
15	+13	0			+11	- 2 ^b		
16	+18	+10	7.0	8.2	+17	+13	6.9	9.8
17	+14	+14	5.7	5.4	+10	+ 8 ^b	2.7	6.5
18	+10	0	3.0	3.8	+ 6	+ 2 ^b	2.9	4.1
19	+ 6		1.4		+ 2	0	0.2	<0.5
20	+ 6		2.7		+ 3	+ 4 ^b	1.6	

^aExperimental site shifts $\pm 4 \text{ cm}^{-1}$; data from Ref. 13.

^bShift and splitting due in part to increase Fermi resonance in solid (see Ref. 13).

TABLE XIII. Calculated and observed sym-C₆H₃D₃ site shifts (Δ) and site splittings (δ_{ss}) (potential set I).

ν	Gas	IMC ^a	Δ		δ_{ss}	
			Calc	Obs	Calc	Obs
1	950.6	953.7	+ 4	0		
2	3070.1	3076.3	+ 6	-9 ^b		
3	1257.0	1262.0	+ 5			
4	692.5	704.3	+11	+7		
5	909.4	919.3	+10	+10		
6	591.4	597.1	+ 5	0	1.0	1.7
		596.1				
7	2281.3	2285.3	+ 4	+2	1.3	4.8
		2284.0				
8	1575.1	1576.9	+ 2	-4 ^b	0.2	1.0
		1576.7				
9	1085.0	1096.9	+10	0 ^b	2.6	2.6
		1094.3				
10	718.9	731.7	+12	+12	4.3	4.5
		727.4				
11	527.5	544.3	+16	+15		
12	1003.9	1006.8	+ 2	0		
13	2285.3	2289.1	+ 4	-3 ^b		
14	1318.4	1325.5	+ 7			
15	930.0	942.0	+12	-2 ^b		
16	370.4	391.8	+18	+13	7.0	8.5
		384.8				
17	947.8	964.5	+15	+14	5.1	3.7
		959.4				
18	840.2	850.5	+ 9	0	2.4	3.0
		848.1				
19	1419.2	1425.0	+ 5	-2	1.1	<3
		1423.9				

TABLE XIII. (continued)

ν	Gas	IMC	Δ		δ_{ss}	
			Calc	Obs	Calc	Obs
20	3061.4	3068.2 3065.8	+ 7	-2 ^b	2.4	<4

^aIdeal mixed crystal value. (Ref. 13)

^bShift due in part to increased Fermi resonance in the solid
(see Ref. 13).

TABLE XIV. Calculated and observed orientational effect for C_6H_5D (potential Set I).

No.	Gas	Sites ^c			Orientational Effect		
		1	2	3	2-1	3-2 (Arbitrary Sign)	Observed ^a
1	979.0	982.2	982.2	982.3	0	+0.1	+0.4
2	3078.6	3085.7	3085.4	3083.3	-0.3	-2.1	-
3	1296.4	1299.9	1299.6	1299.6	-0.3	0	+1.0
4	692.7	704.4	704.3	704.5	-0.1	+0.2	+0.1
5	1001.2	1016.3	1015.2	1016.3	-1.1	-1.1	+1.0
6a	604.2	608.8	609.1	609.1	+0.3	0.0	
6b	604.9	609.8	609.8	609.9	0.0	0.1	
7a	2282.7	2285.0	2285.9	2287.5	+0.9	+1.6	
7b	3043.7	3050.4	3049.5	3048.3	-0.9	-1.2	
8a	1595.6	1597.2	1597.3	1597.3	+0.1	0.0	
8b	1591.8	1593.8	1593.6	1593.6	-0.2	0.0	+0.2
9a	1172.0	1187.1	1184.9	1184.6	-2.2	-0.3	
9b	1157.1	1169.3	1170.4	1170.5	+0.9	+0.1	+0.1
10a	853.6	869.8	875.2	868.4	+5.4	-6.8	
10b	784.3	800.5	797.8	800.5	-2.7	+2.7	
11	606.9	624.3	624.2	625.2	-0.1	+1.0	2.2 L
12	1006.0	1008.8	1008.8	1009.1	0.0	0.3	
13	3053.7	3059.1	3059.7	3060.0	+0.6	+0.3	
14	1327.5	1337.9	1336.8	1336.5	-1.1	-0.3	
15	1080.6	1091.2	1091.4	1091.4	+0.2	0.0	+1.7
16a	400.0	416.4	421.6	417.2	+5.2	-4.4	
16b	377.7	397.4	391.5	397.2	-5.9	-6.3	4.5 H
17a	994.2	1006.5	1010.8	1006.0	-4.3	-4.8	
17b	944.3	957.8	958.5	957.6	+0.7	-0.9	-0.7
18a	1031.9	1042.9	1040.8	1040.2	-2.1	-0.6	2.8 L
18b	858.6	865.8	868.8	869.8	+3.0	+1.0	+2.9 +1.1 (~3.5) ^b
19a	1474.1	1481.2	1480.2	1480.1	-1.0	-0.1	
19b	1451.4	1456.9	1457.4	1457.3	+0.5	-0.1	+0.2
20a	3069.6	3076.0	3075.3	3074.6	-0.7	-0.7	
20b	3075.2	3080.8	3080.7	3081.5	-0.1	+0.8	

^aL = low energy component more intense; H = high energy component more intense; see Refs. 13a and 13b. Signs on the experimental numbers are arbitrary and are given by convention in Ref. 13b, where the "middle site" is the common one in the subtraction.

^bIR and UV data differ.

^cThe meaning of "sites" is discussed in the text.

TABLE XV. Calculated and observed orientational effect for p-C₆H₄D₂ (potential Set I).

No.	Gas	Sites ^b			Orientational Effect		Observed ^a (arbitrary sign)	
		1	2	3	2-1	3-2		
1	975.6	978.6	978.5	978.5	-0.1	0.0		
2	3063.2	3070.2	3069.5	3067.9	-0.7	-1.6		
3	1308.6	1320.7	1318.8	1318.4	-1.9	-0.4	+1.3	-3.4
4	629.2	641.1	637.0	642.5	-4.1	+5.5	+3.3	+2.4
5	988.9	1006.8	1010.7	1006.2	+3.9	-1.5		
6a	598.8	603.4	603.2	603.2	-0.2	0.0		
6b	598.9	603.8	604.4	604.5	+0.6	0.1		
7a	2278.5	2280.8	2281.7	2283.3	+0.9	2.6		
7b	3043.7	3050.5	3049.6	3048.3	-0.9	-0.7		
8a	1588.2	1589.6	1589.6	1589.6	0.0	0.0		
8b	1581.4	1583.6	1583.4	1583.4	-0.2	0.0		
9a	1169.5	1184.6	1182.4	1182.1	-2.2	-0.3		
9b	912.6	919.7	922.1	922.5	+2.4	+0.4	-1.9	+2.6
10a	853.6	869.7	875.2	868.9	+5.5	-6.3		
10b	738.6	748.2	747.4	747.3	-0.8	-0.1	-1.9	+0.5
11	598.9	617.9	618.2	617.1	-0.3	-1.1		<1 L
12	994.2	992.3	992.6	993.0	+0.3	+0.4		3.1 L
13	2287.0	2289.4	2290.3	2291.9	+0.9	+1.6		
14	1291.5	1292.5	1292.6	1292.6	+0.1	0.0		<1.0
15	1103.6	1116.3	1114.8	1114.6	-1.5	-0.2		~2.0
16a	357.3	376.8	370.4	377.2	-6.4	+6.8		4.7 H
16b	400.0	416.2	421.6	416.9	+5.4	-4.7		
17a	971.2	984.7	988.5	984.2	+0.8	-1.3		2.0 H
17b	897.3	908.8	910.6	908.3	+1.8	-1.3	1.0	1.6
18a	1029.5	1040.0	1037.9	1037.2	-2.1	-0.7		3.1 L
18b	819.1	826.4	829.8	830.4	+3.4	+0.6		3.7 H
19a	1468.5	1475.7	1474.6	1474.6	-0.9	0.0		
19b	1412.0	1417.4	1416.7	1416.4	-0.7	-0.3		
20a	3071.2	3077.8	3076.6	3075.7	-1.2	-0.9		
20b	3078.5	3085.7	3085.2	3083.3	-0.5	-1.9		

^aL = low energy component more intense; H = high energy component more intense; see Refs. 13a and 13b. The signed numbers are from Ref. 13a. Signs of the experimental numbers are arbitrary and are given by convention in Ref. 13b, where the "middle site" (0,0²) is the common one in the subtraction.

^bThe meaning of "sites" is discussed in the text.

TABLE XVI. C₆H₆ experimental data.

#	D _{6h} Sym.	Gas ^a	Liquid ^b	IMC ^c	Exciton Components ^d			
					A	B ₁	B ₂	B ₃
ν_1	a _{1g}	992.8	993	990.5			990.3	
ν_2	a _{1g}	3073.5	3062	(3062)			3062.7	
ν_3	a _{2g}	1350	1346					
ν_4	b _{2g}	707	707	704.9				
ν_5	b _{2g}	990	991	1004.9			1012.5	
ν_6	e _{2g}	607	606	606.3 609.4	[605.2	606.3	609.0	611.0]
ν_7	e _{2g}	3055	3041	3042.0 3047.5	[3042.2	3047.0		3048.3]
ν_8	e _{2g}	1600	1594	1584.2				
ν_9	e _{2g}	1177	1177	1174.3 ₄ 1174.8 ₈	[1168.1	1173.5	1177.3	1181.4]
ν_{10}	e _{1g}	845	850	861.8	[852.8	854.8	858.0	864.6]

TABLE XVI. (continued).

#	D_{eh} Sym	Gas	Liquid	IMC	Exciton Components			
					A	B_1	B_2	B_3
ν_{11}	a_{2u}	673	675	696.9	708.9	681	708.7	689
ν_{12}	b_{1u}	1010	1010	1011.3	1020.0	1009.7	1008.6	1006.7
ν_{13}	b_{1u}	3057	3048					
ν_{14}	b_{2u}	1309	1309	1312.6	1309.5	1312.2	1313.4	1315.3
ν_{15}	b_{2u}	1146	1147	1146.9	1146.2	1140.6	1150.3	1142.5
ν_{16}	e_{2u}	398.1	399	404.8	[402.5		404.7	419.0]
				413.0				
ν_{17}	e_{2u}	967	969	978.3	[972.0	978.6	982.3	988.1]
				983.9		974.7		987.5]
ν_{18}	e_{1u}	1037	1035	1034.9	[1030.0	1033.3	1034.6	1038.8]
				1038.7		1032.5		1038.9]
ν_{19}	e_{1u}	1482	1479					
ν_{20}	e_{1u}	3064	3053					

TABLE XVI. (continued).

#	D_{eh} Sym	Gas	Liquid	IMC	Exciton Components			
					A	B_1	B_2	B_3
					(100)	136	(100)	136
				g	86	86	100	107
					64	69	86	(86)
				PHONONS ^{e,f}		102	74	
					u	90		
						0	0	0

^aJ. H. Callomon, T. M. Dunn, I. M. Mills, Phil. Trans. Roy. Soc. (London) A259, 499 (1966).

^bS. Brodersen and A. Langseth, Mat. Fys. Skr. Dan. Vid. Selak 1, 6 (1956).

^cRef. 10 and 13; ideal mixed crystal value.

^dRef. 11 and 12; polarization for band not in square brackets from Ref. 28.

^eRef. 24, 26, and 27; frequencies in parentheses are not observed but have been predicted on the basis of qualitative arguments to be degenerate with observed ones. These assumed degeneracies are not believed to be correct. See text.

^fThe polarizations from Ref. 27 for the B_{2u} and B_{3u} phonons have been reassigned on the basis of this calculation.

TABLE XVII. C_6D_6 experimental data.

#	D_{6h} Sym	Gas ^a	Liquid ^b	IMC ^c	Exciton Components ^d			
					A	B ₁	B ₂	B ₃
ν_1	a_{1g}	945.6	945				944.5	
ν_2	a_{1g}	2303	2293				2291.9	
ν_3	a_{2g}	1059	1055					
ν_4	b_{2g}	599	599					
ν_5	b_{2g}	829	830					
ν_6	e_{2g}	580.2	579		[576.4		579.1]
						578.4	583.1	
ν_7	e_{2g}	2274	2266		[2261.8		2267.7	2269.4]
ν_8	e_{2g}	1558	1553		[1549.9	1552.2]
ν_9	e_{2g}	869	869		[849.2		852.6	879.6]
						851.5	855.5	
ν_{10}	e_{1g}	660	664		[666.5		674.0	681.6]
						670.1	680.2	

TABLE XVII. (continued).

#	D_{6h} Sym	Gas	Liquid	IMC	Exciton Components			
					A	B_1	B_2	B_3
ν_{11}	a_{2u}	496.2	497	511.3	518	502	519.0	506
ν_{12}	b_{1u}	970	970	971.0	978.1	970.3	969.6	966.8
ν_{13}	b_{1u}	2285	2275	2268.1				
ν_{14}	b_{2u}	1282	1282	1285.1	1278.0	1288.7	1287.5	1286.2
ν_{15}	b_{2u}	824	823	820.6	(808.0)	824.1	826.9	823.4
ν_{16}	e_{2u}	347.4	351	354.8	[351.3 354.0 370.1]			
				364.6		353.7 367.3 373.0]		
ν_{17}	e_{2u}	787	789	791.3	[789.4 795.0 797.8]			
				797.8		790.3 795.4 801.2]		
ν_{18}	e_{1u}	814	812	810.5	[808.2 811.2 814.9]			
				814.6		809.3 812.5 815.5]		
ν_{19}	e_{1u}	1333	1330	1329.2	[1325.4 1329.5 1335.1]			
						1328.4 1330.3 1336.0]		
ν_{20}	e_{1u}	2288	2276	2278.9				
				2282.5				

TABLE XVII. (continued).

#	D_{6h} Sym	Gas	Liquid	IMC	Exciton Components				
					A	B_1	B_2	B_3	
					g {	(91)	123	(91)	123
						77	77	90	97
						57	62	77	(77)
				PHONONS ^f					
					u {				
							0	0	0

^aJ. H. Callomon, T. M. Dunn, and I. M. Mills, *Phil. Trans. Roy. Soc. (London)* A259, 499 (1966).

^bS. Brodersen and A. Langseth, *Mat. Fys. Skr. Dan. Vid. Selak* 1, 1 (1956).

^cRef. 10 and 13; ideal mixed crystal value.

^dRef. 11 and 12; polarization data for bands not in square brackets, assumed to be the same as C_6H_6 .

^e ν_{15} , ν_{17} , and ν_{18} are in Fermi resonance in the crystal.

^fRef. 24 and 26; frequencies in parentheses have not been observed but have been predicted on the basis of qualitative arguments to be degenerate with observed ones. These assumed degeneracies are not believed to be correct. See text.

TABLE XVIII. Observed phonon frequencies for C_6H_6 (Ref. 25;^a Ref. 26 used to assign polarizations) in cm^{-1} .

A_g	B_{1g}	B_{2g}	B_{3g}
61.0	66.5	83.1	98.1
83.1	83.1	93.7	132.2
	132.2		

^a Obtained with ionized argon laser (4880 Å line) at 0.5 cm^{-1} resolution (see Ref. 12).

Fig. 1

Plot of force constant versus distance for H-H potentials 8 through 12 presented in Table I. The large variation in magnitude of the force constants, especially at $R > 2.8 \text{ \AA}$ is of particular interest.

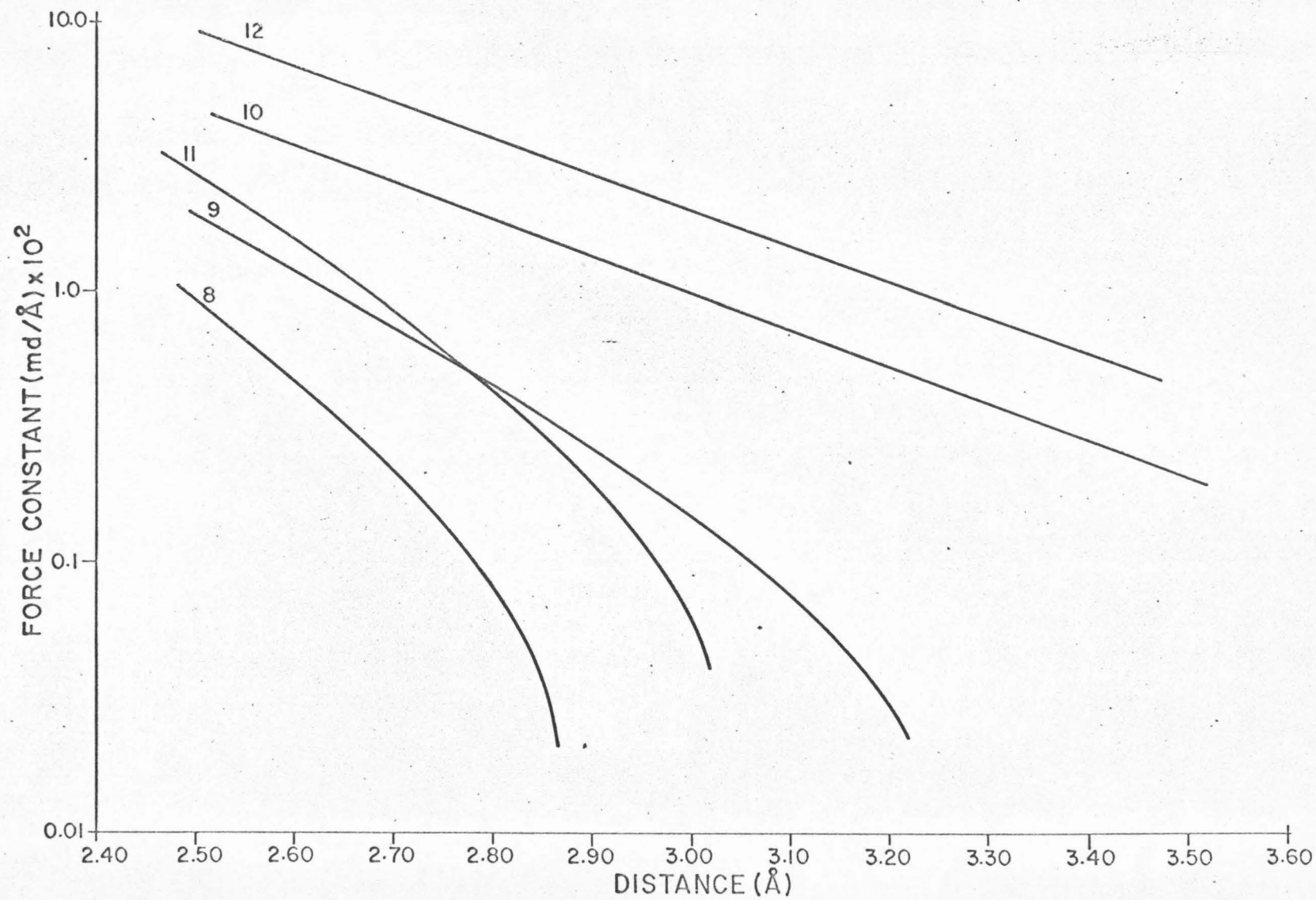


Fig. 2

A plot of force constant versus distance for the H-H potentials 13, 14 and 15 given in Table I. Potential 15 was derived to find the A constant necessary to fit potential 13 to the desired form.

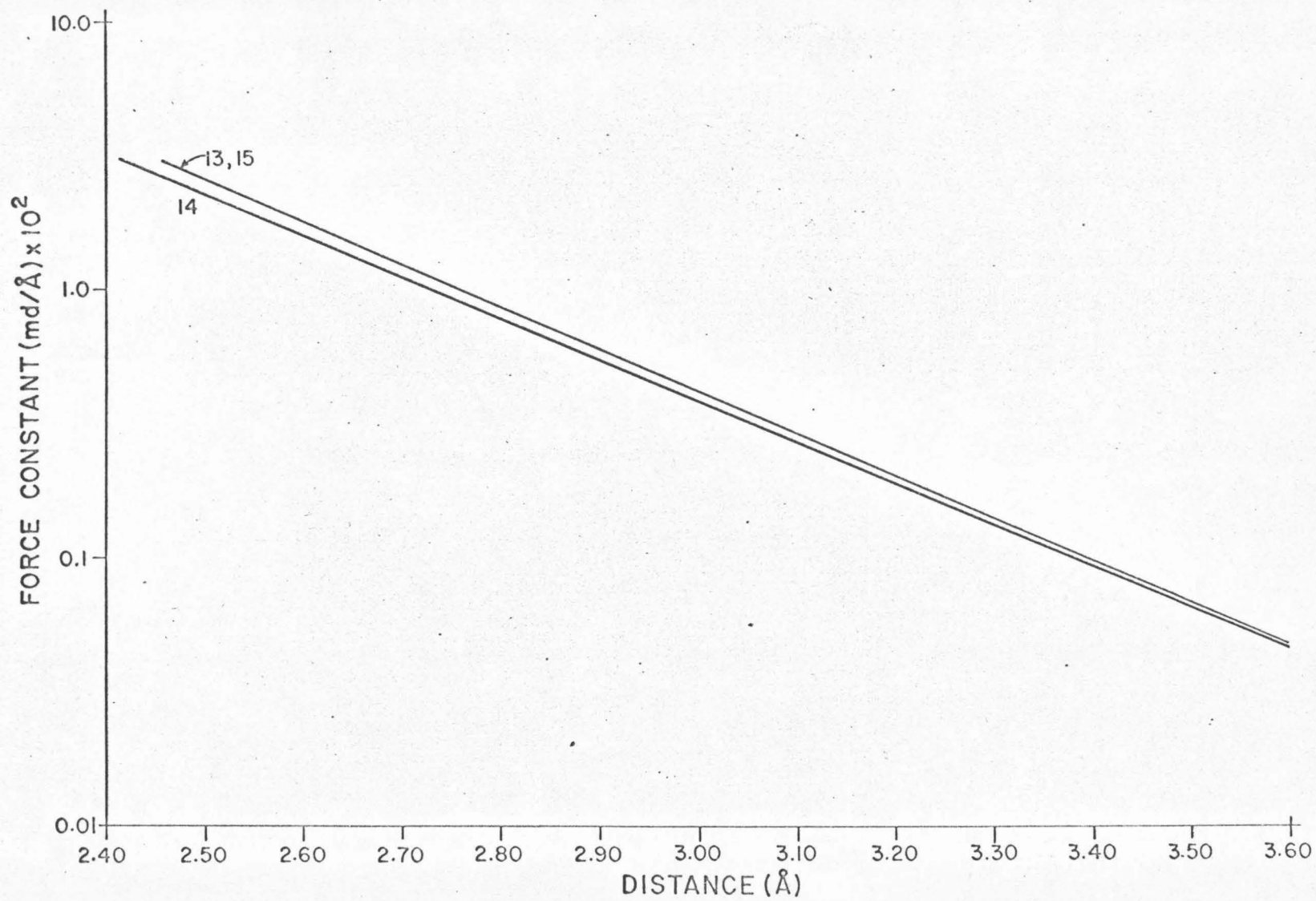


Fig. 3

A plot of force constant versus distance for the H-H(20) and C-H(21) potentials suggested by Kitaigorodskii. The parameters for these potentials are found in Table I.

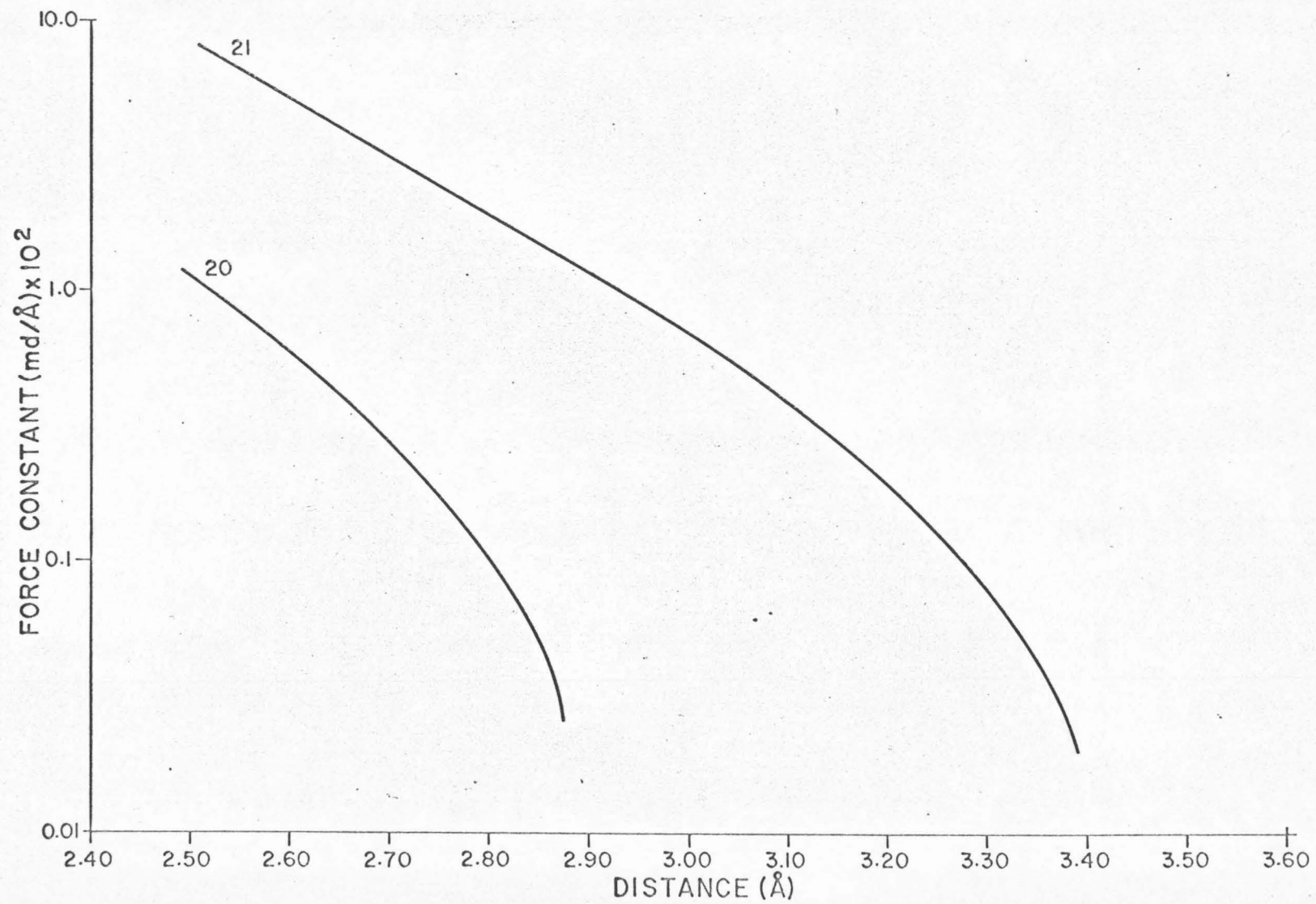


Fig. 4

A plot of the force constants versus distance for the potentials derived by Williams (see table). Note that these potentials are determined in sets and that they pair (16, 22), (17, 23), (18, 24) and (19, 25). The best results are obtained from (16, 22).

Potentials 16 through 19 represent H-H and 22 through 25 C-H interactions. The H-H potential 13 is also shown for a comparison.

Lines a and b represent force constant curves for two separate C-H potentials (ref. 1) used to describe the interaction in benzene and naphthalene respectively.

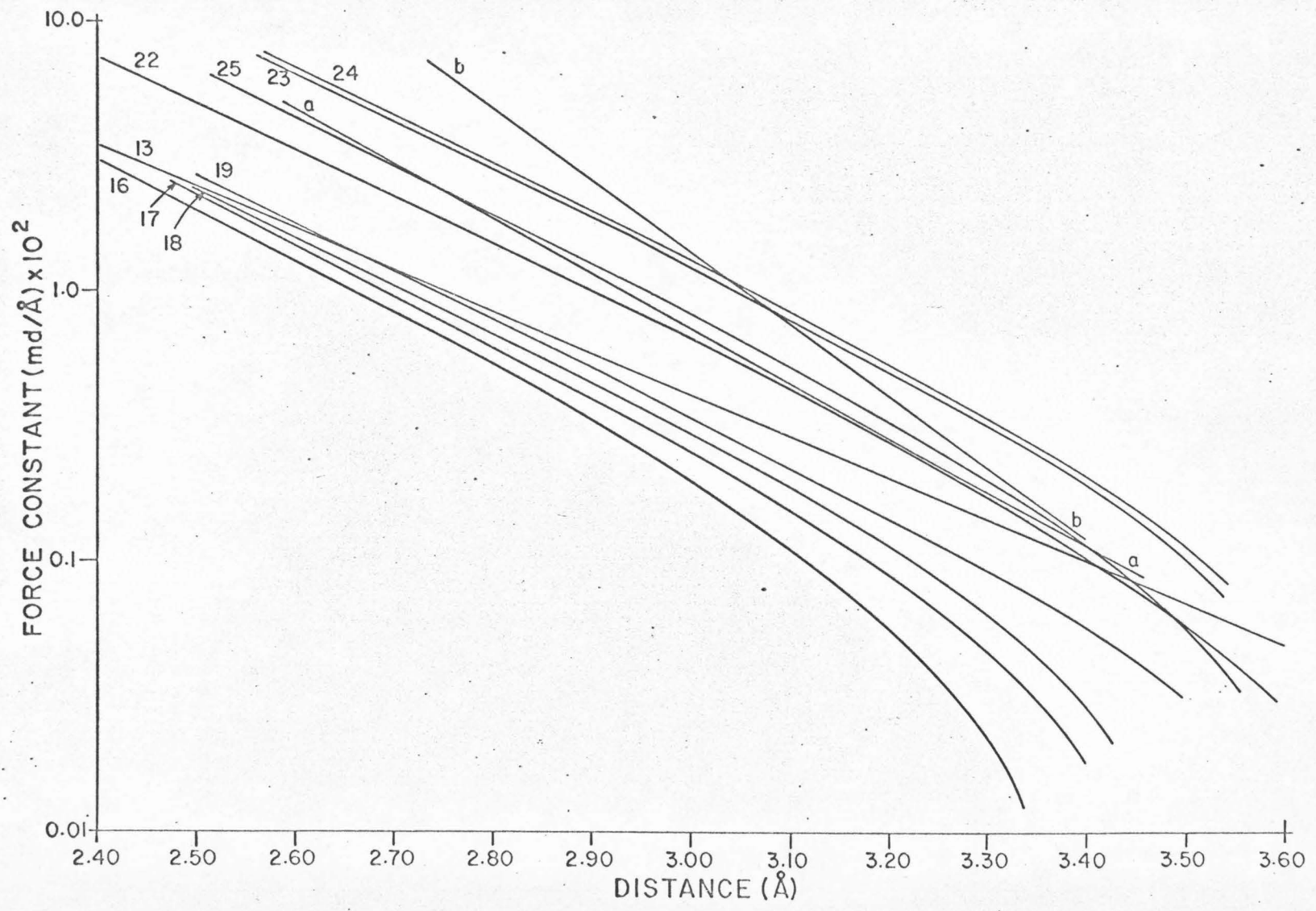


Fig. 5

Plot of the C-C force constants versus distance for the potentials derived by Williams (Table I). These C-C force constants pair with the C-H and H-H potentials of Fig. 4 such that the sets are: (16, 22, 26), (17, 23, 27), (18, 24, 28) and (19, 25, 29).

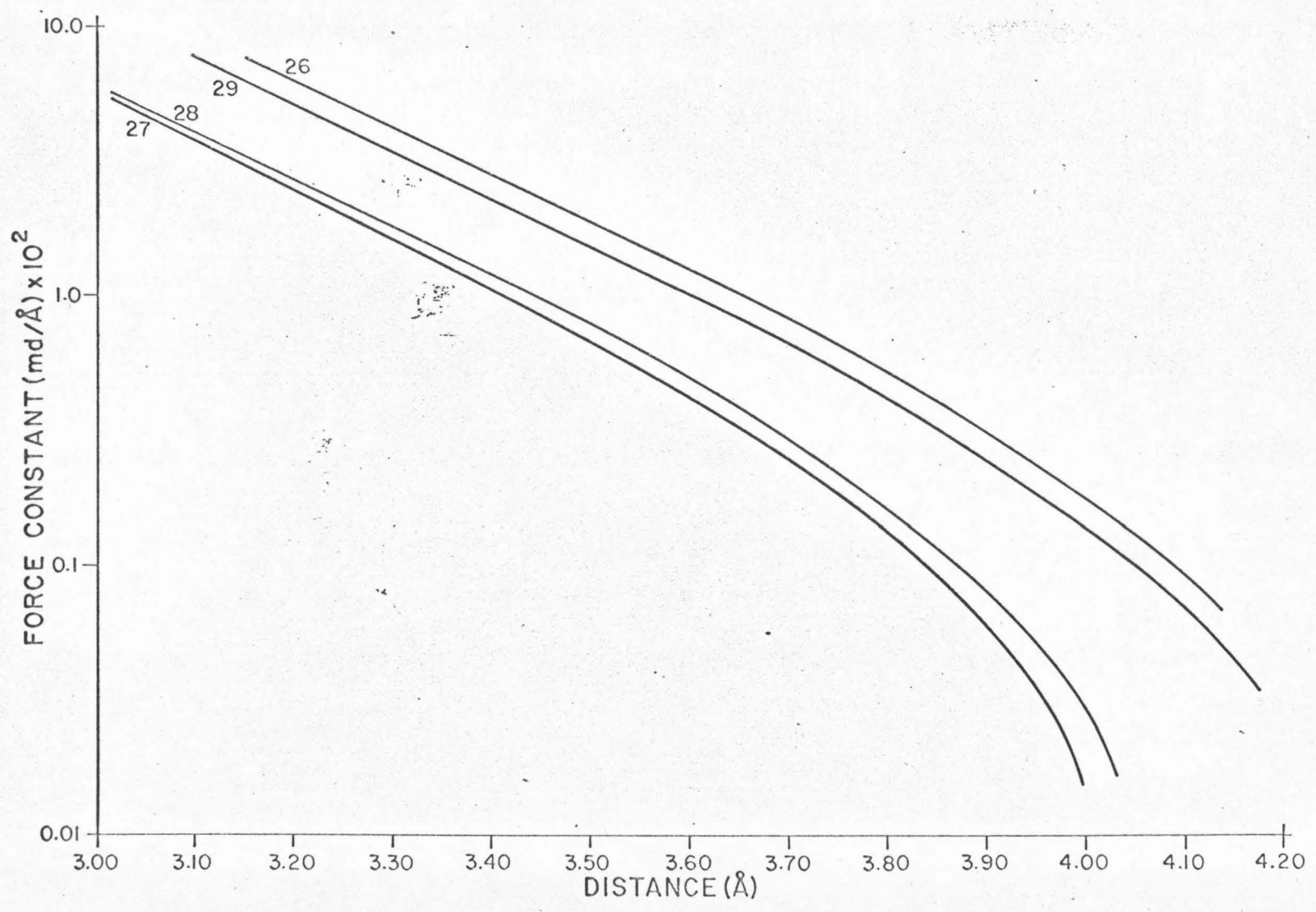
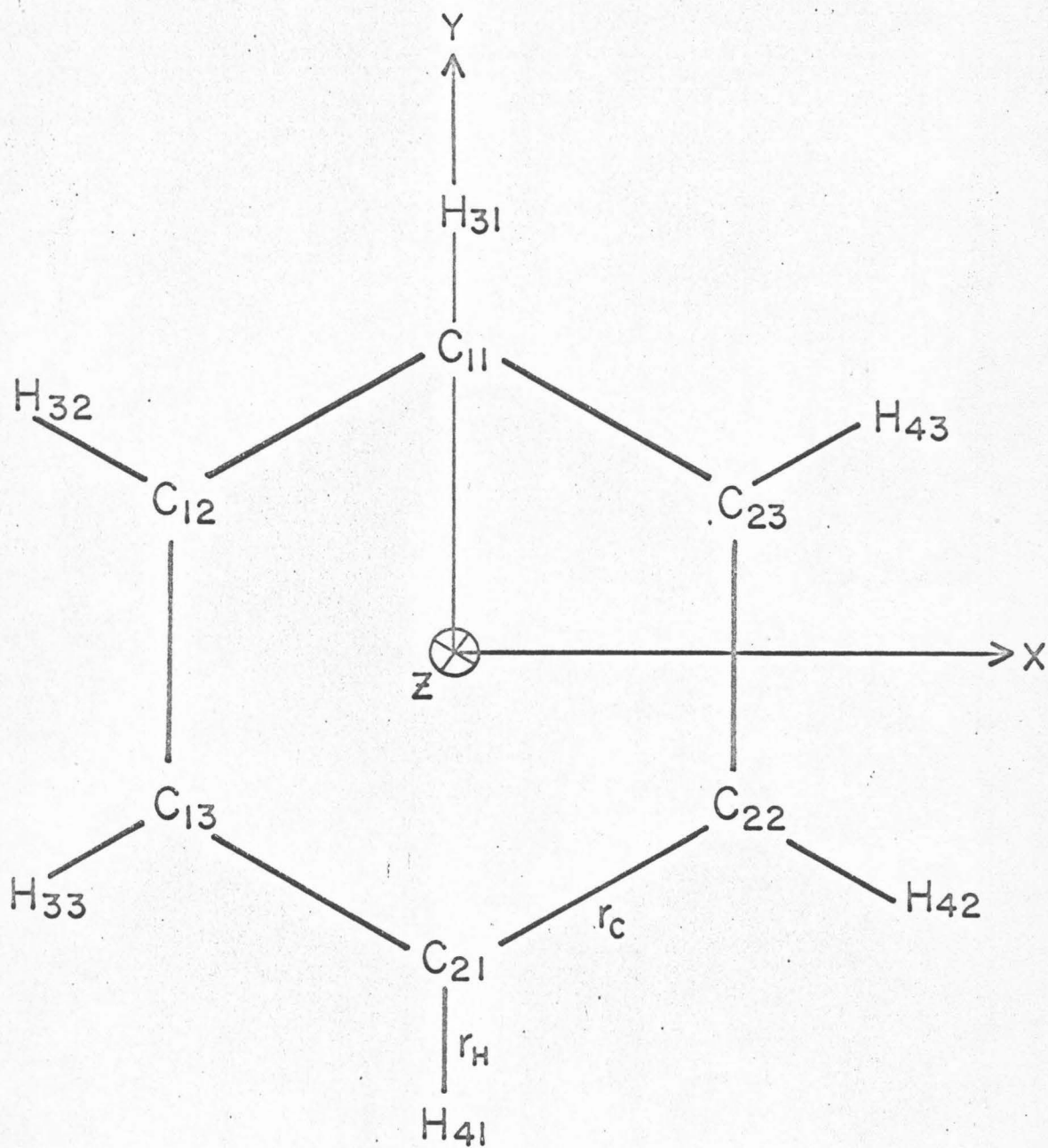


Fig. 6

The structure and numbering of the benzene molecule I at 77°K
(see ref. 22).



$$r_H = 1.083 \pm 0.004 \text{ \AA}; r_c = 1.390 \pm 0.002 \text{ \AA}$$

PART II

First and Second Triplets of Solid Benzene*

STEVEN D. COLSON AND ELLIOT R. BERNSTEIN

Gates and Crellin Laboratories of Chemistry,† California Institute of Technology, Pasadena, California

(Received 1 March 1965)

Absorption spectra have been taken of the O_2 -perturbed first (${}^3B_{1u}$) and second (${}^3E_{1u}$) triplets of solid benzene at 4.2°K. Spectra of both C_6H_6 and C_6D_6 were obtained. The (0-0) bands of the first triplet occur at $29\,674 \pm 25\text{ cm}^{-1}$ for C_6H_6 and $29\,851 \pm 25\text{ cm}^{-1}$ for C_6D_6 . For the second triplet they lie at $36\,560\text{ cm}^{-1} \pm 50$ for C_6H_6 and $36\,784 \pm 50\text{ cm}^{-1}$ for C_6D_6 . The result for the first triplet of C_6H_6 compares very favorably with Evans' gas-phase O_2 -perturbed spectrum. It is also in satisfactory agreement with Nieman's accurate phosphorescence measurements on isotopic mixed crystals of benzene which place the C_6H_6 (0, 0) band position in the crystal at $29\,657.1\text{ cm}^{-1}$. Many precautions were taken to eliminate the possibility of misidentification of the second triplet. The observation that the O_2 -enhanced first triplet and the O_2 -enhanced bands in the $36\,600\text{-cm}^{-1}$ region always appear together and with approximately the same relative intensities is considered to be the best evidence for the assignment. However, the rather broad structure obtained by the O_2 -perturbation technique does not allow all the uncertainties in the identification to be completely removed, nor does it allow a detailed study of this interesting state.

A detailed evaluation of the purity of the benzene is made, and a method is described for the preparation of material having ultrahigh spectroscopic purity. Crystals, up to 5 cm in length, of this very highly purified C_6H_6 and C_6D_6 were studied at 4.2°K to ascertain if the singlet-triplet absorptions could be seen in the absence of a perturbation. The long crystals showed some sharp and some broad ($\Delta\nu \approx 150\text{ cm}^{-1}$) absorptions starting at $36\,947 \pm 50\text{ cm}^{-1}$ in C_6H_6 and at $37\,147 \pm 50\text{ cm}^{-1}$ in C_6D_6 . The broad absorptions correlate reasonably well with the features assigned to the second triplet in the O_2 -perturbation experiments. The first triplet is too weak to be observed in the long-crystal experiments. The position of the second triplet lies about 3000 cm^{-1} above that given by the Pariser-Parr calculation. This places the second triplet about nine-tenths rather than half of the distance from the lowest triplet to the lowest excited singlet.

INTRODUCTION

FOR many years the location of the second triplet state of benzene has been the object of much research, both theoretical and experimental.^{1,2} This intense interest has been generated by theoretical predictions, many and varied, of the energies of the excited states of aromatic hydrocarbons. All theoretical predictions identify the second triplet of benzene as the orbitally degenerate ${}^3E_{1u}$ state, and most of these predictions place the second triplet in the experimentally accessible region between the lowest triplet and the

lowest singlet.³ Semiempirical theories^{4,5} for these energy levels, which are based partially on spectral data, have seemed fairly promising. Thus it becomes of great importance to fix experimentally as many of the states of the lowest π - π^* manifold of benzene as possible. Up to now, all three singlet states, but only one triplet state, the lowest, have been identified.⁶

³ J. W. Moskowitz and M. P. Barnett, *J. Chem. Phys.* **39**, 1557 (1963); note that the use of a Goepfert-Mayer-Sklar core, accurate integrals, and extensive configuration interaction (Column *e* of Table I in this reference) places the second triplet above the first singlet.

⁴ R. Pariser and R. G. Parr, *J. Chem. Phys.* **21**, 466, 767 (1953).

⁵ H. E. Simmons, *J. Chem. Phys.* **40**, 3554 (1964).

⁶ G. W. Robinson, in *Methods of Experimental Physics*, edited by D. Williams (Academic Press Inc., New York, 1962), Vol. 3, p. 244.

* Supported in part by the U. S. Atomic Energy Commission. † Contribution No. 3211.

¹ J. R. Platt, *J. Mol. Spectry.* **9**, 288 (1962).

² D. R. Kearns, *J. Chem. Phys.* **36**, 1608 (1962).

DETECTION OF HIGHER TRIPLETS IN AROMATIC HYDROCARBONS

Phosphorescence

The lowest triplet can be studied in emission (phosphorescence) since it can be populated by excitation into nearby singlets. The lowest triplet is the lowest excited state, and, even though the radiative transition probability for the emission process is extremely small, competing nonradiative processes are themselves sufficiently slow to allow detectable quantum yields of light emission. For higher triplets, however, nonradiative paths to lower triplets are so much more important than the highly forbidden radiative process back to the ground singlet state that quantum yields are vanishingly small.

Triplet-Triplet Absorption

Triplet-triplet absorption from the long-lived, lowest triplet state of benzene could yield information about higher triplets, just as it has done in other aromatic hydrocarbons.⁷ However, $g \leftrightarrow u$ selection rules would not allow strong absorption into the nearby higher triplets since these have the same parity as the lowest triplet. This selection rule is weakened if the molecule distorts and its center of symmetry is lost. The distortion may occur through molecular vibrations, solvent effects, or simply because the equilibrium configuration for the triplet is distorted. In any case the transition is not expected to be strong. This fact combined with the inconveniently low energy of the transition would cause detection of the second triplet in benzene by this technique to be difficult. Actually no evidence has yet been obtained for any kind of triplet-triplet absorption in benzene.⁸

Heavy-Atom Perturbations

Passing over phosphorescence and triplet-triplet absorption, there remain three other experimental methods which can be used to study the second triplet state of benzene: heavy-atom perturbation, O₂ perturbation,

⁷ G. Porter and M. W. Windsor, Proc. Roy. Soc. (London) A245, 238 (1958).

⁸ The most favorable system in which to search for the triplet-triplet absorption is probably the C₆D₆-argon system at 4.2°K. Here a gaseous mixture of less than 1% C₆D₆ with argon is condensed on a liquid-helium-cooled surface. The ³B_{1u} lifetime in this system is nearly 30 sec, and all observed vibronic components are quite sharp. The study in our laboratory of this system using intense, steady illumination for triplet excitation plus a continuum for detection of triplet-triplet absorption showed negative results for the region 2650-7000 Å. In contrast, using the same technique for naphthalene, the ³B_{1u} ← ³B_{2u} absorption in the 4000-Å region could be detected routinely with much greater intensity than that of the 3200-Å ¹B_{2u} ← ¹A_{1g} absorption even though the latter transition involves the ground state! No attempt was made to search for the ³E_{1u} ← ³B_{1u} transition of benzene which, according to results presented in this paper, should have its origin near 1.5μ.

and direct unperturbed absorption studies. Heavy-atom perturbations can arise from the environment or from substituents. Assuming the theoretical ideas of Robinson⁹ concerning environmental heavy-atom perturbations to be correct, perturbed oscillator strengths of not much more than $f \approx 10^{-7}$ may be obtained from solvent perturbations.¹⁰ If the heavy atom is chemically substituted onto the benzene ring, much larger oscillator strengths may result.¹¹ Even though future work may concern pure-crystal studies at 4.2°K of benzenes containing heavy-atom substituents, the primary interest in this paper revolves about the second triplet of benzene itself or of externally perturbed benzene.

Unperturbed Absorption

The experimental value of the oscillator strength for the spin and orbitally forbidden transition ³B_{1u} ← ¹A_{1g} (the first triplet) is $f \approx 10^{-10}$. This value has been derived from phosphorescence-lifetime measurements^{9,12} on both C₆H₆ and C₆D₆ combined with the accurate quantum-yield results of Lim.¹³ Purely theoretical values¹⁴ of 10^{-9} - 10^{-10} for the oscillator strength of the spin-forbidden but orbitally allowed second-triplet transition therefore seem too small. Such calculations may be plagued by cancellation effects in the spin-orbit energy of aromatics,¹⁵ in which case small wavefunction

⁹ G. W. Robinson, J. Mol. Spectry, 6, 58 (1961).

¹⁰ See Ref. 9, pp. 71-77. It is envisioned that the heavy-atom enhancement is caused by weak exchange interactions that couple the triplet state of the molecule to a Russell-Saunders triplet component of the electronically excited heavy-atom perturber. The triplet component of the perturber is in turn coupled to the singlet component of the perturber through strong spin-orbit mixing. In this manner the triplet state of the perturbed molecule borrows some singlet character from the perturber. For heavy-rare-gas perturbations, second-order perturbation theory yields,

$$f_p = [z\delta^2\zeta^2/2(F_0 - \bar{E}_T)^4] (\bar{E}_T/F_0)f_r$$

for the perturbed oscillator strength caused by the lowest ³P₁, ¹P₁ pair of the rare gas. Here z is the coordination number of solvent atoms around the perturbed molecule, δ is the electrostatic "excitation transfer" matrix element which is of the exchange type, ζ is the spin-orbit coupling constant for the ¹P₁ and ³P₁ states of the rare gas, F_0 is the term value for the rare gas, \bar{E}_T is the average triplet-state energy of the perturbed molecule, and f_r is the oscillator strength for the rare gas. A summation of such terms should be made over all perturbing states. For the most effective rare-gas perturber, solid xenon, the observed f_p for benzene is roughly 2.5×10^{-8} compared with the unperturbed value $f \approx 10^{-10}$. Here $z \approx 10$, $\delta \approx 50 \text{ cm}^{-1}$, $\zeta = -6086 \text{ cm}^{-1}$, $F_0 = 71\,095 \text{ cm}^{-1}$, and $\bar{E}_T \approx 29\,800$ (see Table II of Ref. 9). Neglecting other states as a first crude approximation, a rare-gas ¹P₁ ← ¹S₀ oscillator strength of $f_r \approx 0.4$ would be required to explain the experimental result. This is a very reasonable value for f_r . To find a "clean" perturber which would push the perturbed oscillator strength to a factor of, say, more than 100 of what it is in xenon, would be difficult.

¹¹ A chemically bound heavy-atom substituent is expected to yield a δ which is 10-100 times larger than that for an intermolecularly bound entity.

¹² M. R. Wright, R. P. Frosch, and G. W. Robinson, J. Chem. Phys. 33, 934 (1960).

¹³ E. C. Lim, J. Chem. Phys. 36, 3497 (1962).

¹⁴ E. Clementi, J. Mol. Spectry, 6, 497 (1961).

¹⁵ D. S. McClure, J. Chem. Phys. 20, 682 (1952). Deviation of the molecular eigenfunction from a $2p$ (carbon) representation in the D_{6h} molecule or in a distorted form of the molecule would cause the cancellation to be inexact.

errors would give rise to serious errors in the oscillator strengths. Semiempirical estimates can, however, be made and are probably more reliable. For example, assume that the primary singlet-triplet mixing mechanism is spin-orbit coupling between ${}^1E_{1u}$ and ${}^3E_{1u}$ with further vibronic coupling between ${}^3E_{1u}$ and ${}^3B_{1u}$.¹⁶ The vibronic coupling constants for benzene singlets can be computed from the observed oscillator strengths and excitation energies for the ${}^1E_{1u}$, ${}^1B_{1u}$, ${}^1B_{2u} \leftarrow {}^1A_{1g}$ transitions.⁸ One obtains $\langle {}^1E_{1u} | {}^1B_{1u} \rangle \approx 2000 \text{ cm}^{-1}$ and $\langle {}^1E_{1u} | {}^1B_{2u} \rangle \approx 800 \text{ cm}^{-1}$. Assuming the same kind of values hold in the triplet manifold and taking the energy separation between the ${}^3B_{1u}$ and ${}^3E_{1u}$ states to be roughly 7000 cm^{-1} , one finds that absorption into the ${}^3E_{1u}$ state should be from 12–75 times more intense than absorption into the ${}^3B_{1u}$ state.

It has been estimated that well over a meter of path length of liquid benzene would be required for the detection of the unperturbed first triplet transition.⁹ According to the above semiempirical estimate, the ${}^3E_{1u} \leftarrow {}^1A_{1g}$ transition would presumably require 12–75 times less path, providing the line breadths were comparable. In such long paths of benzene, impurity absorption and hot-band structure from nearby intense singlet-singlet transitions become dominant. The hot-band structure is an especially severe problem when searching for the second triplet of benzene, since this state lies virtually in the shadow of the first singlet. The hot-band structure can be eliminated completely by working at liquid-helium temperatures.

The sharpening of structure is an added bonus at these low temperatures. Spectral line sharpening increases the chance of observing weak transitions. For instance, consider the oscillator strength for a transition

$$f = 4.3 \times 10^{-9} \int \epsilon_{\nu} d\nu, \quad (1)$$

where the integration is carried out over the extinction coefficient for all vibronic components, the units of ν being cm^{-1} . Taking a Gaussian line shape for each of m vibronic components, assumed for simplicity all to have equal intensity, one has⁹

$$f = (4.3 \times 10^{-9}) (m) (1.06 \epsilon_{\text{max}} \Delta\nu_{\frac{1}{2}}), \quad (2)$$

where $\Delta\nu_{\frac{1}{2}}$ is the width (in cm^{-1}) at half-maximum of each component, and ϵ_{max} is the extinction coefficient at maximum absorption. If half of the incident light is absorbed at the maximum extinction, detection of the absorption is well above threshold. In that case the required path length in centimeters is given by,

$$l(\text{cm}) = 1.4 \times 10^{-9} (m \Delta\nu_{\frac{1}{2}} / C f), \quad (3)$$

¹⁶ A. C. Albrecht, *J. Chem. Phys.* **33**, 156, 169 (1960); **38**, 354 (1963).

where C is the concentration of the absorber in moles per liter.

There are about five intense components in the benzene ${}^1B_{2u} \leftarrow {}^1A_{1g}$ absorption spectrum. Assume the same holds true for the triplets; thus $m \approx 5$. In pure crystalline benzene $C \approx 12$, and for the benzene transitions thus far observed at 4.2°K , the narrowest absorptions have $\Delta\nu_{\frac{1}{2}} \approx 2 \pm 1 \text{ cm}^{-1}$. This means that a path length of about 5–20 cm would be necessary to give $(I/I_0)_{\text{max}} = 0.5$ for absorption into the first triplet providing the absorption components were sharp. At room temperature in the liquid, the $\Delta\nu_{\frac{1}{2}}$ of each of the five most intense components is around 500 cm^{-1} , and Eq. (3) yields a path length of 30 m.¹⁷ This simple estimate illustrates the great advantages of working at low temperatures where the lines are of minimum width. For the second triplet, as noted earlier, one expects an increase of around one to two orders of magnitude in the oscillator strength compared with that of the first triplet. Thus it would seem to be a relatively easy matter to detect the second triplet in long-path absorption at low temperatures. It will be seen, however, that line broadening substantially lessens the ease with which the absorption can be detected.

O₂ Enhancement

In our initial search for the second triplet state of benzene, the method of O₂ enhancement¹⁸ was decided upon because of the extremely small oscillator strengths for unperturbed, multiplicity-forbidden transitions in aromatic hydrocarbons. In the present work, the O₂-perturbation method has been extended to low temperature in order to sharpen structure and to remove hot-band interference from the nearby ${}^1B_{2u}$ state. A perturbed oscillator strength of 10^{-5} would allow detection of the triplets in 0.01-cm paths of solid benzene even though the respective $\Delta\nu_{\frac{1}{2}}$ were as broad as 150 cm^{-1} . Such paths lengths can easily be obtained through deposition techniques.⁹ The O₂-perturbation method, while yielding broad absorption lines and inaccurate vibrational spacings, would fix, within experimental accuracy, the position of the (0–0) band for the high triplets of aromatic hydrocarbons.

EXPERIMENTAL

Purification of Benzene

In the study of emission spectra or weak absorption spectra of organic molecules, the question of chemical

¹⁷ An earlier estimate of 1.5 m by Robinson, Ref. 5, was based on a detection threshold suggested by Craig *et al.*, *J. Chem. Phys.* **29**, 974 (1958). It is felt that for the broad spectra, on top of a rapidly rising background absorption, such a threshold is unrealistic. The 30-m value above, it should be stressed, is not a threshold value. It is the path at which $(I/I_0)_{\text{max}} = 0.5$.

¹⁸ D. F. Evans, *J. Chem. Soc.* 1957, 1351

purity must always be carefully considered. For this reason a section devoted to the benzene purification methods used in this work seems appropriate.

Sources of the raw starting material were as follows. The C_6H_6 was obtained from three different sources: from the Phillips Petroleum Company, from D. R. Davis of the Chemistry Department, UCLA, and from the National Bureau of Standards. Two different samples of Phillips research-grade benzene were employed, one sample stated to have 99.93 mole % purity and another reportedly being 99.89 mole % pure. This material is furnished in capped bottles and is therefore air contaminated. It is stated that toluene is the major impurity, but it has been reported that about half of the impurity is water.¹⁹ The sample from UCLA had been twice purified by vapor-phase chromatography, degassed, and vacuum sublimed into a tube which was then sealed under vacuum. The NBS sample was prepared by carrying out a large number of careful recrystallizations using the Phillips research-grade benzene as starting material. Freezing-point data were used to set the purity level of the NBS benzene at 99.999 mole %.

Long-crystal absorption spectra provide a sensitive test for spectroscopic impurities, i.e., those impurities which alter the absorption or emission spectrum of an otherwise pure material. If the absorption spectrum of the contaminant is sharp, and its oscillator strength is high, impurity levels in the 10^{-7} – 10^{-10} -mole fraction range can be detected in a 5-cm path of crystalline benzene.²⁰ Because of extensive impurity absorption, in none of the three types of raw starting material mentioned above was it possible to get sufficient radiation through a 5-cm crystal to study absorption in the 2650–2800-Å region! A series of experiments on 2-cm crystals was therefore carried out to determine the nature of these contaminants. The UCLA sample was by far the most inferior, showing strong, broad absorption well to the long wavelength side of 3000 Å, and perhaps indicating the inadequacy of VPC purification for the removal of trace impurities. The major spectroscopic impurity in both the NBS sample and the Phillips sample was found to be phenol. An estimate made from absorption intensity indicated that the NBS sample contained 10^{-6} parts of phenol and little else that was spectroscopically observable. Interestingly enough, the Phillips research-grade benzene showed the smallest amount of impurity absorption. However, a wide variety of chemical impurities seemed to be present in the Phillips samples. Again, the major spectroscopic impurity was phenol, but it was present

to only about $\frac{1}{2}$ the extent of that in the NBS sample. A broad absorption band near 2690 Å is perhaps due to monochlorobenzene, while an underlying, nearly continuous absorption might be caused by toluene plus other unidentified impurities in the mole-fraction range 10^{-5} – 10^{-6} .

The C_6D_6 was obtained from Merck, Sharp & Dohme, of Canada, Ltd. It was said to be 99.5 at. % isotopically pure. The chemical purity was much like that of the NBS C_6H_6 sample, showing a mole fraction of about 10^{-5} perdeuterophenol as the major spectroscopic impurity.

The occurrence of phenol as a trace impurity in benzene has been noted previously.²¹ Its wide occurrence suggests that benzene may react with O_2 from the atmosphere. The reaction must be autoinhibited, however, since large amounts of phenol never seem to be produced. Care must therefore be exercised when handling high-purity benzene, just as it must be for higher aromatic homologs, so as not to allow atmospheric contamination.

It should be stressed that impurities at the concentration levels existing in the Phillips research-grade or NBS C_6H_6 , or the Merck C_6D_6 caused no problems for sample thicknesses up to about 0.2 mm. That is, in the absence of O_2 , only extremely weak impurity absorption could be detected in such samples at wavelengths through the near ultraviolet all the way down to the benzene cutoff at 2650 Å. Certain spectra appeared when 2% O_2 was present. They are discussed more fully later on.

For spectroscopic investigation of 5-cm benzene crystals much better purity is required than exhibited by any of the "raw starting materials." The benzene used in the long-crystal experiments is purified in the following manner. From the beginning of the process until after the crystal is grown, the benzene is kept in a vacuum system. A schematic diagram of the apparatus is shown in Fig. 1. The vacuum system is isolated from the oil diffusion and mechanical pumps by a $\frac{1}{2}$ -in. Kerotest metal valve (a) having a Teflon gasket. The benzene is transferred from a breakseal tube (b) to a vessel (c) where it is dried over vacuum distilled potassium. It is then degassed and transferred by two vacuum distillations through (c_1) to a vessel (i) mirrored with vacuum-distilled high-purity cesium (j). After the initial reaction, the sample is degassed and the cesium reaction vessel is sealed off at the constriction (f_5) from the rest of the vacuum system. The benzene is then refluxed over the cesium at about 100°C for 1 h. Conditions very much more severe than these were found to degrade the benzene and produce a large amount of undesirable impurity absorption. During the cesium refluxing, the parts of the system previously used are "pulled off" under vacuum at the constrictions (f_1), (f_2), and (f_3). The remainder of the

¹⁹ International Union of Pure and Applied Chemistry, Commission on Physico-Chemical Data and Standards, "Cooperative Determination of Purity by Thermal Methods," Report of the Organizing Committee, July 14, 1961, Vol. I.

²⁰ For example, 0.1% phenol can easily be detected as an impurity in a 10- μ -thick crystal of benzene. For a 5-cm crystal, which is 5000 times thicker, 2×10^{-7} parts of phenol would be easily detected. The oscillator strength of the phenol transition is roughly 0.03.

²¹ V. L. Broude, Soviet Phys.—Uspekhi 4, 584 (1962) [Usp. Fiz. Nauk 74, 577 (1961)].

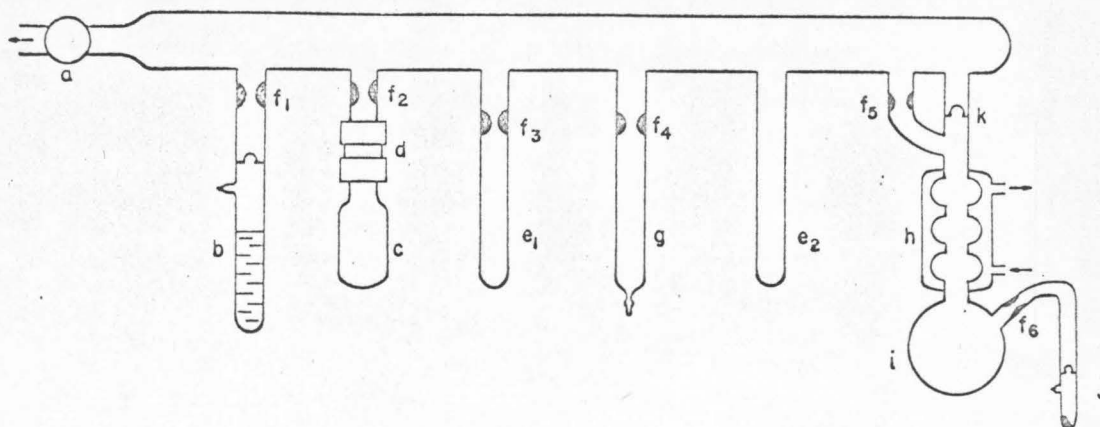


FIG. 1. Benzene purification manifold. (a) Kerotest (Kerotest, Inc., Pittsburgh, Pennsylvania) metal valve to cold traps, gauges, and oil-diffusion pump. (b) Benzene to be purified. (c) Potassium mirrored drying vessel. (d) Swagelok union, $\frac{1}{2}$ in., (Crawford Fitting Company, Cleveland, Ohio) for adding potassium. (e) Receiving vessel for primary vacuum distillations. (f) Constrictions for pulling off under vacuum. (g) Bridgman crystal-growing tube (14 mm \times 10 cm). (h) Water-cooled condenser. (i) Cesium reflux vessel (\sim 30 cc). (j) Cesium. (k) Breakseal.

system is thoroughly flamed until the limiting vacuum of 2×10^{-6} mm of Hg is attained. By means of a breakseal (k), the cesium vessel is reopened to the main vacuum manifold. The benzene is degassed thoroughly, and by two vacuum distillations through the intermediate tube (e_2) it is transferred into a Bridgman crystal-growing tube (g).²² It is then cooled to liquid-nitrogen temperature, and the tube is pulled off at (f_4). A 5-cm crystal purified in this way showed little or no absorption throughout the ultraviolet down to the 2700-Å region. In particular the mole fraction of phenol was estimated to be less than 10^{-8} !

Benzene- O_2 Experiments

The central idea here is to observe the spectrum of a mixture of benzene and oxygen in the region just to the long-wavelength side of the singlet-singlet system (${}^1B_{1u} \leftarrow {}^1A_{1g}$; $f \approx 0.0014$) whose origin lies near 2650 Å. Since thin (< 0.2 -mm) samples are used, purity is not a problem for the O_2 -perturbed experiments. Phillips research-grade benzene, degassed but without further purification, was therefore used for these experiments.

As mentioned earlier, low temperatures are required to eliminate hot-band structure associated with the relatively much stronger singlet-singlet system.²³ Liquid-helium temperature is used in all of

²² D. Fox, M. M. Labes, and A. Weissburger, *Physics and Chemistry of the Organic Solid State* (Interscience, Publishers Inc., New York, 1963) p. 267.

²³ For example, according to this paper, the separation of the unperturbed (0, 0) bands of the first singlet and the second triplet is only about 900 cm^{-1} . At room temperature, hot-band structure from the first singlet in the vicinity of the (0, 0) band of the second triplet is therefore expected to be down in intensity by only a factor of 150. Since even under O_2 perturbation the second triplet is at least 100 times weaker than the first singlet, there would be no chance whatsoever of detecting the second triplet at room temperature. The very highest temperature at which one can expect to separate the second triplet from the hot-band structure of the first singlet is 100°K , and much lower temperatures are to be preferred.

the experiments reported here. Another advantage of low temperatures, the sharpening of band structure, is not realized to its fullest extent in the O_2 -perturbation experiments.

Because of the broad structure, a spectrograph of relatively low resolution is adequate for this portion of the work. The instrument used was a Bausch & Lomb medium quartz prism spectrograph. A 150-W Xe lamp was used as source for the absorption studies, while a Bausch & Lomb $f/3.5$ grating monochromator, in conjunction with the Xe lamp, was used to excite emission. Combinations of bromine gas, Corning Glass #9863, and aqueous nickel sulfate filters were used to reduce stray light from longer wavelength radiation.

Some earlier experiments in our laboratory attempted to detect the second triplet state of benzene by depositing at liquid-helium temperature benzene with excess oxygen; i.e., benzene in an oxygen "matrix." Only the well-known visible and near-ultraviolet bands of condensed oxygen²⁴ were discernible. Besides, in oxygen-rich systems it is very difficult, because of scattering, to get light through the thick deposits necessary for such low concentrations of benzene.

To avoid the problem of O_2 absorption which is caused by O_2 - O_2 interactions and simultaneously to increase the path length of benzene, a mixture rich in benzene containing a few percent O_2 was used. In order for most of the benzene molecules in the solid to have nearest-neighbor contact with at least one oxygen molecule, an optimum concentration of oxygen would lie perhaps in the 5%-10% range. However, the maximum amount which was actually used was 2%, since higher concentrations seem to give deposits which strongly scatter the light.

The gaseous mixture containing 98% benzene and 2% oxygen was deposited on a window cooled to liquid-

²⁴ L. J. Schoen and H. P. Broida, *J. Chem. Phys.* **32**, 1184 (1960).

TABLE I. First and second triplet-state energies (in cm^{-1}) of C_6H_6 and C_6D_6 in O_2 -perturbed systems and pure crystals.

	O_2 perturbed		Benzene crystals	
	C_6H_6^a	C_6D_6	C_6H_6	C_6D_6
$^3B_{1u}$	29 674 \pm 25	29 851 \pm 25	29 657.1 ^b	29 855.1 ^c
	30 581	30 628		
	31 446	31 446		
	32 258	32 362		
$^3E_{1u}$	36 560 \pm 50	36 784 \pm 50	36 947 \pm 50	37 147 \pm 50
	37 170	37 495	37 496	not identified

^a Evans¹⁸ values in the gas phase for this system are 29 440, 30 350, 31 250, and 32 100 cm^{-1} .

^b G. C. Nieman, Ph.D. thesis, California Institute of Technology, 1965, observed in 1% C_6H_6 in 99% C_6D_6 mixed-crystal phosphorescence. The corresponding value of the (0, 0) band position for the $^3B_{1u} \rightarrow ^1A_{1g}$ transition is 37 855 cm^{-1} . It should be noted that the pure-crystal value would be lower by about 50 cm^{-1} [see G. C. Nieman and C. W. Robinson, J. Chem. Phys. 39, 1298 (1963)].

^c Obtained from C_6H_6 value by adding 198 cm^{-1} [see Ref. (b)].

helium temperature in a manner similar to that described by Robinson.⁹ Because of light scattering, the maximum deposit thicknesses that could be used were somewhere around 200 μ . This value was estimated from absorption intensities of the singlet-singlet systems of pure benzene and of a phenol-in-benzene standard sample. It is known that when pure benzene is deposited from the vapor phase at 4.2°K, the electronic spectrum appears very broad compared with the spectrum of a crystal of benzene more carefully prepared. It was discovered that benzene deposited at liquid-nitrogen temperature and then cooled to 4.2°K shows a sharp spectrum, just as in the case of a good crystal. Unfortunately, attempts revealed that little oxygen could be trapped in the benzene under these conditions. Furthermore, strong fluorescence emission from crystalline regions in this deposit masked any weak absorption bands which otherwise might have appeared. Therefore, this technique was abandoned in favor of the 4.2°K deposition experiments. No fluorescence occurred from the 4.2°K depositions containing O_2 . Perhaps deposit temperatures intermediate between 4.2° and 77°K would have been optimum, but no attempt was made to check this point.

Long-Crystal Experiments

Thick crystals of benzene are prepared in the following manner. The crystal-growing tube containing the ultrapure benzene is lowered into a -20°C cold room through a temperature gradient of 30°C/in. at a rate of $\frac{1}{8}$ th in./h. The over-all temperature differential is about 50°C. The crystal is removed from the growing tube and both ends are cut off with a hot wire. The crystal is then polished with a warm brass block and

the 5-cm sample is placed in a loosely fitting Teflon holder, the crystal being kept in an inert atmosphere during all these manipulations. At this stage the crystal is completely transparent with only minor imperfections. During radiation cooling in two stages, first to 77°K, then to 4.2°K, the crystals become somewhat cracked. However, they remain fairly translucent in spite of this difficulty.

All spectra are taken at 4.2°K with the sample in a horizontal position. The optical arrangement and light sources were the same as before. However, a 2-m grating spectrograph having a resolution of about 35 000 was utilized in place of the low-resolution prism instrument in the event that sharp structure, such as factor-group structure, exists in the $^3E_{1u} \leftarrow ^1A_{1g}$ transition in the crystal.

IDENTIFICATION OF SECOND-TRIPLET ABSORPTION

There are three major problems in determining a weak absorption such as the second triplet of benzene. The absorption can be due to an impurity; a photoproduct can be produced during the experiment; or there can be broad but structured emission whose inverse may appear to be weak absorption. The experimental procedure is aimed at the elimination of these possibilities.

Benzene- O_2 System

The benzene- O_2 mixtures were prepared in the manner described in a previous section. A summary of absorption spectra obtained from these mixtures is presented in Table I. It is gratifying that the first triplet ($^3B_{1u}$) is easily detected by this technique. In addition to the first-triplet bands, two broad ($\sim 300\text{-cm}^{-1}$) features in the 36 600- cm^{-1} region of the spectrum occur under O_2 perturbation. Microdensitometer

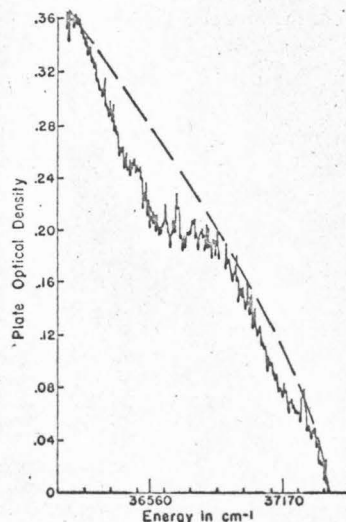


FIG. 2. Densitometer tracing of O_2 -perturbed second triplet of benzene; ---, assumed base line.

tracings of these features are depicted in Fig. 2. It is these features which are attributed to the second triplet (${}^3E_{1u}$). No absorption except that assigned to the first- and second-triplet bands occurs for wavelengths longer than the benzene first-singlet cutoff near 2650 Å.

After first observing the absorption thought to be caused by the second triplet, the system was completely taken apart and cleaned, and the experiment was repeated in the clean system. The absorption appeared as before. Then a completely different deposit Dewar (one previously used only for NH_3 , ND_3 , NH_2D , etc., and HCl and DCl) was used with an entirely new glass manifold. Again the same results were obtained.

To check for an impurity in the benzene, two different sources of C_6H_6 , the Phillips and the NBS, and one sample of C_6D_6 , the Merck, were tried, all giving consistent, corroborating results. An absorption spectrum of 1% phenol in C_6H_6 was taken, the second-triplet absorption was compared with this, and the two were found to be entirely different.

Spraying on benzene without O_2 showed absolutely no absorption for $\lambda > 2650$ Å. This fact combined with the simultaneous observation, when O_2 is added, of the well-known first-triplet absorption and the 36 600- cm^{-1} bands provides fairly convincing evidence for the existence of the second triplet in the 36 600- cm^{-1} region.

Three different supplies of O_2 were used; two types of Linde high-purity O_2 and an O_2 of standard purity. No evidence for the absorption spectrum of condensed O_2 was found.

The possibility of a photoproduct being formed during the experiment was also explored. Plates were taken of the O_2 -benzene mixtures after sample exposure times of from less than 1 sec to 1 h using a 150-W Xe lamp, and the absorption intensity was not seen to increase or decrease. No new absorptions were produced. Furthermore, varying the light intensity over a rather wide range by means of filters and a monochromator, showed no detectable change in the observed absorptions. This fact indicates that the absorptions are not caused by transitory photoproducts. The possibility that the absorption is an artifact due to broad emission was eliminated by using a Bausch & Lomb $f/3.5$ grating monochromator with a 150-W Xe source. Fluorescence spectra using 252- $\text{m}\mu$ exciting light (bandpass of 200 Å) from this monochromator were searched for. In a $\frac{1}{2}$ -h exposure, no emission in the region of interest was observed. Typical absorption exposure times are of the order of 1 sec, so we have convinced ourselves that neither photoproducts nor stray emission can account for the 36 600- cm^{-1} bands.

Based on deposit times and bandwidths, it is possible to determine the relative perturbed intensities of the two triplet states. Our estimates give

$$I({}^3E_{1u}):I({}^3B_{1u}) \approx 10-100 \quad (\text{O}_2 \text{ perturbed}).$$

It is interesting, and perhaps even surprising, that the ratio of the perturbed intensities is so similar to that expected on the basis of our earlier semiempirical estimates for the unperturbed intensities.

Crystalline-Benzene Experiments

As mentioned earlier, impurities are of much more concern in this system than in the previous one because of the long path length required for detection of the weak, unperturbed singlet-triplet absorption. It can be estimated that a sharp-lined impurity absorption with an oscillator strength of $f \approx 0.1-1.0$ could be detected for an impurity concentration of 1 part in 10^{10} ! For this reason, a positive assignment of an absorption caused by the ${}^3E_{1u} \leftarrow {}^1A_{1g}$ transition without a knowledge of detailed vibronic structure in the spectrum or without the O_2 -perturbation results would be impossible. Since the ${}^3E_{1u}$ state is so close to the relatively strong ${}^1B_{2u}$ state, little vibronic structure can be observed. Thus one must rely on a correspondence between any observed bands and the O_2 -perturbed spectrum.

Several absorptions, some sharp and some broad, were observed in the 2650-to-2800-Å region in both C_6H_6 and C_6D_6 . However, only two broad absorption features could be consistently identified in both samples, considering the expected perdeutero shift of about 200 cm^{-1} to higher energy. The intensity of these two features has always been observed to follow, in an expected manner, any changes in benzene path length. Furthermore, the intensity of these bands was found not to be dependent on the extent of purification of the sample, while the intensity of impurity lines change according to the purification method used. The most extensive purification was obtained with cesium refluxing, as described earlier in this paper. For one 5-cm crystal of C_6H_6 so purified, all impurity absorption was reduced to below or barely above the level of detection, while the two broad absorptions showed the same intensity as in less well purified samples.

The broad absorptions, which appear to belong to benzene itself, lie at $36\,947 \pm 50 \text{ cm}^{-1}$, and $37\,496 \pm 50 \text{ cm}^{-1}$ in C_6H_6 , and at $37\,147 \pm 50 \text{ cm}^{-1}$ in C_6D_6 . The second absorption feature in C_6D_6 was obviously present but was strongly overlapped by a series of sharp impurity lines and was therefore difficult to measure. The impurity was perhaps an isotopic or a chemical impurity that was not completely removed by the purification technique.

The broadness of the absorption was disappointing and somewhat unexpected at first, considering the sharpness of emission and absorption lines in other crystalline-benzene transitions. After a little reflection, however, one can find many mechanisms that could broaden the ${}^3E_{1u} \leftarrow {}^1A_{1g}$ transition. For instance, it is certain that the orbital degeneracy of the ${}^3E_{1u}$ state is removed by the crystalline field whose symmetry is

only C_1 . (This effect may be called *electronic site-group splitting*.) Further contributions to the degeneracy removal from the Jahn-Teller effect may also be important. The removal of this twofold degeneracy on top of the expected 100–200 cm^{-1} factor-group splitting²⁵ divides the (0–0) band and other totally symmetric vibronic bands into eight components, transitions to six of which are allowed. It is noteworthy that the observed 150- cm^{-1} total breadth of each band is of reasonable magnitude on the basis of such contributions. Further line-broadening mechanisms must be postulated, however, in order to explain the complete lack of resolution of any of this fine structure, since, ordinarily, individual components are not more than about 5–10 cm^{-1} broad, and the instrumental resolving power of the 2-m spectrograph used is not a limiting factor. The nature of this extra broadening is not known at the present time, but crystal strain to which the site-group splitting is sensitive may be responsible.

Estimating from the plates that $(I_0/I)_{\text{max}}$ for the second-triplet absorption bands is about 1.3 and applying Eq. (2) yields an oscillator strength of

$$f(^3E_{1u} \leftarrow ^1A_{1g}) \approx 7 \times 10^{-9} \quad (\text{unperturbed}).$$

It has been assumed that $\Delta\nu_3 \approx 150 \text{ cm}^{-1}$ and that $m=5$, but that three of the bands are overlapped by the singlet. The oscillator strength so obtained is wholly reasonable.

In all fairness it must be pointed out that the absorptions observed in the long-crystal experiments, in spite of all our precautions, could still be due to impurities. If this were the case, one would have to conclude that either the oscillator strength and breadth of the $^3E_{1u} \leftarrow ^1A_{1g}$ bands are such that the absorption could not be observed in crystals of this length, or that the transition energy lies above that of the first excited singlet. However, the correlation between the long-crystal absorptions and the O_2 -perturbed bands makes the second-triplet identification plausible. The $^3B_{1u}$ state was never observed in these long crystals. This fact is consistent with the oscillator strength $f \approx 10^{-10}$ for this transition.

SUMMARY

The following constitutes a summary of the reasons that the absorption bands in C_6H_6 and C_6D_6 , whose origins lie, respectively, at 36 560 and 36 784 cm^{-1} in the O_2 -perturbed system and at 36 947 and 37 147 cm^{-1} in the pure crystals, are believed to belong to the second-triplet ($^3E_{1u}$) transitions in these molecules.

(1) Evidence that the bands are not caused by impurity absorptions.

(a) The bands in C_6D_6 are shifted $220 \pm 50 \text{ cm}^{-1}$ to higher energy from those in C_6H_6 . The size of the

shift compares reasonably well, considering the accuracy of the measurements, with the deuterium shift in the other benzene transitions. This is not a binding argument, however, since protonated vs deuterated chemical impurities may well behave in the same manner.

(b) The absorption was seen in two sources of C_6H_6 and a totally different source of C_6D_6 .

(c) Varying the source of O_2 produced no effect.

(d) *Except for the 5-cm crystals, the absorption is not seen without O_2 in the sample.* This is the case not only for a deposited sample but also for a 2-cm-thick crystal of C_6H_6 or C_6D_6 .

(e) After making various checks, the sample used in the O_2 -perturbation experiments was found to be much too thin to show impurity absorption from C_6H_6 , C_6D_6 , or O_2 .

(f) The O_2 -perturbed absorption was seen in two entirely different deposit systems.

(g) Varying the exposure time and the light intensity produced no change whatever in the observed spectra, indicating that photoproducts are not responsible for the absorption.

(2) After careful investigation, the possibility was eliminated that the weak, broad absorption is an artifact caused by the presence of broad emission.

(3) Absorption spectra of 5-cm crystals of ultrapure benzene indicate that the $^3E_{1u} \leftarrow ^1A_{1g}$ transition lies higher than 36 900 cm^{-1} providing its oscillator strength is of the expected magnitude.

(4) That this absorption is the second triplet is evidenced by the following facts:

(a) *In the O_2 -perturbed system, the second triplet and the first triplet were observed in all instances during the same experiment in the same sample, and with approximately constant relative intensities.*

(b) The relative intensities of the three absorptions ($^1B_{2u}$, $^3B_{1u}$, $^3E_{1u} \leftarrow ^1A_{1g}$) are roughly of the expected magnitude.

(c) The absorption is indeed O_2 enhanced. This meets a criterion for a multiplicity-forbidden transition.

(d) The position of the absorptions is reasonable.

CONCLUSIONS

In the past, the search for the second triplet of benzene has usually been carried out at room temperature and in the liquid phase,²⁶ using O_2 - and heavy-atom-perturbation methods.²⁷ In all of these attempts no great pains were taken to purify the benzene or the perturbers. It is obvious from the earlier discussion that experiments of this nature are not likely to give positive evidence about higher triplet states in benzene. Hot bands, impurities, and spreading out of intensity are just a few of the reasons that data from such experi-

²⁵ G. C. Nieman and G. W. Robinson, *J. Chem. Phys.* 39, 1298 (1963); E. R. Bernstein, S. D. Colson, R. Kopelman, and G. W. Robinson (to be published).

²⁶ A. C. Pitts, *J. Chem. Phys.* 18, 1416 (1950); J. S. Ham and K. Ruedenberg, *ibid.* 25, 1 (1956).

²⁷ For a general review of these experiments see Ref. 1.

ments are not definitive. Bands observed by Ham²⁸ at 77°K in a carbon tetrachloride glass have been assigned^{29,30} as the (0, 0) progression of the ${}^1B_{2u} \leftarrow {}^1A_{1g}$ transition intensified by solvent-solute interactions. We consider this assignment to be much more reasonable than the original suggestion that the Ham bands are the second triplet.

Even though positive identification of the broad absorptions observed in our 5-cm samples of pure benzene, as belonging to the ${}^3E_{1u} \leftarrow {}^1A_{1g}$ transition, is not possible, these experiments are very useful in placing a lower limit to the energy of this state. The ${}^3E_{1u}$ state of crystalline C_6H_6 cannot lie below 36 900 cm^{-1} . In the O_2 -perturbed C_6H_6 system no absorption (aside from the first triplet) was observed below 36 560 cm^{-1} . These results are consistent with the empirical lower limit of 37 000–38 000 cm^{-1} for the ${}^3E_{1u} \leftarrow {}^1A_{1g}$ transition as discussed by Platt.¹

Pariser-Parr theory⁴ places the position of maximum intensity of the ${}^3E_{1u} \leftarrow {}^1A_{1g}$ transition exactly halfway between the maxima of the ${}^3B_{1u} \leftarrow {}^1A_{1g}$ and the ${}^1B_{2u} \leftarrow {}^1A_{1g}$ transitions. Due to the lack of experimental data, these authors were forced to employ empirically evaluated integrals derived from the energies of observed singlet states to calculate triplet-state energies. There is no theoretical justification for this, since singlet and triplet wavefunctions, even though from a common configuration, are expected to require a different basis representation. The discrepancy between our experimental energy and that calculated for the ${}^3E_{1u}$ state on the basis of Pariser-Parr theory is about 3000 cm^{-1} . This value is based on (0, 0) band positions (see Table I) rather than on absorption maxima as specified in the theory, but for the states in question there should be no great difference.³¹ Thus, the second triplet lies

nearly $\frac{1}{10}$ rather than $\frac{1}{2}$ of the way from the lowest triplet to the lowest excited singlet state of benzene.

It should be noted that from our experiments no information can be obtained concerning the energy of the proposed O_2 -benzene charge-transfer states.²⁹ These states would have a continuous absorption spectrum and therefore could not be differentiated from light loss due to scattering in the deposit experiments.

Note added in proof: It is conceivable that the absorption observed in the 37 000- cm^{-1} region of the O_2 -perturbed system is due to the benzene- O_2 "double" transition [${}^3B_{1u} \leftarrow {}^1A_{1g}$] \leftarrow [${}^1A_{1g} \leftarrow {}^3\Sigma_g^-$]. Addition of the gas-phase value of the ${}^1\Delta_g \leftarrow {}^3\Sigma_g^-$ transition to the crystal-phase value of the ${}^3B_{1u} \leftarrow {}^1A_{1g}$ transition "predicts" the double transition to lie about 1000 cm^{-1} above that observed. This is not particularly close. Nevertheless, it would be unrealistic to exclude this as a possibility, considering the assumptions inherent in the prediction. Observing the transition using NO perturbation would eliminate this possibility. Deposit experiments were attempted in which the O_2 was replaced by NO. These proved to be unproductive as NO is a weaker perturber than O_2 , neither the first nor second triplet being observed. We are now working on new techniques that will hopefully yield long, transparent crystals of benzene containing NO. NO-benzene mixed crystals about 2 cm long have been produced, but so far have been so badly cracked that they are opaque in the 37 000- cm^{-1} region. The first triplet has, however, been detected in such crystals. We are also trying to grow crystals long enough to observe the first triplet (${}^3B_{1u} \leftarrow {}^1A_{1g}$) transition in the absence of external perturbations. We acknowledge B. Stevens of Sheffield University for suggesting the double transition to Robinson as a possible cause of the 37 000- cm^{-1} absorptions in the benzene- O_2 mixed crystal. It should not be forgotten, however, that similar absorptions have been seen in 5-cm crystals containing no O_2 where, of course, the double transition cannot occur.

ACKNOWLEDGMENTS

The many hours of discussion with and advice from Professor G. W. Robinson are greatly appreciated by the authors. Preliminary O_2 -perturbation work was done on this project by Mrs. Lelia Coyne.

²⁸ J. S. Ham, *J. Chem. Phys.* 21, 756 (1953).

²⁹ E. C. Lim and V. L. Kowalski, *J. Chem. Phys.* 36, 1729 (1962).

³⁰ N. S. Bayliss and L. Hulme, *Australian J. Chem.* 6, 257 (1953).

³¹ A recent theoretical calculation (Ref. 5) which employs more extensive configuration interaction within the framework of the Pariser-Parr theory, appears to give very good agreement with our experimental ${}^3E_{1u}$ energy. However, the calculated energies refer to intensity maxima. The theoretical (0-0) band position is 1000 to 2000 cm^{-1} lower than our experimental value. It should also be noted that "experimental values" for the ${}^3E_{1u}$ energy reported in Refs. 3 and 5 are not experimental values at all, only semiempirical estimates.

Observation of the Second Triplet of Solid Benzene Using NO Perturbation*

ELLIOT R. BERNSTEIN AND STEVEN D. COLSON

*Gates and Crellin Laboratories of Chemistry†
California Institute of Technology, Pasadena, California*

(Received 14 July 1966)

AS mentioned in our previous paper on the first and second triplets of solid benzene,¹ the absorptions observed in the 37 000-cm⁻¹ region under O₂ perturbation could conceivably be "due to the benzene-O₂ 'double' transition [³B_{1u} ¹Δ_g]←[¹A_{1g} ³Σ_g⁻]." To eliminate this possibility, benzene-NO mixed crystals have been grown and their spectra taken. The mixed crystals were prepared in the following manner: The benzene was purified as before and checked for purity by taking its spectrum. No impurity absorptions in the 37 000-cm⁻¹ region were observed in 2-cm-thick crystals at 4.2°K. The NO was purified by a series of vacuum sublimations until the originally multicolored solid was white. NO, thus purified and placed in a hydrocarbon glass at 77°K, shows no absorption in the 37 000-cm⁻¹ region. However, in the 40 000-cm⁻¹ region a strong cutoff was observed, believed to be caused by the γ bands of NO, indicating that NO had dissolved in the glass.

Several NO-benzene mixed crystals were prepared by loading a sample cell containing purified benzene with 10⁻¹ to 10⁻² liter·atm of the purified NO gas. Crystals were grown by lowering the cell at the rate of 1 mm/h through a temperature gradient of about 100°C/cm (10° to ~-100°C), and then directly into liquid N₂. This technique gives excellent pure benzene crystals

but the mixed crystals were highly cracked. The mixed crystals containing large amounts of NO were so cracked that only the (0-0) band of the first triplet absorption system could be seen. However, the crystals more dilute in NO were sufficiently less scattering to be investigated in the 37 000-cm⁻¹ region.

New absorptions are observed at 36 983±50 and 37 324±50 cm⁻¹. These are assigned to the second triplet transition (³E_{1u}←¹A_{1g}) of the perturbed solid benzene system. The reason for the difference between the energy of these absorptions and those observed under O₂ perturbation (36 560±50 and 37 170±50 cm⁻¹) is not obvious. It does not appear to be large enough to justify a new interpretation. It therefore seems improbable that the absorptions observed in the O₂-perturbed system are due to a benzene-O₂ "double" transition. The absorptions both in the benzene-O₂ and the benzene-NO systems in the 37 000-cm⁻¹ region are, as concluded earlier,¹ most likely caused by the perturbed second triplet of benzene.

The support and encouragement from Professor G. W. Robinson is gratefully acknowledged by the authors.

* Supported in part by the U.S. Atomic Energy Commission.

† Contribution No. 3395.

¹S. D. Colson and E. R. Bernstein, *J. Chem. Phys.* **43**, 2661 (1965).

APPENDIX

APPENDIX I

Discussion of experimental apparatus and procedures

A. The Dewar

At the time this investigation was begun, a versatile spectroscopic helium temperature dewar was not commercially available. Moreover, dewars in our laboratory were either quartz or Pyrex immersion dewars, or metal systems for deposition of gases. It was clear at this time that due to the problems involved with the transmission of infrared radiation, a metal dewar with windows must be developed that would allow samples to be both immersed in liquid helium and placed at the end of a helium cold finger. Thus the design of a new, and in many ways radical, dewar was undertaken. There were major design difficulties with the existing metal dewars in the laboratory at this time. For one, the soft solder joints were extremely prone to developing low temperature leaks which were difficult to locate and once these leaks were located, the dewar had to be completely disassembled to replace them. There was, of course, no guarantee that in so doing more leaks would not be created than were repaired. On the other hand, the Pyrex or quartz dewars were all of very small internal diameter so that only samples of approximately 15 mm O. D. could be used in them. Thus the three guiding principles in the construction of this new dewar were: to avoid soft solder joints wherever possible by the use of demountable indium flange seals and welds; to make the "cans" nest such that the dewar could be taken

apart at flanges for easy repair and interchange of internal helium cans (deposit, cold finger, or immersion); and finally to enlarge the inside diameter of the immersion can within the confines of the ~5 inch total outside diameter which allows the dewar to be placed into the sample compartment of a standard commercial infrared instrument (Beckman, in this case). The end result of these considerations is given in Figures 1, 2, and 3. All low temperature vacuum seals are either welds (for flange to tube seals) or indium pressure seals for the flanges. These are clearly indicated on the figures. The room temperatures seal between the top and the base was accomplished with a rubber "o"-ring. Such construction allows for the removal of the inside helium can and thus it can be readily interchanged with many other designs. The straight-through design of this can allows a 5.0 cm sample to easily pass into the optical path.

The dewar is evacuated through a 2 inch "gate valve" which allows for very fast pumping, not necessary for present operation, but a necessity in deposit systems. The dewar could easily be modified for use as a variable temperature deposit system with the proper feed-throughs fitted into the base and a new internal helium can. Such a helium can should have a bottle shape instead of the straight form design now used, as this would cut down the helium evaporation rate (1.5 l. lasts about 4 to 5 hours). Such a design change could potentially decrease the evaporation rate by probably a factor of two.

The vacuum sealing of the room temperature windows was accomplished by either rubber "o"-rings or various epoxy resins (see

Sec. Ic). Each technique has its advantages: the epoxy kept the windows on the dewar when it was assembled for the cold finger mode of operation while the "o"-ring technique required the windows to be held on with flanges; but, on the other hand, the epoxy was subject to mechanical shock which caused leaks after some time.

Operation of the dewar in the immersion mode is reasonably obvious and need not be discussed here in detail. The windows were sealed to the inside can in different ways (depending on the type of window) and will be discussed in the next section. It was possible to keep about 1.5 l. of either normal or superfluid helium for 4 to 5 hours under conditions of irradiation of the sample with infrared or ultraviolet radiation.

The dewar when operated with the cold finger can was a little more difficult to use. The problems stem from two causes: the dewar must be assembled free from water to be used in the infrared and to generally decrease sample scatter, and the sample, liquid benzene, is a high vapor pressure liquid at room temperature. The technical problems presented by these factors were or could have been eliminated in a few different ways; the exact choice of one method was arbitrary and dependent upon many variables. The solution to this problem centers around the sample holder. If this is vacuum tight, the dewar can be assembled at room temperature, evacuated without pumping away the sample, and then cooled down with liquid nitrogen. On the other hand, if the sample holder is not evacuable, the dewar must be flushed with dry N_2 , assembled cooled down and only after the sample is frozen can the dewar be evacuated. Both of these techniques have been employed

in sample preparation and while the first is more aesthetically pleasing both render the same final result — a polycrystalline sample of reasonable quality at 4.2°K.

A different approach (not employed in this work) is to place the dewar into the especially prepared port of a vacuum dry box. The entire system may then be evacuated to insure dryness. A crystalline (cold) sample may then be placed on the cold finger of the cooled dewar which is then assembled and further evacuated at its own pumping station. Such a procedure would allow single oriented crystals to be studied at helium temperature in this dewar.

B. Low Temperature Vacuum Seals for Various Windows:

The vacuum sealing of windows to metal at low temperature is an exceedingly burdensome problem in many instances. The difficulty is especially acute for the soft windows used in the infrared region of the spectrum 1.0 to 50.0 μ (10,000 to 200 cm^{-1}). The windows used in this investigation were BaF, KBr, NaCl, CsI, "KRS-5" (thallium bromide . iodide), and AgCl; all of which are finally taken to liquid helium temperature and recycled many times by the technique discussed below. Before we discuss this method in detail, it would be useful to enumerate a few of the more notable failures encountered prior to the development of the successful technique in order that one may appreciate the extreme measures undertaken.

For quartz, sapphire, Pyrex, and LiF (all quite hard substances with small thermal expansion coefficients) low temperature window seals can be affected by indium or certain epoxy resins (see next

section). Both of these techniques fail for any of the soft window materials due to the contraction of the window with respect to the sealant. Such failures usually result in the destruction of the windows. One partially successful attempt was made that is probably worth noting. The technique is described in detail in the literature.^{1,2} It involves using a spring to keep constant tension on the seal as the window moves. This method was found to be not very reliable and only worked for AgCl.

The problem was eventually solved by epoxying the window to a drawn Cu foil (0.003" before drawing) which was soft soldered to a 304 stainless steel ring. The ring was then indium sealed to the dewar. The Cu foil, the frame with the foil, and a complete window assembly with indium are shown in Figure 4. The solder must be a high temperature alloy which melts at temperatures over 200°C, as the Aerobond 2902, Epibond 100-A, and the Araldite Stick-I epoxy resins must all be cured at 180-200°C for 1 hour. The method of epoxying is quite simple: the powdered epoxy is applied to the space between the foil side and the window edge. Upon heating the epoxy is sucked under the window by capillary action, but a large portion of it remains at the edge of the window. Thus, both the edge of the window and the side of the Cu foil and the face of the window and the flat surface of the foil are sealing surfaces (see Figure 4). These windows, recycled upwards of ten times, have never caused any problems, even upon rapid cooling. To remove the windows for major polishing, one must heat the assembly to about 250°C, replace the foil and re-epoxy the polished window to the foil. It was also possible to do light polishing of the window in the frames. Such windows can also be used to assemble vacuum-tight

sample cells which may be filled from a vacuum line (see Sec. Id).

C. Epoxy:

Since almost no epoxy has been explicitly developed to be used at 4.2 and 1.8°K, one must search about for those that can be used in vacuum applications at low temperatures. Such a partial search has been undertaken, the results of which follow. Each epoxy found to be useful is listed below with comments on its performance.

1. Aerobond 2902 - Adhesive Engineering Co., 1411 Industrial Road, San Carlos, California 94070. This epoxy was cured between 180 and 190°C for 1 hour and applied as a powder. It is also available in solid form. Much like Araldite I, this epoxy is very reliable and the one most used.

2. Araldite I - (and many others in this line - both with and without metal) Ciba Co., Duxford/Cambridge, England. This epoxy is virtually impossible to obtain in the U. S. A., but Adhesive Engineering and Furane Plastics Company claim their products to be equivalent. It is the best one to use for low temperature applications.

3. Epibond 100-A - Furane Plastics Co., 4516 Brazil Street, Los Angeles, California. About the same as 1 and 2 - cure at 190-200°C for 1 hour.

4. 50% Epon 828 (Shell Oil Co.) and 50% Versamid 125 (General Mills Inc.). A room temperature cure can be affected in 24 hours. It is a very good epoxy although not as reliable as others probably due to the liquid being more difficult to apply evenly and

without bubbles. Thorough mixing has been found to be an important factor in the performance of this epoxy resin.

D. Sample Cells and the Growth of Crystals:

The sample cells employed with the previously described infrared dewar are discussed in publications stemming from part of these investigations and are contained in this thesis in reprint form (Chapter I, II, and III). Sample cells used in connection with the electronic absorption and emission spectra are also discussed in detail in Chapters IV and VI. The techniques employed in the growth of benzene crystals in the above cells are also described. The essential point for the growth of crystals for the ultraviolet spectra is the maintenance of a sharp temperature gradient, slow growth rate, and constant temperature above and below the gradient. For samples from about 1 to 25 mm, the gradient was maintained by butting a copper tube, with one end in liquid nitrogen against a heating element surrounded by styrofoam, while for larger samples a standard Bridgman furnace in a cold room was used to develop the gradient at which the crystal was grown (see Chapter VI).

The purpose of this section of the experimental appendix is not to redevelop these points but to discuss similar attempts and techniques used to grow samples of single or optical quality crystals for the infrared. The difficulties this presents, especially when the liquid-solid technique, which has been employed in the previous work, is chosen, should be quite obvious. The major problem, of course, is that of constructing a sample cell that can be filled on a vacuum line, evacuated

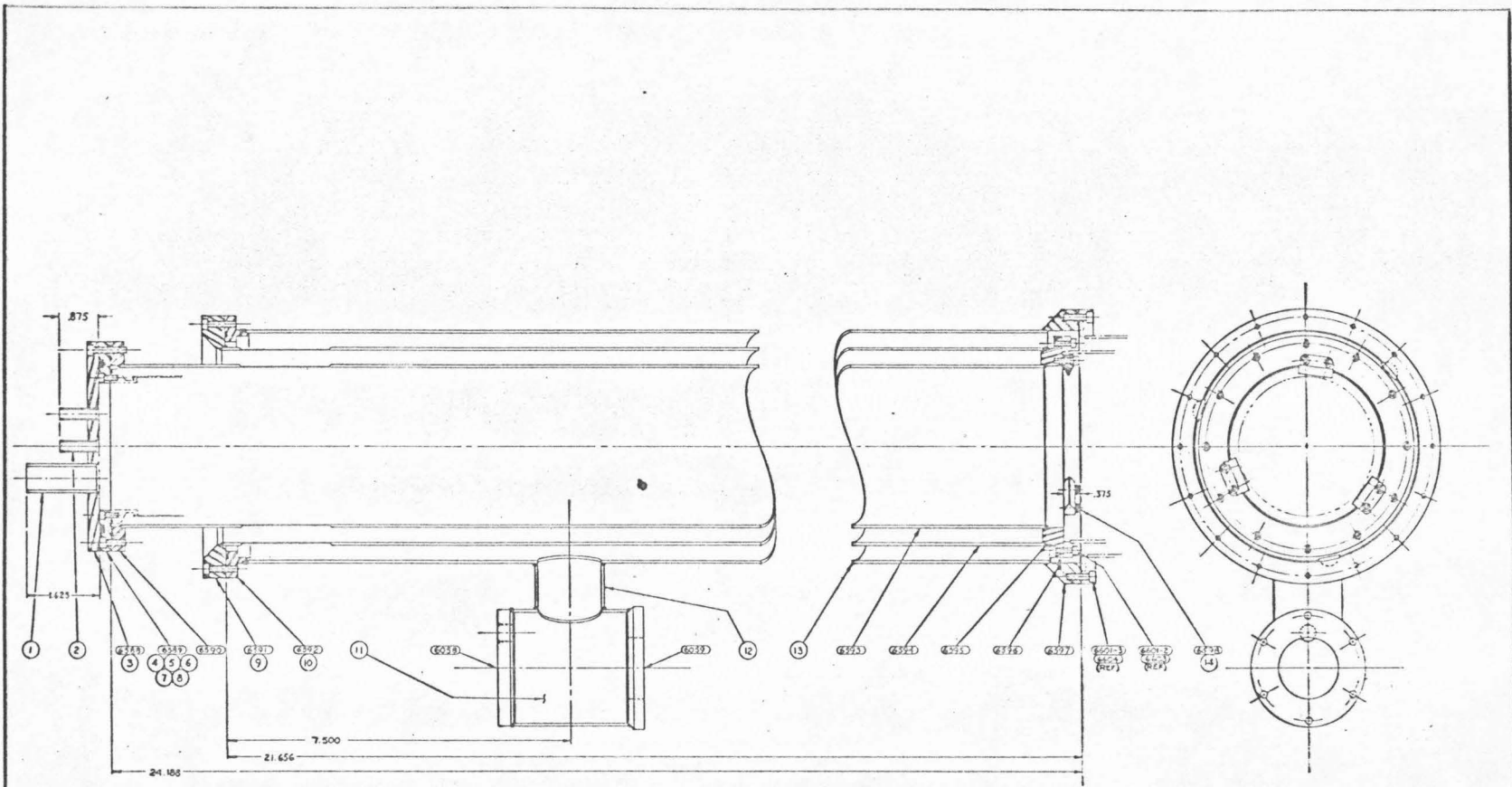
and taken to low temperatures under vacuum, with soft and water soluble infrared windows. Once the technique for sealing windows to the internal helium can of the dewar was developed, this difficulty could be surmounted by a simple extension of that method. The solution to this problem was to make a flange with a glass-to-Kovar 1/8" vacuum feed-through to which two previously described window frames could be afixed with indium. These frames were slightly modified to keep the cell as small as possible. This assembly was then glass-blown to a vacuum line, loaded with benzene and then glass-blown off the line as near as possible to the Kovar seal. The benzene had to be frozen in the cell before the glass could be heated; the windows were protected from water by the use of a few rubber prophylactics.

The major problem with the growth of a crystal concerns the fact that the cell contains a large amount of 304 stainless steel, which, while not a good conductor of heat, is certainly much better than Pyrex or quartz. It thus becomes impossible to develop the temperature gradient that is needed to grow a good crystal across the cell. In fact the best crystals were either grown in the dewar which cooled down slowly, or by simply placing a well insulated cell in a -30°C cold room for about 12 hours. The project was abandoned when these crystals turned out to be no better than the ones grown in the previously described cells (Chapters I, II, and III), as judged from their infrared absorption spectra.

References

1. L. Parts and H. R. DuFour, Rev. Sci. Inst., 36, 1271 (1965).
2. J. L. Mack and G. B. Wilmot, Rev. Sci. Inst., 36, 1265 (1965).

Figure 1. Upper section of infrared helium dewar. At the far left of figure (near the top of dewar) the internal can assembly is indicated in broken lines. The section at the right is the dewar viewed from the bottom. The port at the center is used for vacuum gauges. The part numbers refer to drawings on file (V-554) with the Department of Chemistry Machine Shop and Drafting Room.



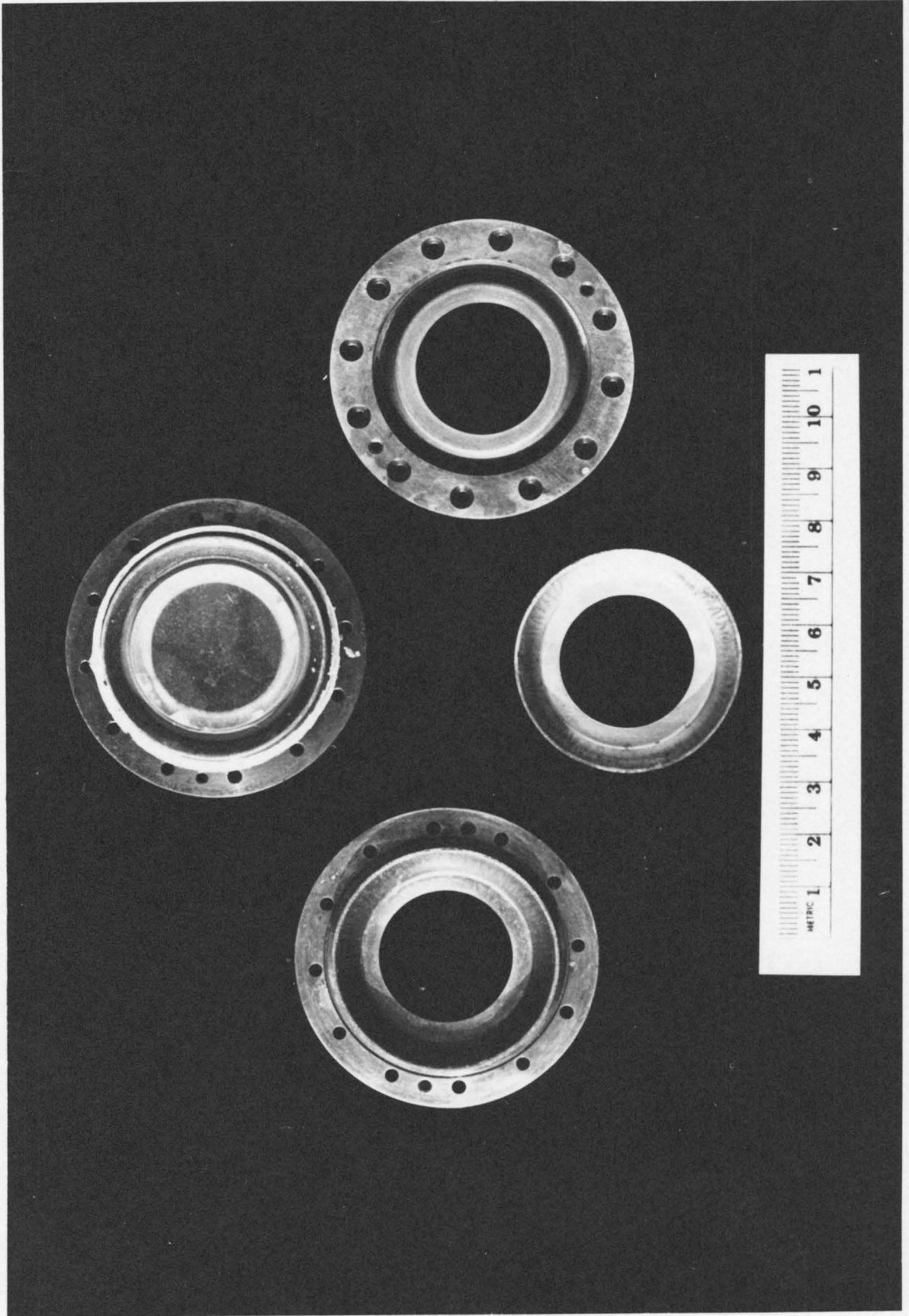
- NOTES
1. BRASS AND STAIN. STEEL
 2. CONSTRUCTION: MILL-AC. SEAL WELDED. FULL PENETRATION CORNER WELD.
 3. BRASS WELD (LARGE SIZE) DIMENSIONS: 1/16" BRASS FILLING ALTERNATE 1/8" BRASS SURFACE: 1/8" W/CH. 1/100 IN 10,000

SCALE: FULL		DATE	BY	CHKD
CALIFORNIA INSTITUTE OF TECHNOLOGY - DEPARTMENT OF CHEMISTRY				
PROJECT: 6537				
DRAWN BY: W. W. W. 1/10				
DEWAR SUB-ASSEMBLY - UPPER				6537
INFA RED - HELIUM				

Figure 2. Base of infrared helium dewar with liquid nitrogen heat shield. The internal can is the cold finger one with the helium heat shield in place. The dewar is evacuated through pumping port (protruding flange at dewar bottom). Inserts at top right give window configuration. Again numbers refer to drawing on file (V-554) in Department of Chemistry Machine Shop.

Figure 3. Same as Figure 2 with internal immersion can. Window assembly is given at upper right.

Figure 4. Photograph of the window frame assembly for the internal immersion helium can. The four articles in the picture are: at 12 o'clock - a completed window assembly with a CsI window and the indium gasket in place; at 3 o'clock - an empty frame with a Cu foil soldered to it - the frame is upside down; at 6 o'clock - a 0.003" Cu foil, the top rim of which is for soldering and the lower ledge is the epoxying surface; at 9 o'clock - a right-side up frame with the foil soldered in place.



PROPOSITIONS

ABSTRACT OF PROPOSITIONS

by Elliot R. Bernstein

1. The study of the complex optical rotatory dispersion phenomenon in single oriented crystals composed of non-active molecules is proposed. The one-electron theory is discussed for the case of the urea crystal.

2. The study of the "chemical" or "local field" shift of Xe^{129} , Ne^{21} , and He^3 is suggested, using the various rare gases and H_2 as solvents. Of particular interest would be the liquid and solid mixed systems in which "exchange interactions" or "diatomic molecule" formation has been suggested as the dominant mechanism for the relaxation and the shift.

3. Using the combined experimental techniques of optical pumping, epr, and uv emission spectroscopy, the study of the ($n - \pi^*$) triplet states of pyridine, pyrazine, and sym-triazine is proposed. The type of information that can be obtained concerns spin orbit coupling, signs of D and E, locations of the optically forbidden states, molecular geometry, and in sym-triazines the Jahn-Teller distortion of the triplet state.

4. In order to study phase transitions in solids, a study of nuclear quadrupole resonance of single crystals of diborane as a function of temperature is suggested. The quadrupolar coupling constant, asymmetry parameter, and resonant frequency are calculated for an isolated diborane molecule.

5. After a discussion of the Watson-Crick-Pauling-Corey hydrogen bonding structure in DNA and a quantum mechanical calculation dealing with it, a suggested series of experiments on base pair crystals is presented. These experiments are designed to shed light on the nature and properties of the hydrogen bonds holding together the complementary bases.

PROPOSITION I

The phenomena of optical rotation (circular birefringence) and circular dichroism have been known to exist for quite some time. Condon,¹ Condon, Altar, and Eyring,² Kauzmann et al.,^{3,4} and Kauzmann⁵ have discussed these effects in detail. Unfortunately very little quantitative understanding of the theory as outlined here is available due mostly to a lack of complete and accurate experimental data with which to check the model (e. g., these effects are supposed to be of a tensorial nature and this fact has not as yet been investigated and verified). The best method for obtaining such data would be to measure the circular dichroism and optical rotatory dispersion of a single crystal of known orientation as a function of crystal direction. Such a complete study has never been made and represents an excellent test of the theory of complex optical rotatory dispersion and of the optical properties of crystals. It is proposed then that the tensor properties of the optical complex rotatory dispersion be evaluated in crystals both theoretically and experimentally. Discussed in what follows are some of the considerations and factors that govern the theoretical and experimental investigations.

There are certain classes of crystals (having no center of symmetry — no S_n point operations) that exhibit circular birefringence and optical rotatory dispersion due solely to the molecular arrangement (i. e., the space group) and not the individual molecule. The so-called "active" space groups can be determined to be: C_1 , C_2 , D_2 , C_3 , D_3 , D_4 , C_4 , C_6 , T , O and those members of C_{2V} , C_S , S_4 , and D_{2d} without,

in general, the $\bar{4}$ and m operations. It can be further demonstrated, however, that classes m , $mm2$, $\bar{4}$, $\bar{4}2m$ can theoretically evidence circular birefringence and dichroism even though they are not enantiomorphic. These crystals simply cannot show rotation along the direction of any of the above mentioned symmetry operations. In classes $\bar{4}$ and $\bar{4}2m$ the rotation along the optic axes must be zero (both classes are uniaxial). In these classes rotation exists in the direction off the optic axis where the normal or linear birefringent effects are quite large. Such phenomena have as yet not been observed. The above space groups all have in common screw axis symmetry operation, and as a direct consequence of this fact the molecules are arranged in long polymer-like chains of helical configuration. Interesting examples of such molecular arrays are: urea ($P\bar{4}2_1m = D_{2d}^3$, 2 molecules per unit cell in sites of C_{2v} symmetry where only off axis activity exists); phenol ($D_2^2 = P222_1$ with 2 molecules per unit cell in sites of C_2 symmetry); phenanthrene ($P2_1 = C_2^2$ 2 molecules per unit cell with a site of only trivial symmetry); and benzophenone ($D_2^4 = P2_12_12_1$ with 4 molecules per unit cell and also a site of trivial symmetry) to name just a few.

Phenomenologically the complex optical rotation can be written as (in cgs units and radians/cm):

$$\tilde{\Phi} = (\varrho - i\theta) = \frac{\pi\nu}{c} (\tilde{N}_L - \tilde{N}_R) \quad (1)$$

where $\tilde{N}_L = \tilde{n}_L - i\tilde{k}_L$ and $\tilde{N}_R = \tilde{n}_R - i\tilde{k}_R$. \tilde{N}_L and \tilde{N}_R are the complex refraction tensors of left and right circularly polarized light, and \tilde{n}

and $\underline{\kappa}$ are the refraction and absorption tensors, respectively. $\underline{\rho}$ is the optical rotatory dispersion tensor and $\underline{\theta}$ is the ellipticity tensor, which are the quantities of interest in the active crystal systems. Quantum mechanically the complex rotation tensor $\underline{\Phi}$ can be obtained as,

$$\underline{\Phi} = - \frac{4\pi\eta e\nu^2}{\hbar mc^2} \sum_A \frac{[\underline{\mu}_{OA} \times (\underline{pr})_{AO}]}{[(\nu_{AO}^2 - \nu^2) + i\nu\Gamma_{AO}]} \quad (2)$$

which from eq. (1) gives:

$$\underline{\rho} = - \frac{4\pi\eta e\nu^2}{\hbar mc^2} \sum_A \frac{(\nu_{AO}^2 - \nu^2)[\underline{\mu}_{OA} \times (\underline{pr})_{AO}]}{[(\nu_{AO}^2 - \nu^2)^2 + \nu^2\Gamma_{AO}^2]} \quad (3)$$

$$\underline{\theta} = - \frac{4\pi\rho e\nu^2}{\hbar mc^2} \sum_A \frac{\nu\Gamma_{AO}[\underline{\mu}_{OA} \times (\underline{pr})_{AO}]}{[(\nu_{AO}^2 - \nu^2)^2 + \nu^2\Gamma_{AO}^2]}, \quad (4)$$

where Γ_{AO} is the width of the absorption band ($A \leftarrow 0$) at half maximum, η is the number of molecules per cm^3 , $\underline{\mu}$ is the electric moment vector ($= e\underline{r}$), \underline{p} is the linear momentum vector, \underline{r} is the position vector of the electron and the product (\underline{pr}) is the angular momentum tensor. The summation is over all excited states giving $\underline{\Phi}$, the total complex rotation, for all electronic transitions. Typically one electronic transition is determined to be the most important in a given frequency region and the partial complex rotation $\underline{\Phi}_A$, is of most interest. It should be noted that in order to have rotation ($\underline{\Phi}_A$ to be non-zero) for a given transition, neither the electric nor magnetic

dipole moments of this transition can be zero. If an electron moves in a straight line, $\underline{\mu}$ the electric dipole moment, will be large (large oscillator strength) while if the electron moves in a circle, (\underline{pr}) the magnetic dipole moment, will be large (small oscillator strength). It is therefore obvious that a weak absorption such as the $n \rightarrow \pi^*$ transition in the carbonyl system can very well produce a large optical rotation. An electron constrained to move on a helical path (i. e., undergo a transition in a potential field of helical - pseudo scalar - symmetry) would be an example of an instance in which neither the magnetic or electric dipole moments vanish for a given transition.

Using this formulation as a basis Moffitt⁶ has derived, for the case of a helical polymer, the exciton contribution to the rotation. It is found that this term has an anomalous dispersion with $\underline{\Phi}_A$ depending on $(\nu_{OA}^2 - \nu^2)^{-2}$. With only minor revisions it is believed that the work of Moffitt is applicable directly to optically active crystals,⁷ in which the molecules due to a screw axis of the space group form long chain-like helical configurations. There are, however, some minor corrections to be noted for the application to molecular crystals, and these can be taken over from standard exciton theory.⁸ Moffitt's wave function for the σ^{th} excited crystal state must take on the form,

$$\Phi_q^\sigma(\underline{k}) = \frac{1}{\sqrt{N}} \sum_{m=1}^{N/q} \exp[i\underline{k} \cdot \underline{R}_{mq}] \phi_{mq}^\sigma \quad (5)$$

with

$$\phi_{mq}^\sigma = \chi_{mq}^\sigma \prod_{m' \neq m}^{N/q} \chi_{m'q}^\sigma \quad (6)$$

Here \underline{k} is the wave vector which due to the crystal translational symmetry and can have a zero value, m is the unit cell index, q is the number of sites per unit cell and \underline{R}_{mq} is the vector to the q^{th} site of the m^{th} unit cell from some arbitrary origin. The χ_{mq} 's are the crystal site wave functions.⁸ Moffitt's selection rules must now be altered to accommodate the molecular crystal model for which the maximum number of allowed crystal transitions ($\Delta \underline{k} = 0$) for a given molecular one is at most equal to the number of molecules (monomers) per unit cell.

It is thus proposed that "pure exciton" or "crystal" circular birefringence and dichroism be studied in detail, using "optically active" molecular crystals whose molecules are not themselves "active" (i. e., have an S_n operation). The circular birefringence and circular dichroism are observed as a function of direction in the crystal and of particular interest are the two directions parallel and perpendicular to the axis of the "crystal helix." The major difficulty with such experiments is the strong linear birefringence most crystals exhibit off their optic axes. This can be dealt with however by various techniques, the easiest of which is the use of a compensator.⁹

When the circular dichroism of such crystal is observed, it would be of great interest to be able to resolve the vibrational structure of the electronic transition and determine the contribution to the dichroism of each vibronic band separately. In the case of weak transitions ($n \rightarrow \pi^*$ for example) one would expect to find different polarizations and dichroic ratios for the various bands depending on the vibronic

coupling or other "intensity stealing" mechanism involved. One can also determine if the magnetic or the electronic dipole term is associated with this coupling. In order to facilitate such a study the crystal measurements must be carried out at 4.2°K, employing high spectral resolution. On the other hand, from the temperature variation of these phenomena, the contribution from nearly degenerate or low-lying molecular states and lattice modes could be evaluated.

The superiority of crystal systems over one of say unoriented or even oriented polymers is fourfold: first, and perhaps most important, in the oriented single crystal system, the complete and unambiguous tensorial nature of the complex rotation phenomenon can be observed directly; second, the crystals can be purified and refined to such an extent that impurities no longer become a problem; third, the individual molecules composing the crystals are non-active and thus the exciton or crystal determined contribution to the complex rotation tensor is not masked by the molecular one; and fourth, the exact configuration of the molecules is precisely known and constant, making relatively good and extensive calculations on these systems possible. (For example in the urea crystal, even the H-atom positions have been accurately determined.) Through these experiments and the subsequent checks on the existing theories, it is possible to better understand not only the phenomenon of optical rotation and the states involved with it, but also the intermolecular interaction involved in molecular crystal exciton effects. Since the "path" of the electron during the transition in the crystal is a very sensitive function of the intermolecular

interactions, optical rotation and circular dichroism studies should be a very useful probe to aid in the understanding of such crystal perturbations.

The question now arises which of the space groups and which molecule should be examined first. In considering a space group it would be useful to choose one which is predicted to be "active" off the optic axis if only in order to prove that such a phenomenon can occur and that the circular birefringence and dichroism can be measured in the presence of large linear birefringence. The choice of a molecule is somewhat more difficult to make, in that one must have a calculational model or procedure in mind to do this intelligently. The most promising of these is the "one electron" model¹⁻⁵ in that it is the one to which perturbation techniques may be most readily applied, and it provides the greatest physical insight into the phenomena. In the light of such considerations urea is an obvious choice. The $n - \pi^*$ carbonyl transition is well isolated and localized, essentially involving only one electron and the detailed crystal structure is available.

The specific example of urea will now be considered in detail. The crystal structure¹⁰ and all atomic positions¹¹ have been accurately determined, and the C_{2v} site symmetry preserves all the molecular states and does not complicate the symmetry arguments for the states of the crystal site. The general configuration of the molecules in the bulk crystal is that of parallel chains of urea molecules, hydrogen bonded to one another, each chain flanked by two skewed chains whose sense is opposite to the first. The skewing, or helical

configuration, due to the 2_1 screw axis, gives rise to the asymmetric potential, $V(\underline{r})$. This potential, interacting with the $n - \pi^*$ transition of the carbonyl group, must give rise to the optical rotation associated with the electronic band. The ground state configuration of the carbonyl group is $n^2\pi^2$ ($\langle n |$) and the excited state is $n\pi^2\pi^*$ ($|\pi^*\rangle$). These orbitals in the first order have the form

$$\begin{aligned} |n\rangle &= 2p_{y,O} \\ |\pi^*\rangle &= A2p_{x,O} + B2p_{x,C} \end{aligned} \quad (7)$$

and it can be shown that, from symmetry arguments alone,

$$\begin{aligned} \langle n | \underline{\mu} | \pi^* \rangle &= 0 \\ \langle n | (\underline{pr}) | \pi^* \rangle &\neq 0 \end{aligned} \quad (8)$$

and the $n - \pi^*$ transition is, to first order, dipole forbidden. For the complex rotation tensor to be non-zero $[\underline{\mu}_{n\pi^*} \times (\underline{pr})_{\pi^*n}]$ must be non-zero. There are two approaches to the problem. The standard method is to use configuration interaction and mix into the $|\pi^*\rangle$ state a third state. In this case $(C3d_{yz,C} + B3d_{yz,O})$ is a function that can be used, as we are looking for a dipole moment component along the bond axis (z-direction) — the cross product $[\underline{\mu}_{n\pi^*} \times (\underline{pr})_{\pi^*n}]$ must not vanish. The coefficients are of the form,

$$C = \frac{A \langle 2p_{x,O} | \frac{1}{r} | 3d_{yz,O} \rangle}{\Delta E_O}$$

$$D = \frac{B \langle 2p_{x,C} | \frac{1}{r} | 3d_{yz,C} \rangle}{\Delta E_C} \quad (9)$$

An alternate approach, somewhat better suited to this problem, in which the $|\pi^*\rangle$ and $|n\rangle$ states are directly mixed together by a perturbing potential has been recently developed.¹² We must then find

$$\langle n | V(\underline{r}) | \pi^* \rangle \neq 0 \quad (10)$$

where $V(\underline{r})$ is the intermolecular potential. Obviously V must be of the same symmetry (xy) as $|\pi^*\rangle$ for eq. (10) to be true. This gives each state some "character" of the other state and makes $\mu_{n\pi^*}$ non-zero. We can thus determine the nature and symmetry of the interaction producing the partial complex rotation due to this $n \rightarrow \pi^*$ transition, and we will be able to calculate the directional rotation phenomena we observe in the region of the $n \rightarrow \pi^*$ transition.

References

1. E. U. Condon, *Rev. Mod. Phys.*, 9, 432 (1937).
2. E. U. Condon, W. Altar, and H. Eyring, *J. Chem. Phys.*, 5, 753 (1937).
3. W. J. Kauzmann, J. E. Walter, and D. H. Eyring, *Chem. Rev.*, 26, 339 (1940).
4. W. J. Kauzmann and H. Eyring, *J. Chem. Phys.*, 9, 41 (1941).
5. W. J. Kauzmann, *Introduction to Quantum Chemistry*, Academic Press, Inc., New York (1961), pp. 617 and 703.
6. W. Moffitt, *J. Chem. Phys.*, 25, 467 (1956).
7. Moffitt's original work was later corrected by Moffitt, Fitts, and Kirkwood, *Proc. Natl. Acad. Sci. (U. S.)*, 43, 723 (1957). The basis of this criticism and subsequent correction was that Moffitt's wave function

$$\Phi_K^\sigma = \frac{1}{\sqrt{N}} \sum_m \exp[2\pi i m \underline{k}/N] \Phi_m^\sigma$$

where σ is the excited electronic state, m is the residue, N the number of residues in the helix and \underline{k} a wave or phase "vector" ($k, m = 1, 2, \dots, N$), was incorrect for the case of a simple helical polymer. The objection was that the coefficient of Φ_m^σ was not proper, as the helix is not reentrant. However, this criticism is not valid for molecular crystals. With a few minor changes to be listed in the text it is believed that Moffitt's original treatment is valid for the case in point.

8. A. S. Davydov, *Usp. Fiz. Nauk*, 82, 393 (1964); [English translation: *Soviet Physics-USpekhi*, 7, 145 (1964)], and E. R. Bernstein, S. D. Colson, R. Kopelman, and G. W. Robinson, *J. Chem. Phys.*, (to be published).
9. G. N. Ramachandran and S. Ramaseshan, *Handbuch der Physik (BdXXV/I)* Springer (1947) and G. N. Ramachandran, *Handbuch der Physik (Band XXVII)* Springer (1961).
10. P. Vaughan and J. Donohue, *Acta Cryst.*, 5, 530 (1952).
11. J. E. Worsham, Jr., H. A. Levy, and S. W. Peterson, *Acta Cryst.*, 10, 319 (1957).
12. J. A. Schellman and P. Oriol, *J. Chem. Phys.*, 37, 2114 (1962).

PROPOSITION II

Over the last few years there has been a great deal of experimental and theoretical controversy concerning the "chemical shift" and nuclear spin relaxation rates of the rare gases in all three phases. After a brief review of these findings and problems a series of experiments, designed to shed some light on the mechanism of the "chemical" or "local field" shift and the relaxation processes, is suggested.

It has been found experimentally,¹⁻⁵ that the chemical (local field) shift of Xe^{129} ($I = 1/2$) in natural Xe in gas, liquid and solid phases is dependent on the temperature, density (pressure) of the sample and the magnetic field where the shift is measured relative to "an isolated" Xe^{129} nucleus. It is further observed that the relaxation rate is very slow and that this too is a function of density. It is postulated⁶⁻¹¹ that both the shift and the relaxation can be described theoretically by "momentum dependent interactions."⁶⁻⁸ What this means is that relaxation and the chemical shift in these systems are due to collisions. One can look upon this, depending on the time scale, as a consequence of "diatomic molecule formation" and then the well-known Ramsey theory,¹² relating the magnetic shielding, relaxation mechanism and the nuclear-spin rotational coupling constant, is applicable.

The chemical shift is attributed to the fact that the nuclei see a different magnetic field than the applied one \underline{H}_0 , due to the presence of the electrons. This can be expressed in the form¹³

$$\underline{H}_1 = - \underline{\sigma}^N \underline{H}_0 \quad (1)$$

where \underline{H}_1 is the field seen by the nucleus and σ^N is the symmetric nuclear shielding tensor. Due to this effect of electron shielding, the resonant frequency for a given nucleus is changed. The nuclear moment $\underline{\mu}_N$ will interact with the total local "shielded" field to give an energy,

$$\begin{aligned} E &= - \sum_N \underline{\mu}_N \cdot \underline{H}_0 + \sum_N \underline{\mu}_N \cdot \underline{\sigma}^N \cdot \underline{H}_0 \\ &= - \sum_N \underline{\mu}_N \cdot (\underline{1} - \underline{\sigma}^N) \cdot \underline{H}_0 \end{aligned} \quad (2)$$

Therefore, to learn about the chemical shift we are interested in terms proportional to $\underline{\mu} \cdot \underline{H}_0$ in the Hamiltonian. From analogy with classical physics, we know that the Hamiltonian for a molecule with a nuclear and electronic dipole moment can be written as

$$\begin{aligned} \mathcal{H} &= \mathcal{H}_0 - \sum_N \underline{\mu}_N \cdot \underline{H}_0 - \sum_k \underline{\mu}_{kN} \cdot \underline{H}_0 + \\ &\quad \left\{ \frac{e}{mc} \sum_k \frac{\hbar}{i} (\underline{A}_k \cdot \nabla_k) + \frac{e^2}{2mc^2} \sum_k \underline{A}_k^2 \right\} \end{aligned} \quad (3)$$

The summations over N and k refer to nuclei and electrons respectively, \mathcal{H}_0 is the Hamiltonian for the system in the absence of the external magnetic field and the second and third terms are the nuclear and electronic Zeeman terms, respectively. The terms in { } produce the shielding or the electron coupled interaction of the nuclear magnetic moment $\underline{\mu}^N$ and the external magnetic field H_0 . \underline{A}_k is the vector potential at the k^{th} electron, and if we choose the origin to be the nucleus N, \underline{A}_k is

$$\underline{A}_k = \frac{1}{2} (\underline{H}_0 \times \underline{r}_{kN}) + \frac{\underline{\mu}_N \times \underline{r}_{kN}}{r_{kN}^3} \quad (4)$$

for the approximation in which electron-electron interactions are neglected. This is a convenient gauge (or coordinate system in this case) choice for two reasons. First it allows the orbital Zeeman perturbations to be put in terms of angular momentum measured about nucleus N and second, it makes the calculation of exchange and overlap integrals less complicated. In the first consideration calculations are simplified because it is now possible to eliminate that part of the electronic distribution possessing spherical symmetry with respect to the nucleus under consideration. In the second case this choice is more essential. For these two center calculations the choice of vector potential causes an apparent induced polarization of the closed electronic shells of atom N' which, through exchange interactions, is calculated to be the major contribution to the chemical shift in Xe¹²⁹. This point will be further discussed in more detail shortly.

The last two terms in eq. (3) can be expanded to give

$$\frac{e}{mc} \sum_k \frac{\hbar}{i} (\underline{A}_k \cdot \underline{\nabla}_k) = \frac{e}{2mc} \sum_k \underline{l}_{kN} \cdot \underline{H}_0 + \frac{e}{mc} \sum_{N,k} \left(\frac{\underline{\mu}_N}{r_{kN}^3} \cdot \underline{l}_{kN} \right) \quad (5a)$$

$$\frac{e^2}{2mc^2} \sum_k \underline{A}_k^2 = \frac{e^2}{2mc^2} \left[\sum_k (\underline{H}_0 \times \underline{r}_{kN}) \right] \cdot \left[\sum_n \left(\frac{\underline{\mu}_N \times \underline{r}_{kN}}{r_{kN}^3} \right) \right] \quad (5b)$$

keeping only those terms to $\underline{\mu}_H$. If we now define the first order correction to the wave function in the field direction ν as,

$$|\psi_{0\nu}'\rangle = - \sum_{n=1}^{\infty} \frac{|\psi_n\rangle \langle \psi_n | \frac{e}{2mc} \sum_{\mathbf{k}} (\mathbf{l}_{\mathbf{k}N})_{\nu} | \psi_0 \rangle}{E_n - E_0}$$

we find that the total shielding tensor is given by

$$\begin{aligned} \sigma_{\nu\lambda}^N &= \frac{e^2}{2mc^2} \langle \psi_0 | \sum_{\mathbf{k}} \left(\frac{\mathbf{r}_{\mathbf{k}N} \cdot \mathbf{r}_{\mathbf{k}N} \delta_{\nu\lambda} - (\mathbf{r}_{\mathbf{k}N})_{\nu} (\mathbf{r}_{\mathbf{k}N})_{\lambda}}{r_{\mathbf{k}N}^3} \right) | \psi_0 \rangle \\ &+ \frac{2e}{mc} \operatorname{Re} \langle \psi_0 | \sum_{\mathbf{k}} \frac{(\mathbf{l}_{\mathbf{k}N})_{\nu}}{r_{\mathbf{k}N}^3} | \psi_{0\lambda}' \rangle, \end{aligned} \quad (6)$$

with the origin of the vector potential taken at nucleus N. The first term in eq. (6) is the "diamagnetic term" and the second is the "paramagnetic term." The decomposition of the total measurable shielding tensor into a paramagnetic and a diamagnetic shielding term is clearly not unique in the sense that it is a gauge dependent separation. The gauge invariance of physically observable quantities applies only to the total shielding tensor σ^N . Expanding the second part of eq. (6) we find

$$\begin{aligned} \sigma_{\nu\lambda}^{PN} &= - \frac{e^2}{m^2 c^2} \sum_{n=1}^{\infty} \operatorname{Re} \left(\frac{1}{E_n - E_0} \right) \langle \psi_0 | \sum_{\mathbf{k}} \frac{(\mathbf{l}_{\mathbf{k}N})_{\nu}}{r_{\mathbf{k}N}^3} | \psi_n \rangle \times \\ &\langle \psi_n | \sum_{\mathbf{j}} (\mathbf{l}_{\mathbf{j}N})_{\lambda} | \psi_0 \rangle. \end{aligned} \quad (7)$$

It is this paramagnetic term that is of interest to us with our choice of gauge.

Adrian⁹ and Torrey¹⁰ have found that both shift and relaxation terms for Xe¹²⁹ due to van der Waals forces are vanishingly small and cannot account for the relatively large experimentally observed effects. Further the diamagnetic shielding due to van der Waals interactions is also vanishingly small, as the slowly varying term $(1/r)$ [see the first term in eq. (6)] is very insensitive to small changes in the tails of the wave functions. It is possible however that a paramagnetic current [eq. (7)] could be produced at the nucleus due to a "van der Waals excitation" or distortion of the Xe¹²⁹ orbitals (5p). These orbitals could then produce a magnetic field at the nucleus through Zeeman interactions with the applied magnetic field. Such terms would give rise to a large magnetic shielding and thus a sizeable chemical shift. However it is found that there is almost complete cancellation of these effects.¹⁰ On the other hand considering "short range exchange terms" between outer shell electrons from "diatomic molecule" formation it is possible to get order of magnitude agreement with the observed shifts and relaxation time. Adrian has shown¹⁰ that the change in diamagnetic shielding due to exchange interaction is negligible when averaged over all collisions and that the second order paramagnetic shielding is the important term. Throughout this calculation the distortion of the ground state wave functions is neglected. The crux of Adrian's technique for the calculation of the paramagnetic contribution to the shielding is the placing of the origin of the vector potential at the nucleus of one of the colliding atoms, say A. Then the angular momentum of the atom B electrons is given by

$$\sum_j^B (\chi_{jA})_\nu = \sum_j^B \left\{ (\chi_{jB})_\nu - R \left(\frac{\partial}{\partial y_B} \right)_j \right\} \quad (8)$$

where R is the inter-nuclear or "intermolecular" separation. The second term on the right-hand side of eq. (8) is the gauge variant term that produces the mixing of the occupied with the unoccupied orbitals on the B atom. This term is thus responsible for the polarization of the electron cloud around the B center and is definitely gauge variant. Now unless there is either exchange or direct overlap of A and B electron orbitals, the A nucleus is unaware of this polarization of the B electronic orbitals. During a collision between atoms A and B (diatomic molecule formation), this "polarization" is transmitted from B to A producing the current flow associated with the induced field and it is this field which produces the observable shift or shielding tensor. The "exchange of orbital polarization" or current flow can take place in two ways. The first is through direct orbital overlap of the electronic orbitals of atoms A and B (taking into account the Pauli principle) and the second through "excitation transfer" or "exchange coupling." Adrian¹⁰ shows that the first method produces only small effects while the second is responsible for most of the observed chemical shift. With the foregoing ideas as a foundation and employing the average energy approximation, an ensemble average of g^P over all collisions, and exchange interactions to second order, Adrian was able to obtain reasonable (order of magnitude) agreement with the experimental chemical shift and relaxation data.

It is felt, however, that very little is known about these exchange interactions and much more experimental work is needed in order to elucidate the mechanisms of the chemical shift and relaxation in these systems. It is proposed that Xe^{129} , Ne^{21} ($I = 3/2$), and He^3 ($I = 1/2$) resonances should be studied as a function of solvent and helium, neon, argon, krypton, xenon, and hydrogen should be solvent gases used. The chemical shift and spin-lattice relaxation T_1 of Xe^{129} (Ne^{21} and He^3) should be determined as a function of sample density (pressure), magnetic field, and temperature in all the above solvents. Due to the long relaxation times and weak signals, the experiments should be carried out at about 5% isotopic concentration in the liquid and solid phases employing large samples. These are of course the most interesting in terms of intermolecular exchange interactions. It is expected that the shift in the solid would be about 5 times as great as that in liquid³ even in these systems and it is hoped that experimental conditions could be such that the isotopic concentration could be lowered to about 2% but this would depend heavily on the apparatus used and its sensitivity. It is necessary to lower the "probe" atom concentration as much as possible in order to reduce Xe-Xe, Ne-Ne, or He-He interactions, since if these became too great, we would not be able to measure the desired shifts or relaxation times due to the Xe (Ne, He) solvent interaction, but only an effect averaged over the probe isotopes in different sites in the liquid and solid. It would be possible, however, to measure a change in shift from solvent to solvent (holding the concentration of these

nuclei constant) and thus "subtract out" the "guest-guest" interactions. In this latter technique one would have to assume implicitly that the coordination number of these atoms in the different solvents (or number of nearest neighbors in the crystal) did not change appreciably from host to host.

The relaxation time for these systems would be a very sensitive function of the above experimental parameters, especially, the solvent. Over a wide range of pressure and density for both the liquid and the gas, Torrey has shown that T_1 , the spin-lattice relaxation, is due to nuclear spin-rotational coupling which allows the "exchange" of orbital angular momentum during the formation of and lifetime of the "diatomic molecule." In the solid T_1 would become an even more important relaxation process³ and much useful information could be gained about this relaxation by using different solvents as outlined above. In these simple systems where other interactions are not so large as to mask van der Waals and exchange forces, the spin-lattice relaxation should be an effective probe into the nature of these interactions.

N. B. Some of the experimental ideas put forward in this proposition, first written in the fall of 1964, seem to be under current exploration [see e. g., J. Lurie and G. K. Horton, *Phys. Letters*, 22, 560 (1966)].

References

1. R. S. Streever and H. Y. Carr, Phys. Rev., 121, 20 (1961).
2. E. R. Hunt and H. Y. Carr, Phys. Rev. 130, 2302 (1963).
3. W. M. Yen and R. E. Norberg, Phys. Rev., 131, 269 (1963).
4. D. Brinkmann and H. Y. Carr, Phys. Rev., 150, 174 (1966).
5. W. W. Warren and R. E. Norberg, Phys. Rev., 154, 277 (1967).
6. I. Oppenheim and M. Bloom, Can. J. Phys., 39, 845 (1961).
7. M. Bloom and I. Oppenheim, Can. J. Phys., 41, 1580 (1962).
8. I. Oppenheim, M. Bloom, and C. Torrey, Can. J. Phys., 42, 70 (1964).
9. C. Torrey, Phys. Rev., 130, 2306 (1963).
10. F. J. Adrian, Phys. Rev., 136, A980 (1964).
11. J. Lurie, J. L. Feldman, and G. K. Horton, Phys. Rev., 150, 180 (1966).
12. N. F. Ramsey, Phys. Rev., 78, 699 (1950).
13. C. P. Slichter, "Principles of Magnetic Resonance," Harper and Row (1963), Chapter 4, pp. 69-72.

PROPOSITION III

It is proposed that a quantitative and complete study of the lowest (phosphorescing) triplet states of pyridine (I), pyrazine (II), and sym-triazine (III) be undertaken using the combined techniques of



I



II



III

selective optical pumping, electron paramagnetic resonance (epr) and uv spectroscopy. It is believed generally, (with the possible exception of pyridine) that the phosphorescing transition of these three systems, and hence the lowest singlet - triplet transition, is $n - \pi^*$.

There are many theoretical reasons to investigate these prototype systems aside from the obvious biological importance of the N-heterocyclic compounds in general and specifically the $n - \pi^*$ transitions. The extreme theoretical interest in small N-heterocyclic molecules falls into two categories: how can the $n - \pi^*$ transitions be best described and what can we understand about triplet states in general, their transition intensities and interactions. The n (sp^2 hybrid orbital) π^* ($2p_z$ -perpendicular to the molecular plane) transitions have been described by two formalisms: the molecular orbital (delocalized) and exciton (localized).^{1, 2} Due to the believed breakdown of both the σ - π separation and the molecular orbital approximation, the exciton model is thought to be the most accurate physical description of such

transitions. The combined techniques of optical pumping and epr are quite well suited to such an investigation, as from the spectra (at $\underline{H} = 0$ and $\underline{H} \gg 0$) it is an easy matter to determine the degree of localization of the "triplet exciton" (hole-pair state) and also the geometrical configuration of the molecule.³ On the other hand, selective optical pumping coupled with observation of the phosphorescence and magnetic resonance (both at $\underline{H} = 0$ and $\underline{H} \neq 0$), can shed light on the mechanism of the triplet state population and depopulation (e. g. spin-orbit and vibronic mechanisms).

The $n \rightarrow \pi^*$ triplet transition is characterized by its relatively large oscillator strength ($f \approx 10^{-7}$, whereas on $\pi \rightarrow \pi^*$ triplet transitions, $f \approx 10^{-9} - 10^{-12}$), short lifetime ($\tau \sim .02$ sec while for benzene crystal $\tau > 10$ sec) and a large zero field splitting ($D \approx .5 \text{ cm}^{-1}$ and, when symmetry is low enough, $E \approx .05 \text{ cm}^{-1}$), all giving strong evidence for large spin-orbit and spin-spin interactions. These are a direct consequence of the high degree of localization of the $n \rightarrow \pi^*$ transition and the assumed nonplanar geometrical configuration of these ring systems in the excited $^3\pi^*$ state. One further expects resonance at high field and with a large g value (electron magnetic field coupling parameter). This kind of information strongly suggests the exciton approach to the problem, in which the " π^* electron" is attracted back to its "n hole."

Let us first examine the interactions (Hamiltonians) in which we are interested and then discuss the experimental techniques proposed for these systems. We eventually want to determine zero field

parameters, configuration of the phosphorescing state, the nature of the hyperfine interaction and spin orbit and vibronic coupling routes. The most general spin-spin Hamiltonian³ is

$$\mathcal{H} = \beta \underline{H} \cdot \underline{g} \cdot \underline{S} + (g\beta)^2 \sum_{i>j} \left\{ \frac{(\underline{S}_i \cdot \underline{S}_j)}{r_{ij}^3} - 3 \frac{(\underline{r}_{ij} \cdot \underline{S}_i)(\underline{r}_{ij} \cdot \underline{S}_j)}{r_{ij}^5} \right\} \quad (1)$$

where β is the Bohr magneton and \underline{H} is the constant magnetic field.

Using spin functions

$$\begin{aligned} T_x(1, 2) &= \frac{1}{\sqrt{2}} (\beta_1 \beta_2 - \alpha_1 \alpha_2) \\ T_y(1, 2) &= \frac{1}{\sqrt{2}} (\beta_1 \beta_2 + \alpha_1 \alpha_2) \\ T_z(1, 2) &= \frac{1}{\sqrt{2}} (\alpha_1 \beta_2 + \beta_1 \alpha_2) \end{aligned} \quad (2)$$

($\beta = |-1\rangle$, $\alpha = |+1\rangle$), for the case of no magnetic field and integrating over all space coordinates

$$\mathcal{H} = D(S_z^2 - \frac{1}{3} S^2) + E(S_x^2 - S_y^2) \quad (3)$$

where D and E are the so-called "zero field parameters." In eq. (1) the interaction assumed is the most general tensor form of the magnetic dipolar interaction and thus zero field splitting (the energy difference between T_x , T_y , and T_z with $\underline{H} = 0$) is due to magnetic dipole-magnetic dipole spin interactions.⁴ We find D and E, by expanding (1) in a matrix form and integrating over the spin variables, to be,

$$D = \frac{1}{2} (X + Y) - Z \quad E = \frac{1}{2} (Y - X) \quad (4)$$

where (for 2 electrons)

$$X = \frac{(g\beta)^2}{2} \langle \psi(r_1, r_2) | \frac{3x^2}{r_{12}^5} - \frac{1}{r_{12}^3} | \psi(r_1, r_2) \rangle , \quad (5)$$

Y and Z follow from this definition. It is obvious that if the molecule has D_{3h} asymmetry or higher (implying the x, y directions are equal, as is the case for sym-triazine) then $E = 0$ identically. In these systems E is expected to be less than D.

The fine structure, due mostly to hydrogen nuclei, is given by the interaction

$$\mathcal{H}_f = \underline{\hat{S}} \cdot \underline{\hat{A}} \cdot \underline{\hat{I}} \quad (6)$$

It would be possible to measure the tensor $\underline{\hat{A}}$ experimentally, as given below, and thus get at the spin densities and electron spin-nuclear spin coupling.

It is known that these proposed experiments are difficult, due mostly to the nature of the $n \rightarrow \pi^*$ triplet state itself. Phosphorescence has not been observed from pyridine and only weakly from sym-triazine. It is proposed that the resonance and emission data be taken using ~1% isotopic mixed single crystals with the spectra of the per-protonated guest to be studied in the perdeuterated host. This system, isotopic mixed crystals, has proven very valuable in the study of electronic emission and absorption spectra. Assuming that triplet β 's

(the nearest neighbor interaction matrix) in these systems are of the order of 10 cm^{-1} , transfer to the trap states would be fast and efficient, giving a high concentration of triplets when the host bands are used to absorb the light, and should be the ideal system for such studies.

Using isotopic mixed crystals it should further be possible to investigate hyperfine interactions both in the molecule itself and with the environment; such studies would give intra- and intermolecular structure and might be very useful information for the interpretation of energy transfer data and the extent of the influence of the environment on the molecule. Using standard epr technique and exciting into the host singlet states of these isotopic single crystals with unpolarized light will enable the D , E , g , and A quantities and the molecular geometry in the triplet state to be determined as in typical epr experiments. Such determinations can be carried out at both zero and high field and as a function of temperature. This latter point is of some interest, as for the N-heterocycles containing more than one nitrogen atom, there is more than one π^* excited state corresponding to a given N atom $n \rightarrow \pi^*$ transition, and optical transitions to some of these may be forbidden in the dipole approximation. For example in pyrazine, due to electron-electron repulsion interactions, the $n \rightarrow \pi^*$ transitions involving N_1 and N_2 are no longer degenerate in energy and under this perturbation the two new states are $[n_{12} \rightarrow (\pi_1^* \pm \pi_2^*)]$ with the antisymmetric combination optically forbidden. In sym-triazine we have three states $[n_{123} \rightarrow (\pi_1^* + \pi_2^* + \pi_3^*), (\pi_1^* + \epsilon \pi_2^* + \epsilon^\dagger \pi_3^*), \text{ and } (\pi_1^* + \epsilon^\dagger \pi_2^* + \epsilon \pi_3^*)]$ where $\epsilon = \exp(2\pi i/3)$ and $\epsilon^\dagger = \exp(-2\pi i/3)$ (the

latter two states are physically degenerate), but transitions can occur to all the states. The epr transitions are not governed by these same selection rules and the observed transitions can be affected by the proximity of an optically forbidden state. Therefore the variation of the spectrum with temperature will enable the $(\pi_1^* + \pi_2^*) - (\pi_1^* - \pi_2^*)$ splitting to be evaluated in pyrazine, in particular. Since however phosphorescence usually originates from the lowest triplet state, such a temperature study of both the resonance absorption and the phosphorescence would also be fruitful for sym-triazine.

The selective optical pumping^{5,6} experiments involve the use of highly monochromatic polarized light (both circular and linear) to excite the triplet states.⁵ The general procedure is to irradiate the triplet state of the sample (once the "magnetic" or zero field axes of the triplet state have been determined) with circularly polarized light, thereby exciting only the $m = +1$ or -1 spin states, depending on the handedness of the circularly polarized light. On the other hand, linearly polarized light ($m = 0$) can be used to irradiate the singlet and the polarization dependence of intersystem crossing and singlet-triplet energy transfer can be determined. To fully exploit this technique which has been mostly ignored over the years for aromatic crystals, the epr ($\underline{H} \neq 0$ and $\underline{H} = 0$) and polarized emission of single crystals should be simultaneously observed as a function of type of polarization ($m = 0, \pm 1$) and crystal (magnetic) direction (with both respect to \underline{H} and direction of propagation of the light). Below are a few of the possible types of observations that can be made with this general approach.

It is very important to determine accurately zero field parameters and their signs, the extent and nature of the spin-orbit interaction and which states it involves; at present no direct determination of such quantities is available. A "double resonance" technique can be employed to do this. At zero field the spin eigenstates are given by T_x , T_y , and T_z and the splitting pattern of these states, due to dipolar spin-spin coupling, is such that $T_z(|0\rangle)$ is removed from T_x and T_y which are (at least in these systems) nearly degenerate. If a large single crystalline sample (2-3 cm) is irradiated with left ($m = -1$) or right ($m = +1$) circularly polarized light, due to selection rules for dipolar transitions only the T_x , T_y states will be populated. The magnetic resonance is found and the absorbed light intensity monitored simultaneously. If the amount of light transmitted decreases when the rf field is turned on, T_x , T_y are below T_z (D is negative). If the T_x , T_y states are above T_z (D is positive) we should see rf stimulated emission and a small decrease in transmitted light. This should be studied as a function of direction in the crystal (as defined by the rf field and the polarized light). Now this same technique could be used at high field where the spin eigenstates are decoupled and are simply $|+1\rangle$, $|-1\rangle$, and $|0\rangle$. It will be possible in this instance to determine which of these spin states is most effective in spin orbit coupling, as the state populated (most strongly absorbing and emitting) would be the one having the most spin orbit derived transition probability.

The loss of full symmetry of the molecule can be directly related to this mixing of triplets with singlets. From the general form

of the optical and esr spectra (see below and ref. 3), the line shape, the fine structure, and their change with temperature, an analysis the triplet state molecular symmetry can be made and a lifetime can be assigned to the (new) geometrical structure. As an example, naphthalene has D_{2h} symmetry, but if it rotates in the ring plane at a rate greater than 10^{10} sec^{-1} , the x and y directions would appear to be equivalent and the naphthalene epr spectrum would reflect this "3-fold or higher" (D_{6h} here) symmetry. On the other hand, consider exciton transfer rates of greater than 10^{10} sec^{-1} . We would not expect to observe any fine structure on its resonance line. Thus, when T_x, T_y appear non-degenerate at zero field ($E \neq 0$), we know the molecule in its triplet state has less than a trigonal axis and that this state lives longer than $10^{-9} - 10^{-10} \text{ sec}$. What this new symmetry is, is indicative of both the spin-orbit and the configurational interactions and the vibronic coupling mechanisms.

The epr and emission spectra in each case should be taken with both polarized and unpolarized light (exciting into both the host and guest singlet and triplet states) and at as many orientations of the crystal in the \underline{H} field as possible. $\Delta m = \pm 2$ transitions should also be looked for (but would be very weak³) in order to check the zero field determinations (find $\Delta m = \pm 1$ and $\Delta m = \pm 2$ transitions for a constant \underline{H} field). The expected anisotropy in the spectra, and thus the \underline{g} tensor, is another method for the determination of spin-orbit interactions. The anisotropy, along with the fine structure data, could enable one to determine the effect of the ring nitrogen atoms on the electron spin density.

Individual Molecules:

Pyridine: Calculations⁷ put the 3B_2 state ($n \rightarrow \pi^*$) at 28,000 to 30,000 cm^{-1} but this state has not been observed. The probable reason for this is the small spatial overlap of the nitrogen 2s and 2p orbitals thus giving rise to the very small transition moment. It is possible here, according to Goodman,⁸ that the lowest triplet state is $\pi \rightarrow \pi^*$ (3A_1). This would be worth-while proving and could be done by the technique outlined above. (For the $\pi \rightarrow \pi^*$ case, D and E would be small and resonance would occur at relatively low fields.)

Pyrazine: The pyrazine crystal has 2 molecules per unit cell with a space group symmetry D_{2h} and the site symmetry, and therefore the molecular symmetry in the crystal, is C_s .

This system is far better understood than is pyridine. Phosphorescence has been observed, oscillator strength calculated ($\sim 10^{-7}$) and the phosphorescing state at 26,000 cm^{-1} has been identified as $n \rightarrow \pi^*$.^{2,9,10} The $n \rightarrow \pi^*$ optically allowed triplet is ${}^1A_{1g} \rightarrow {}^3B_{2u}$, and it is found that the major mixing term due to spin-orbit coupling is ${}^1B_{1u}$.⁸ The state is further believed to be nonplanar.

Due to the molecular and crystal site symmetry we would expect D and E to be non-zero. This is the best characterized of the three systems discussed and probably should be treated first. As previously discussed it would be very interesting to observe the temperature dependence (77 to 1.8°K) of the resonance.

sym-Triazine: The crystal structure of sym-triazine is D_{3d}^6 (rhombohedral) with 2 molecules per cell. The site symmetry is $C_{3i}(S_6)$. This molecule has D_{3h} symmetry and thus E is identically zero if symmetry is kept in the triplet state. It is interesting to note that since the site symmetry is so high, distorted excited states observed in the crystal must be due to intrinsic or molecular effects.

sym-Triazine has three $n\pi^*$ states E'' , A_1'' , and A_2'' . The energy of this $n \rightarrow \pi^*$ triplet is around $26,000 \text{ cm}^{-1}$ and is assigned ${}^3E'' \leftarrow {}^1A_1'$. The state to which this is coupled has not been determined but the ${}^1A_2''$ states at $31,600 \text{ cm}^{-1}$ is a likely candidate. The reason for low quantum yields for this molecule may be connected to the triplet state symmetry. Since this molecule has such a high symmetry in the site and the lowest triplet is supposed to be degenerate, we have a very good opportunity to study the Jahn-Teller Effect in this system. Any observed splitting must be due to a vibronic distortion as the crystal cannot remove this degeneracy. Here again the temperature dependence of the resonance and emission spectra would be of particularly great interest. Such a determination of the Jahn-Teller Effect would be one of the first unambiguous observations of this phenomenon.

References

1. P. R. Kearns and M. A. El Bayoumi, *J. Chem. Phys.*, 38, 1508 (1963), for background and general presentation but it is thought that the conclusion reached by these authors is incorrect. The M. O. and exciton presentation are not at all of the same degree of sophistication and refinement.
2. M. A. El-Sayed and G. W. Robinson, *Mol. Phys.*, 4, 273 (1961).
3. See series of papers by J. H. van der Waals *et. al*, *Mol. Phys.*, 2, 33 (1959), *Mol. Phys.*, 3, 190 (1960), *Mol. Phys.*, 6, 545 (1963), *Mol. Phys.*, 8, 301 (1964), C. A. Hutchison, Jr., and B. Mangum, *J. Chem. Phys.*, 29, 952 (1958); 32, 1261 (1960), 34, 908 (1961); and later discussion of individual molecules in this proposition.
4. We are neglecting spin-orbit effects which for these systems may not be small. If the zero field splitting is exceptionally large for these systems it is possible that spin-orbit effects would account for this. See S. J. Fogel and H. F. Hamerka, *J. Chem. Phys.*, 42, 132 (1965).
5. A. Kastler, *Proc. Phys. Soc. (London)*, 67A, 853 (1954), *J. Opt. Soc. Am.*, 47, 460 (1957).
6. R. A. Bernheim, *Optical Pumping: An Introduction*, Benjamin, Inc., New York, New York (1965).
7. L. Goodman and R. W. Harrell, *J. Chem. Phys.*, 30, 1131 (1959).
8. L. Goodman, *J. Mol. Spect.*, 6, 109 (1961).
9. L. Sidman, *J. Mol. Spect.*, 2, 333 (1958).
10. L. Goodman and M. Kasha, *J. Mol. Spect.*, 2, 58 (1958).
11. J. P. Paris, R. C. Hirt, and R. G. Schmidt, *J. Chem. Phys.*, 34, 1857 (1961).

PROPOSITION IV

It is now quite apparent that the static properties of molecular aromatic hydrocarbon crystals are quite well understood and characterized in terms of pair wise, atom-atom interactions.¹ On the other hand, such a potential model may be very bad in the description of a first or second order phase transition in a crystal of small molecules or in general for non-aromatic but covalently bonded systems. In fact, very little is known about crystal phase transitions in an interaction or mechanistic sense and perhaps even less about intermolecular interactions between non-aromatic, covalently bonded molecules. Such molecules, in many cases (diborane, for example), due to their unusual electronic distribution, may be expected to evidence new and interesting intermolecular interactions in the solid. In order to study the phase transitions and intermolecular interactions in these systems, it is proposed that single crystals of diborane (B_2H_6) be studied by nuclear quadrupole resonance spectroscopy.

The diborane is itself quite interesting: it has D_{2h} symmetry and the two boron atoms are held together by two B-H-B "three center" bridge bonds. The terminal hydrogens all line in a plane which is perpendicular to the plane of the two bridge hydrogens. There is effectively no bond between the two boron atoms in diborane and, thus unlike ethylene, there is a very high barrier to internal rotation about the B-B twofold axis. "Three-center bonds" usually arise when the number of electrons available for bonding is less than the number of atomic orbitals used in the bond formation. The similarities and

differences between the diborane and ethylene orbitals are pointed out and discussed by Lipscomb.²

The crystal structures of the many phases of diborane are as yet not well defined. Investigations by infrared spectroscopy of single crystals revealed evidence for at least three crystal phases,³ one of which was identified as being monoclinic with molecules at sites of \underline{C}_i or \underline{C}_1 symmetry. Another of the phases has been studied by the techniques of x-ray crystallography⁴ and the space group has been determined to be $P2_1/n$ with two molecules per primitive unit, occupying site of inversion symmetry. It is apparently not clear, however, if there is a real conflict between these two studies or if each group was looking at different phases. Both groups believe they have the α or high temperature modification but predict different orientations for the molecules with respect to the crystallographic axes.

The crystal with its many phase transitions and this rather simple molecule with its quite unique electron distribution (three center or bridge bonds), would seem to provide a wealth of possibilities for the study of intermolecular interactions and first and second order phase transitions in the solid. The technique of nuclear quadrupole resonance absorption is particularly well suited for such a study in that quadrupole spectra usually give sharp lines and large, single crystal samples are employed. The greatest advantage of nqr over, say light spectroscopy, is that the resonance absorption can be followed through the phase transition, since the frequency of the absorption ($\nu \sim 10$ mc/s) is of the order of the molecular reorientation

and motion in the solid. Thus the actual kinetics of the motion or orientation undergoing change can be followed, and such dynamic effects are of major importance in phase transitions.

Boron has two isotopes, B^{10} and B^{11} , with $I = 3$ and $I = 3/2$, respectively, the B^{11} isotope being about three times as abundant naturally. The fact that the B^{11} nucleus has a spin of $3/2$ and is more abundant makes it by far the easier of the two to use as a probe of electronic structure of boron compounds. Moreover, since the nuclear spin contributes little to the field gradient tensor at the nucleus (the studied quantity in nqr absorption spectroscopy), both nuclei yield the same information and thus the B^{11} nucleus will be the only one used to probe the molecular electronic structure of diborane in the solid.

For a nucleus with a spin of $3/2$, only one frequency will be observed at zero external magnetic field ($\underline{H} = 0$); we cannot, therefore, find both the z component of the electric field gradient tensor q and the asymmetry parameter ($\eta = q_{xx} - q_{yy}/q$). This single frequency for a nucleus of spin $3/2$ is given by

$$\omega_Q = \frac{e^2qQ}{2\hbar} (1 + \eta^2/3)^{\frac{1}{2}}$$

where e is the charge of the electron, Q is the nuclear quadrupole moment, and e^2qQ is referred to as the nuclear quadrupole coupling constant. In the presence of a weak magnetic field ($\gamma H_0 \ll e^2qQ$, where γ is the nuclear gyromagnetic ratio) however, the m degeneracy is removed and in principle five transitions may be observed as the

magnetic field mixes the $\pm 1/2$ states. Thus $\pm 3/2 \rightarrow \pm$, and $+$ $\rightarrow -$ transitions can be observed and vary in intensity as a function η . A detailed discussion of the equations that govern the intensities and energies of these transitions is given by Das and Hahn.⁵

The technique for finding the electric field gradient tensor, its axes, the number of molecules (physically or chemically inequivalent) per primitive unit cell and the effect of motion on the resonance and line width will now be outlined for $I = 3/2$. The study of the pure quadrupole resonance in single crystals as a function of temperature will give the quadrupole coupling constant and its temperature coefficient in all phases. The observation of more than one resonant absorption frequency indicates the presence of more than one molecule per unit cell: if the principle components of the field gradient tensor are different for the two sites, the sites are chemically inequivalent while if the tensor axes are simply rotated with respect to one another, the sites are interchange equivalent ones. Observing the intensities of these pure quadrupole resonances as a function of the direction of the rf field with respect to the axes of the crystal will allow a rough determination of the orientation of the axes of the field gradient tensors with respect to those of the crystal. Applying a small magnetic field and observing the Zeeman pattern provides a method of finding η and the exact positions of the field gradient axes for all the molecules of the unit cell. If $\eta \neq 0$ there will be no "locus of no splitting" for the Zeeman pattern of four lines even in the case where the rf field is perpendicular to an axis of symmetry. The exact form of these

patterns are quite complex and are discussed in Ref. 5. For more than one interchange equivalent molecule in the unit cell the different Zeeman patterns can be traced separately and the individual axes obtained. The above procedure enables one to find the "static" properties of the molecules in each phase, but we now want to evaluate the effect of the motion of the molecules on the observed resonant absorption lines. The quantities of interest in following such motion are the relaxation time T_1 , the resonant frequency, and the line width as a function of temperature both throughout the regions of constant phase and through the phase transition itself. The various theories that relate these properties to the molecular motion are enumerated by Das and Hahn.⁵ One can in principle find both the barrier height and the frequency of motion from the above data (e. g., the change from free to hindered rotation involves a large change in the temperature coefficient of the frequency in the neighborhood of the transition temperature). The nature of the phase transitions and the cooperative intermolecular interactions causing them can be thus evaluated.

Aside from the obvious information concerning phase transitions and intermolecular interactions, we can also learn about the electronic structure of diborane and how this structure is perturbed by the various crystal environments. Unfortunately, since no quadrupole data are available for diborane in the dilute gas, our knowledge of these changes in any absolute sense will be severely limited. We can, however, estimate the isolated molecule field gradient tensor components using the highly simplified Townes and Dailey theory.⁶ In this severe but

surprisingly useful approximation we obtain the molecular quadrupole coupling constant for the atom of interest as,

$$e^2 Q q_{\text{mol}} = eQ [n_z - 1/2(n_x + n_y)] (eq)_{2p_z}$$

with n_i the square of the coefficient of the $2p_i$ orbital. Using sp^3 hybridization for the boron atom in diborane such that the bridge angle, H-B-H, is $101^\circ 32'$ and the two terminal B-H bonds make an angle of 120° , the B orbitals for the bonds are:

$$\begin{bmatrix} \psi_1 \\ \psi_2 \\ \psi_3 \\ \psi_4 \end{bmatrix} = \begin{bmatrix} +1/\sqrt{6} & -1/\sqrt{3} & +1/\sqrt{2} & 0 \\ +1/\sqrt{6} & -1/\sqrt{3} & -1/\sqrt{2} & 0 \\ +1/\sqrt{3} & -1/\sqrt{6} & 0 & -1/\sqrt{2} \\ +1/\sqrt{3} & -1/\sqrt{6} & 0 & +1/\sqrt{2} \end{bmatrix} \begin{bmatrix} \psi_{2s} \\ \psi_{2p_x} \\ \psi_{2p_y} \\ \psi_{2p_z} \end{bmatrix}$$

with the x-axis between the two terminal bonds. ψ_1 is "up" in the xy-plane, ψ_2 is "down" in the xy-plane, ψ_3 "back" in the xz-plane, and ψ_4 "out" in the xz-plane. If one assumes that ψ_1 and ψ_2 each have 1/2 electron and ψ_3 and ψ_4 each have one electron, one gets the relation:

$$(eq)_{\text{mol}} = 0.58 (eq_{2p_z})_{\text{at}}$$

and

$$\eta = 0.43$$

Now for the B^{11} atom $e^2 q_{\text{at}} Q/h = 5.39$ mc/s and thus for diborane

$$(e^2 q_{\text{mol}} Q/h)_{B^{11}} = 3.14 \text{ mc/s}$$

with the resonance appearing at

$$\nu_Q = \frac{e^2 q Q}{2h} (1 + \eta^2/3)^{1/2} \approx 1.75 \text{ mc/s}$$

It must be borne in mind that this approximate calculation of the quadrupolar coupling constant and asymmetry parameter is highly suspect for a molecule as unique as diborane. Further it must be remembered that the quadrupole coupling constant and asymmetry parameter have been calculated for an isolated diborane molecule; the intermolecular forces between diborane molecules may alter their value considerably in the crystal. It will, however, serve as a useful guide in the search for the resonance and in the interpretation of the experimentally determined q and η .

References

1. E. R. Bernstein, "Calculation of Ground State Vibrational Structure and Phonons of the Isotopic Benzene Crystals," J. Chem. Phys. (to be published).
2. W. N. Lipscomb, Boron Hydrides, W. A. Benjamin, Inc., New York (1963).
3. I. Freund and R. S. Halford, J. Chem. Phys., 43, 3795 (1965).
4. H. W. Smith and W. N. Lipscomb, J. Chem. Phys., 43, 1060 (1965).
5. T. P. Das and E. L. Hahn, Solid State Physics, Supplement 1 (1958).
6. C. H. Townes and B. P. Dailey, J. Chem. Phys., 17, 782 (1949); J. Chem. Phys., 23, 118 (1955).

PROPOSITION V

One of the contributions of the physical sciences to biology in the last two decades has been the determination of the structure of DNA (by Watson and Crick^{1,2}). In this work they determined that DNA has a double helix structure with the two sugar-phosphate chains held together by a sequence of pairs of nucleotide bases (each member of the pair belonging to a different one of the two helices). The bases (adenine, thymine, guanine, and cytosine - Figure 1), and thus the separate chains of the DNA molecule itself, are held together by hydrogen bonding between complementary pairs of bases (A-T and G-C; Figure 2).^{1,2,3} They further argued that, by these hydrogen bonds and lone pair electrons, the genetic code is both recognized and preserved. Errors in the hydrogen bonding scheme then can cause mistakes in the genetic code and thus may lead to the mutations responsible for aging, tumors, evolution, or in some cases, death. This is indeed a very provocative postulate, which has now become virtually accepted without question. As far as is known, however, although no unequivocal evidence has yet been found to contradict it, their postulate has never been scientifically demonstrated. After the ensuing discussion of the quantum mechanical formulation of this postulate, a series of experiments is suggested on some simple, well characterized model systems, designed to shed light on the importance of hydrogen bonds for the genetic code and for DNA, itself.

When Watson and Crick put forth this hypothesis, they believed that the tautomeric forms of the bases incorporated into DNA were

quite rare in solution, as well as in DNA itself. However, recent measurements of the equilibrium constants for the pyrimidine bases (T, C) have shown that around 1% of the bases in solution are in their tautomeric forms (C*, T*).⁴ Unfortunately such a study has not been carried out on the purine bases (A, G). There are two possible ways to accommodate this fact into the Watson-Crick model of genetic specificity. Löwdin^{5, 6} has proposed a "replication plane" consisting of two amino and two keto groups (two base pairs - two bases from the old helices that have just separated and two new entering bases) which can all hydrogen bond together temporarily, and thereby keep out any single tautomeric forms. Pairs of tautomeric bases, which could be thus incorporated, on the other hand, would be quite low in concentration in solution and in rough agreement with the mutation rate of 10^{-8} to 10^{-12} /base pairs/generation.⁷ Thus if at replication time only pairs of tautomeric bases (A*-T*, G*-C*) are included as "errors," which at next replication will yield a "genetic mistake," the Watson-Crick postulate can be retained. The second approach is to allow all mistakes in the genetic processes to be repaired by one of the polymerases, those enzymes active in the replication processes. Of course, physicists (physical chemists) favor the former, while biologists the latter mechanism.

The "purification" procedure for DNA, the replication plane, was actually put forth by Löwdin as only a part of a much larger theory concerning the hydrogen or "proton genetic code" in DNA.^{5, 6} Löwdin has calculated the rate of mutation of a proton code for the DNA base

pair system in a very impressive body of work.^{5,6} The major ideas and results of this calculation are summarized below:

a) Using an asymmetric double well potential model, the tautomerization of a hydrogen bond is a function of the height of the barrier between the wells (V_0), the "non-classical" distance between the two wells from classical turning point to classical turning point ($a_0 \sim 1 \text{ \AA}$), the characteristic frequency of the particle (mass m) in the lowest well ($\nu \sim 10^{13}$ to 10^{14} sec^{-1}), and a Boltzmann factor depending on the separation of the two well minima in energy space (ΔE).

b) The Boltzmann factors are such that the only possible mechanism by which a proton can get from the deeper well to the shallow one is by tunneling. Löwdin, however, appears to neglect the return of the proton to the deep well by classical means which now becomes quite competitive with the quantum mechanical return process.

c) If one assumes the hydrogen bond is of an electrostatic nature and calculates charge densities on the various N and O atoms comprising the bond, then due to the "ionic effect" the well asymmetry is quite large ($\Delta E \sim 2.0 \text{ eV}$) and the tunneling time geological. Unfortunately, in two different calculations the wells were different by about a factor of two ($V_0 = 0.4$ to 0.8 eV).

d) Again for single proton tunneling, it is found that if one of the bases is in an excited state (e. g., base \rightarrow base charge transfer or simple excitation of one of the bases), tunneling is quite fast and efficient as the asymmetry in the well is almost zero. ($\Delta E \sim 0.3 \text{ eV}$ but again we find great variation for two different calculations.)

e) On the other hand, with a simultaneous two proton jump Löwdin shows that due to the overall preservation of base pair neutrality, the well asymmetry markedly decreases ($\Delta E \sim 0.7$ eV), the Boltzmann factor becomes reasonable $\sim 10^{-10}$, and the tunneling times become the observed natural mutation rate.

f) The rate of barrier penetration in most cases (even for the single proton) is quite rapid, 10^5 sec^{-1} (as it should be!), and in all cases it is the Boltzmann factor that governs the overall process of tautomerization of the hydrogen bond. Since the tautomeric equilibrium is quickly arrived at, when observing at times long with respect to the tunneling times, the difference between H and D atoms in the bond (i. e., a mass effect) is lost due to "back tunneling."

All factors considered, this is indeed a remarkable calculation in that it gives a mutation rate that corresponds to the one found in nature and does predict great stability for the "proton genetic code." The two possible points of criticism of this work are the fact that classical (over the barrier) "back-tunneling" is not considered, and that two different calculations give such divergent well energetics. How serious these criticisms are is difficult to say, but it does appear as though a "proton code" could be qualitatively based on the simultaneous proton tunneling and "selective replication plane" joint hypothesis. What Löwdin has shown is that at least such postulates are not self-contradictory and appear not be at variance with current observations.

On the other hand, Chan and co-workers⁸ have recently reported some extremely interesting results concerning base stacking in solution. The stacking seems to be the predominant, detectable interaction between various dinucleotides and pyrimidine and purine bases. It is as yet too early to understand the implication of this partially completed research, but it certainly raises questions concerning the proton or hydrogen bond dominance of the DNA-genetic code system.

Clearly the time is ripe for quantitative studies of the hydrogen bonding and stacking interactions in DNA and it is proposed that a model system be employed in such research; since the in vivo or in vitro DNA system is much too complex for such an investigation, a good model system indeed appears to be the only solution. The proposed model is base pair crystals. In such systems quantitative evaluation of Löwdin's calculation is possible and comments on stacking interaction can also be made. It is proposed that a series of diverse spectroscopic studies of these crystals be made, but before this discussion let us consider the crystals themselves. The hydrogen-bonded base pair crystals thus far observed are:

1. 1-Methyl thymine and 9-methyl adenine (1:1). Space group $P2_1/n$ with two pairs/unit cell and the arrangement of the pair is planar.⁹ Interestingly enough, these molecules do not hydrogen bond in the same way as they are postulated to in DNA.

2. 9-Ethyl guanine and 1-methyl-5-bromocytosine (1:1). The space group is Pa_1/c with two pairs/unit cell.¹⁰ The hydrogen bond structure is the same as that predicted by Pauling and Corey³ for the G-C pair in DNA.

3. 9-Ethyl guanine and 1-methyl cytosine (1:1). The unit cell is triclinic with two base pairs/primitive unit.¹¹ The hydrogen bonding is found to agree with the DNA structure.

4. 9-Ethyl adenine and 1-methyl uracil (1:1). The space group is $P\bar{1}$ with two pairs/unit cell.¹² Strong hydrogen bonding appears between the two molecules in the base pair complex.

5. Two tautomers of isocytosine (1:1 complex). The space is $P2_1/n$ with four pairs of molecules in the unit cell.¹³ The pairs are again planar and strong hydrogen bonding exists between the molecules comprising the pair.

6. 1-Methyl 5-iodouracil and 9-ethyl-2,6-diaminopurine (2:1 complex). The space group is $P2_1/c$ with four asymmetric units/unit cell.¹⁴ This complex shows non-DNA type hydrogen bonding between three molecules.

Two general remarks can be made concerning these base pair crystals. First, not only is the hydrogen bonding scheme not always like that proposed for DNA, but bases excluded from DNA appear to hydrogen bond quite well with those included in DNA. Second, these crystals form in layers of base pairs separated by $\sim 3.4 \text{ \AA}$, a distance often encountered in aromatic molecular crystals in this regard and also in DNA. Of course, these two facts do not negate the Watson-Crick-Pauling-Corey proton genetic code hypothesis, but they do give one cause to reconsider and reinvestigate the nature of the hydrogen bond and the base stacking interactions in these systems. It is with such an open-minded approach that the spectroscopic study of base

pair crystals is proposed. Research on the base pair crystals themselves is, however, far from complete. Neutron diffraction data is completely lacking for these crystals and its need is quite obvious. It would, of course, be important to obtain other pair crystals and to determine whether mixed base pair crystals (containing more than one type of pair) could grow and, if so, what systems could be obtained (again the question of base stacking interactions arises, e. g., could a known code triplet be crystallized?). Further, it may be possible to incorporate known mutagens, such as 5-bromouracil, into these crystals. The possibilities for the model system are indeed almost limitless and should be extremely fruitful. Since it is known that high energy radiation (2537 Å Hg light, x-radiation, proton and electron bombardment) is lethal to the living cell, the crystals can be studied before, during, and after they have been irradiated.

A few of the possible techniques for the investigation of the hydrogen (deuterium) bonding or stacking properties of base pair crystals will now be presented and briefly discussed.

Infrared Absorption: With infrared absorption spectra it will be possible to measure the frequency shift ($\Delta\nu$, is usually a negative shift from gas or non-polar liquid) of the X-H (D) stretch, the half width of the band, and its temperature dependence. This will give us information concerning the energy of the hydrogen bond ($\Delta\nu_s/\nu \propto \Delta H$) and the X-H (D) bond length.¹⁵ One can also look for very low frequency (20 to 200 cm^{-1}) absorption caused by new stretching or bending modes, due to the bond formation. Intensity changes are also of interest but are

usually quite difficult to interpret.

Raman Scattering: Like information can be obtained from Raman scattering experiments, but there are distinct advantages of this technique over the infrared absorption, especially in the solid. Usually the absorption of X-H stretching and bending modes is quite strong requiring very thin crystalline samples, difficult to orient and grow. On the other hand, the Raman scattering intensity of these bands is very small and large single crystals (2 cm^3) can be used. Further, Raman spectra (which are usually much sharper than the infrared absorption bands) can now be obtained with lasers, allowing high resolution techniques to be employed. Again the temperature dependence of the scattering is very important both for shifts in frequency and splittings of different modes; deuterium substitution should prove fruitful in identification of bands and the interpretation of the observed changes upon hydrogen bonding. Raman scattering is a far superior tool in the study of the very low frequency stretching and bending modes.

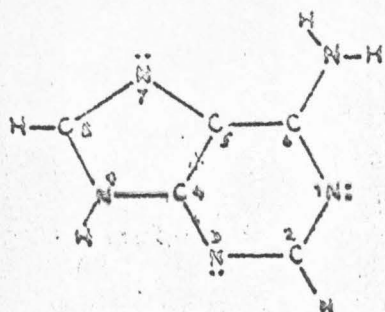
Optical Emission, epr Absorption, and Energy Transfer: At very low temperature (4.2°K) it may be possible to excite selectively one of the bases and monitor the emission (phosphorescence or fluorescence). This may help determine whether the largest interaction is across the hydrogen bonds or between the π systems of the rings (stacking). If phosphorescence is observed, epr absorption can be used to follow the triplet state population and kinetics as a function of temperature. Mixed base pair crystals would be of much interest in such studies.

Nuclear Quadrupole Resonance: The atomic nuclei ^{14}N , ^{17}O , and D have quadrupole moments and can thus be used as probes for the X-D bond in the base pair crystals. Of particular interest with this technique would be the changes in frequency, line width, and spin-lattice relaxation times (T_1) as a function of temperature. These observations would offer kinetic information concerning the motion of the hydrogen (deuterium) atom in the bond and could, therefore, serve as a direct and crucial test of Löwdin's ideas and calculations.

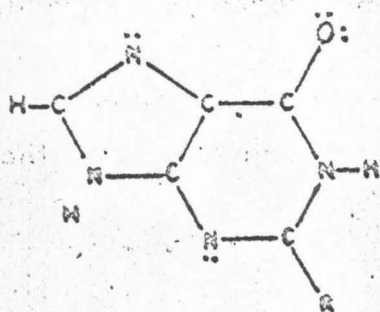
The above suggested methods of observation are only a few of the many ways to obtain accurate quantitative data concerning base pairing and should greatly help in the understanding of the DNA molecule, the genetic transfer or coding of information, and the DNA replication process.

References

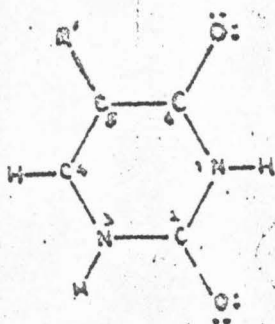
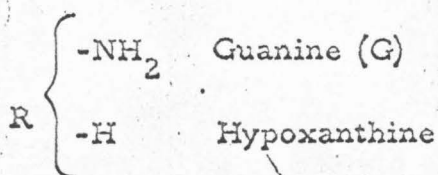
1. J. D. Watson and F. H. C. Crick, *Nature*, 171, 737, 964 (1953).
2. F. H. C. Crick and J. D. Watson, *Proc. Roy. Soc. (London)*, A223, 80 (1954).
3. L. Pauling and R. B. Corey, *Arch. Biochem. and Biophys.*, 65, 164 (1956).
4. A. P. Katritzky and A. J. Waring, *J. Chem. Soc. (London)*, 1540 (1962) and *J. Chem. Soc. (London)*, 3046 (1963).
5. P-O. Löwdin, preprint QB 7, Quantum Chemistry Group, Uppsala Univ., Uppsala, Sweden.
6. P-O. Löwdin, preprint QB 33, Quantum Chemistry Group, Uppsala Univ., Uppsala, Sweden.
7. E. Freese, *J. Theoret. Bio.*, 3, 82 (1962).
8. P. O. P. Ts'o and S. I. Chan, *J. Am. Chem. Soc.*, 86, 4176 (1964); S. I. Chan, M. P. Schweizer, P. O. P. Ts'o, and G. K. Helmkamp, *J. Am. Chem. Soc.*, 86, 4182 (1964); M. P. Schweizer, S. I. Chan, and P. O. P. Ts'o, *J. Am. Chem. Soc.*, 87, 5241 (1965); and S. I. Chan, B. W. Bangerter, and H. H. Peter, *Proc. Nat. Acad. Sci.*, 55, 720 (1966).
9. K. Hoogsteen, *Acta Cryst.*, 16, 907 (1963).
10. H. M. Sobell, K. Tomita, and A. Rich, *Proc. Nat. Acad. Sci.*, 49, 885 (1963).
11. E. J. O'Brien, *J. Mol. Biol.*, 7, 107 (1963).
12. F. S. Mathews and A. Rich, *J. Mol. Biol.*, 8, 89 (1964).
13. J. F. McConnell, B. D. Sharma, and R. E. Marsh, *Nature*, 203, 399 (1964).
14. L. L. Labana and H. M. Sobell, *Proc. Nat. Acad. Sci.*, 57, 459 (1967).
15. See e.g., G. C. Pimentel and A. L. McClellan, The Hydrogen Bond, W. H. Freeman and Co., San Francisco, California (1960).



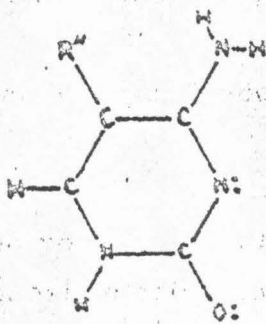
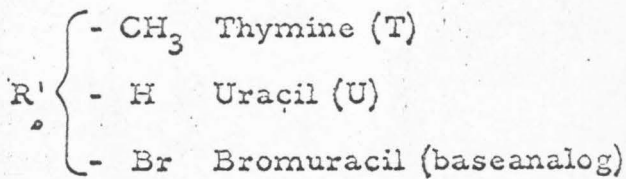
Adenine (A)



Guanine bases:



Thymine bases:



Cytosine bases:

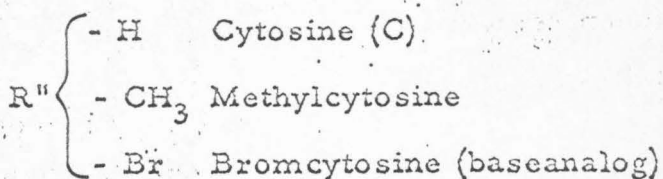


Figure 1. Chemical structure of the common bases and some of the baseanalog; in addition to the σ -skeleton indicated by the figure, there is also a π -electron cloud corresponding to the conventional double bonds. The double dots : indicate electron lone pairs which attract protons and will participate in hydrogen bonding.

Figure Captions

- Figure 2a. The hydrogen bonds between the normal base pairs in DNA resolved into their proton-electron pair components; note that here H denotes a proton and the symbol : an electron pair according to Lewis. Arrows indicate the positions at which bases are joined to the sugar-phosphate chain.
- Figure 2b. The proton-electron pair code of the normal nitrogen bases; compare the schematic templates in Figure 2a.
- Figure 2c. The proton-electron pair code of some rare tautomeric forms of the nitrogen bases; compare the schematic templates in Figure 2b.

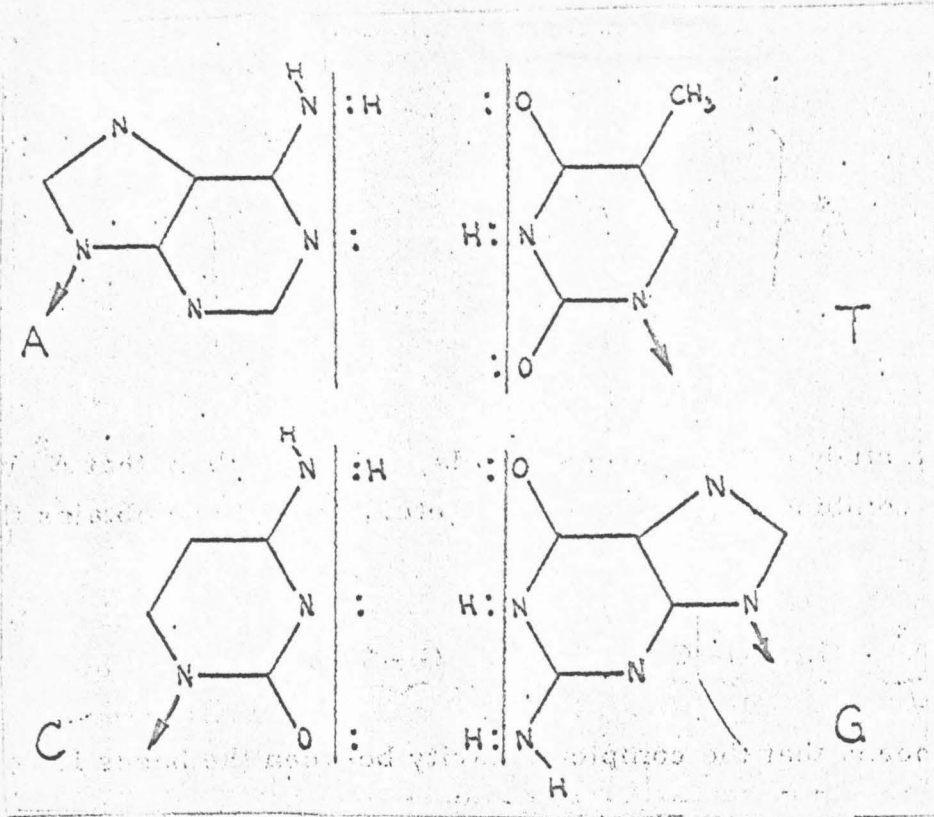


Figure 2a

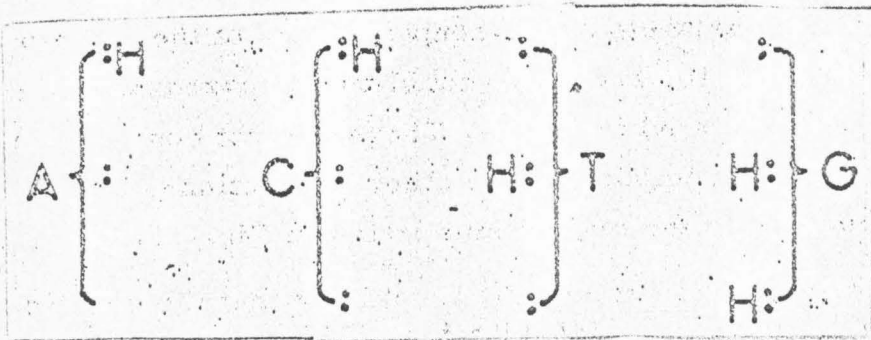


Figure 2b

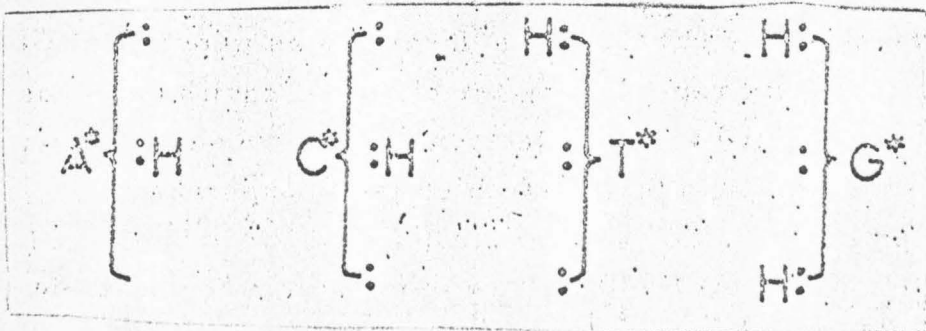


Figure 2c